Packed-Bed Adsorption of Phenol and 2,4 Dichlorophenoxy Acetic Acid on the Macroreticualar Resin Xad-7

by

Yousouf Eydatoula

A Thesis Presented to the

FACULTY OF THE COLLEGE OF GRADUATE STUDIES

KING FAHD UNIVERSITY OF PETROLEUM & MINERALS

DHAHRAN, SAUDI ARABIA

In Partial Fulfillment of the
Requirements for the Degree of

MASTER OF SCIENCE

In

CHEMICAL ENGIEERING

May, 1984

Packed-bed adsorption of phenol and 2,4-dichlorophenoxyacetic acid on the macroreticular resin XAD-7

Eydatoula, Yousouf, M.S.

King Fahd University of Petroleum and Minerals (Saudi Arabia), 1984

PACKED-BED ADSORPTION OF PHENOL AND 2,4 DICHLOROPHENOXY ACETIC ACID ON THE MACRORETICULAR RESIN XAD-7

by

YOUSOUF EYDATOULA

A Thesis presented to the
FACULTY OF GRADUATE STUDIES,
UNIVERSITY OF PETROLEUM AND MINERALS, DHAHRAN,
In Partial Fulfillment of the
Requirements for the Degree of
MASTER OF SCIENCE, CHEMICAL ENGINEERING.

MAY 84

UNIVERSITY OF PETROLEUM AND MINERALS

DHAHRAN, SAUDI ARABIA

This thesis, written by

YOUSOUF EYDATOULA

under the supervision of his Thesis Committee, and approved by all its members, has been presented to and accepted by the Dean, College of Graduate Studies, in partial fulfillment of the requirements for the degree of

MASTER OF SCIENCE IN CHEMICAL ENGINEERING

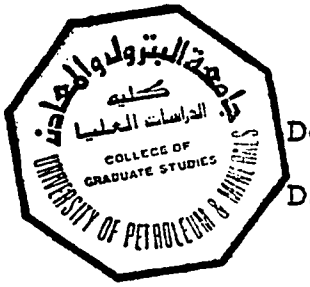

Dean, College of Graduate Studies

Date

Dr. Reda S. Al-Thiga

Department Chairman

THESIS COMMITTEE

Dr. Muhammad A. Hasanain(Chairman)

Dr. Kevin F. Loughlin(member)

Dr. Dulaihan K. Al-Harbi(member)

To

Mahshid, Murielle and Vista,

with all my love.

ABSTRACT

The objective of this research is the study of the adsorption of phenol and 2,4 dichlorophenoxy acetic acid on the macroreticular resin XAD-7. The research was divided into the following parts: experimental work including batch and continuous flow adsorption to determine both the equilibrium isotherms and the adsorption rate-controlling mechanisms in the packed bed system. Experimental breakthrough curves were measured for both adsorption and regeneration and various kinetic models examined.

The parameters studied were:adsorbate initial concentration, temperature , bed height and flow rate.Equilibrium isotherms for each component at 25,40 and 50 degrees centigrade was obtained and modelled. Experimental data were also obtained for equilibrium adsorption of a mixture of the acid and phenol on the resin. Analysis of the data revealed that the adsorption of the individual components was unaffected by the presence of the other one at the loadings studied.

A differential approach was used for the calculation of the mass transfer coefficients and the

rates of adsorption. The data were tested for external, internal and second-order surface kinetic resistances. The reversible second order kinetics model gives the best fit in the case of the DPCA acid, and external diffusion appears to be the rate controlling step in the adsorption of the phenol.

The heat of adsorption was calculated from the data. It was found to be of the same order of magnitude as the latent heat of condensation of each adsorbate.

LIST OF CONTENTS

TABLE OF FIGURES

NOMENCLATURE

b equilibrium constant, lit/umole.

C concentration,umoles/lit.

C_0 initial concentration,umoles/lit.

C' constant in the BET isotherm,dimensionless.

F flowrate,cc/minute.

J Thomas function.

K Henry's constant,lit/gm.

K' equilibrium constant in the Langmuir equation,lit/μmole.

K_I irreversible 2nd order kinetics mass transfer coefficient, lit/hr-μmoles.

k_a reversible 2nd order kinetics mass transfer coefficient, lit/hr-μmoles.

k_1 rate constant for the adsorption term of the Langmuir equation, lit/gm-hr

k_2 rate constant for the desorption term of the langmuir equation. μmoles/gm-hr

$K_F a_F$ external mass transfer coefficient,hr.$^{-1}$

K_K Klotz's external mass transfer coefficient, $hr.^{-1}$

K_V Vermeulen's mass transfer coefficient, $hr.^{-1}$

K_{GE} Geser and Kostecki's mass transfer coefficient, $hr.^{-1}$

$K_p a_p$ internal mass transfer coefficient, $hr.^{-1}$

m,n Freundlich constants.

P pressure, atm.

q uptake of adsorbate, μmoles/gm.

q^* solid composition at equilibrium with C, the concentration, μmoles/gm.

q solid composition at equilibrium with the C_0, μmoles/gm.

Q defined as q/q_∞, dimensionless.

Q_m maximum capacity of the adsorbent, μmoles/gm.

r the rate of adsorption, μmoles/gm-hr.

r^* defined as $1/(1 + K'C)$.

S cross sectional area of tube, $cm.^2$

t time, minutes.

v volume, cc.

V superficial velocity of solution, cm/hr.

V_Z velocity of solution inside the bed, cm/hr.

X defined as C/C_0, dimensionless.

Z bed length, cm.

τ dimensionless time variable.

ξ dimensionless length variable.

ρ_b bulk density of packed bed, gm/cc.

ϵ porosity of packed bed.

ACKNOWLEDGEMENTS

I have been able to complete this thesis because many people helped. I thank Dr. Mohammad Hasanain ,my thesis advisor , for providing me with the opportunity to work on this project. He guided me with his suggestions and criticisms and showed friendly understanding to my personal problems. I thank Dr. S. Gultekin for his interest in my work, and for his discussions and interpretations of the data. He taught me an interesting course in catalysis, which helped me to understand the results of my research. Thanks also to Dr. K. Loughlin and Dr. D. Al-Harbi,the two other members of the thesis committee. Dr. Loughlin was always available for discussions. I do not forget the technicians Mr. P. McQue and Mr. J. Chapman, whose suggestions helped me to resolve some considerable difficulties during the setting-up of the apparatus. Dr. Zakri, the Chairman of the Chemical Engineering Department did his best to help in certain personal matters. I thank him too.

I must also send my thanks to these people I met on the highway.People,whose faces and names I do not remember now, but they helped because somehow they

know that on the road of Life there is no 'here', nor any 'there'.There is just the 'going' and the 'coming'.And that to help a fellow traveler on the road is perhaps the only worthwhile thing.To these people I send my thanks and blessings. Above all, my thanks go to my wife, whose patience and love made everything possible, and to my mother, whose sacrifice and foresight allowed me to continue for higher studies. I thank the few people whose friendship here at the University, made life bearable. Finally, the assistanceship offered by the University of Petroleum & Minerals is gratefully acknowledged.

CHAPTER ONE

INTRODUCTION

The adsorption of organic compounds on activated carbon has been studied extensively for years. Although activated carbon is a good adsorbent for organic compounds, the adsorption bond between the surface and the adsorbate is often so strong that desorption is difficult and complete regeneration is usually unsuccessful. This limits the use of activated carbon as an adsorbent for purifying certain industrial waste waters.

With the advent of macroreticular resins regeneration presented less problems due to the nature of the weak intermolecular forces involved. Thus, by selecting an appropriate organic solvent the resin can be easily regenerated. The XAD resins are cation-exchange catalysts and are in the form of small beads.Many of them are used as acid catalysts for liquid phase reactions. The most common formulation is styrene, cross-linked with divinyl benzene. The compound is then sulfonated. The effective pore radius in these materials is very fine, so that reactions tend to be diffusion-limited.

This can be substantially improved by preparing a so-called *macro-reticular structure* which has a more open set of pores. The structure of phenol,2,4 DPCA acid and the resin are shown below.

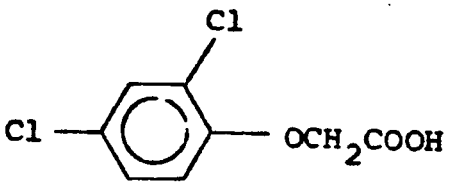

2.4 dichlorophenoxyacetic acid

Amberlite Resin

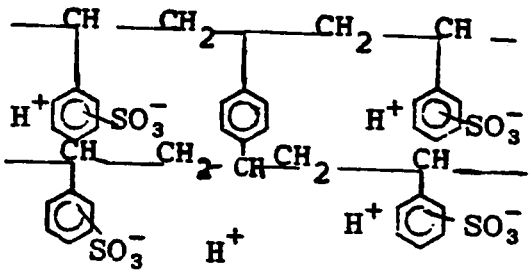

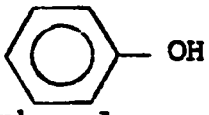

phenol

Only a few studies have been made in which macroreticular resins were used as adsorbent. The advent of these resins is relatively recent, and this might explain the lack of enough study in this area. Among the early researchers in this branch were Gustafson et al.(1) who studied the adsorption of a number of organic compounds from aqueous solutions on Amberlite resins XAD-1,XAD-2 and XAD-3.Further investigations by Paleos(2) involved the adsorption of organic species onto XAD-6 and XAD-7.

Phenol and 2,4 dichlorophenoxyacetic acid, henceforth referred as DCPA acid, have been chosen for investigation of their adsorption properties because they are typical organic compounds to be found in industrial wastewaters. DCPA acid is a by-

product in the manufacture of pesticides. XAD-7 resin is an Amberlite resin, easily regenerated, relatively cheap, produced by Rohm and Haas.

It must be pointed out that the above-mentionned researchers studied mainly the adsorption at equilibrium for a limited range of concentration. The unsteady state adsorption of organics on macroreticular resins does not appear to have been reported in the literature.

The DCPA acid was obtained from the Fluka Chemicals Co.(W.Germany) and was 99.9 percent pure. The phenol was obtained from the Poole Chemical Co. (England) Dept. and was also guaranteed to be 99.99 percent pure. Five liters of XAD-7 were imported and they were used after having been washed. The resin was then dried in an oven at 150 to 200 degrees centigrade for 48 hours. The dried resin was kept in stoppered flasks.

In this work the adsorption of the compounds was investigated under steady flow conditions by placing the XAD-7 in a packed-bed. Breakthrough curves were obtained for various flow rates and initial

concentrations of the solutions.Batch studies were carried out to determine equilibrium isotherms at 298,313 and 323 degrees Kelvin.

In the batch studies, the shaker-bath used had a temperature controller which allowed a temperature variation of about one degree centigrade from the set temperature. The concentrations were measured by a Beckman ultra-violet spectrophotometer.

The heat of adsorption was calculated by two different methods. First, the isosteric heat of adsorption was calculated via the Hersch equation. Then the virial equation was used to find the Henry's constants which was then inserted in the Van't Hoff equation to calculate the heat of adsorption.

The continuous flow adsorption studies were carried out using four beds of different length connected together and packed uniformly with a known weight of the resin. T-connections allowed samples to be taken for analysis.The peristaltic pump was used to pass the solution through the bed. More details of the experimental work are presented in Chapter Five.

CHAPTER TWO

RESEARCH OBJECTIVES

The aim of this research is to investigate the adsorption of dissolved phenol and DPCA acid onto XAD-7. The heat of adsorption of both compounds is calculated. Finally the behaviour of a mixture of both compounds upon adsorption at equilibrium is investigated.

To achieve these goals,the research was divided into several stages:

(1) Batch studies to generate equilibrium isotherms at 298,313 and 323 degrees Kelvin for single component species.

(2) Batch studies to generate equilibrium isotherms for multicomponent mixtures at room temperature.

(3) Continuous packed-bed adsorption studies to obtain experimental breakthrough curves at different operating conditions for both aqueous solutions of the two species.

(4) Evaluation of mass transfer coefficients and rates of adsorption using different rate

equations.

(5) Prediction of theoretical breakthrough curves by simulating three different models.

(6) Experimental measurements of the regeneration curves for both components.

CHAPTER THREE

LITERATURE SURVEY

In order to predict the performance of a packed bed system, two types of information are required.First the relationship between the adsorbate composition and the concentration of the solution (i.e. the equilibrium isotherm) needs to be established. Second, the mechanism governing the rate of adsorption of the adsorbate onto the adsorbent is required. In this chapter a brief review of the literature about a few of the different types of isotherms and the different types of rate limiting mechanisms is presented. In the end, some brief definitions of the heat of adsorption are included.

3.1 EQUILIBRIUM ISOTHERMS

As mentionned before,not only a model for the adsorption of the species on the resin is needed,but also the equilibrium isotherms giving the distribution of the adsorbate molecules between the fluid and the solid phases.In general,equilibrium isotherms are classified into four different categories. These are: 1) Irreversible, 2)

Unfavorable, 3) Linear and 4) Favorable. Brunauer et al.(3) considered that there are five principal forms of equilibrium isotherm as shown in Fig 1. Type I is classified as the Langmuir type which is characterised by a monotonic approach to a limiting adsorption capacity corresponding to a complete monolayer.Type II describes the formation of a multilayer of adsorbate molecules on the solid surface.This type of isotherm is known as the B.E.T(Brunauer,Emmet,Teller).Type III is rare because it suggests an unlimited uptake by the adsorbent. Types IV and V reflect capillary condensation phenomena in that they level off before the saturation pressure is reached and may also show hysteresis effects.

3.1.1 Linear Isotherm

A simple, but important, isotherm is the linear one. Here the plot of the uptake vs the concentration gives a straight line. The general formula is

$$q = K*C \qquad 3.1$$

where

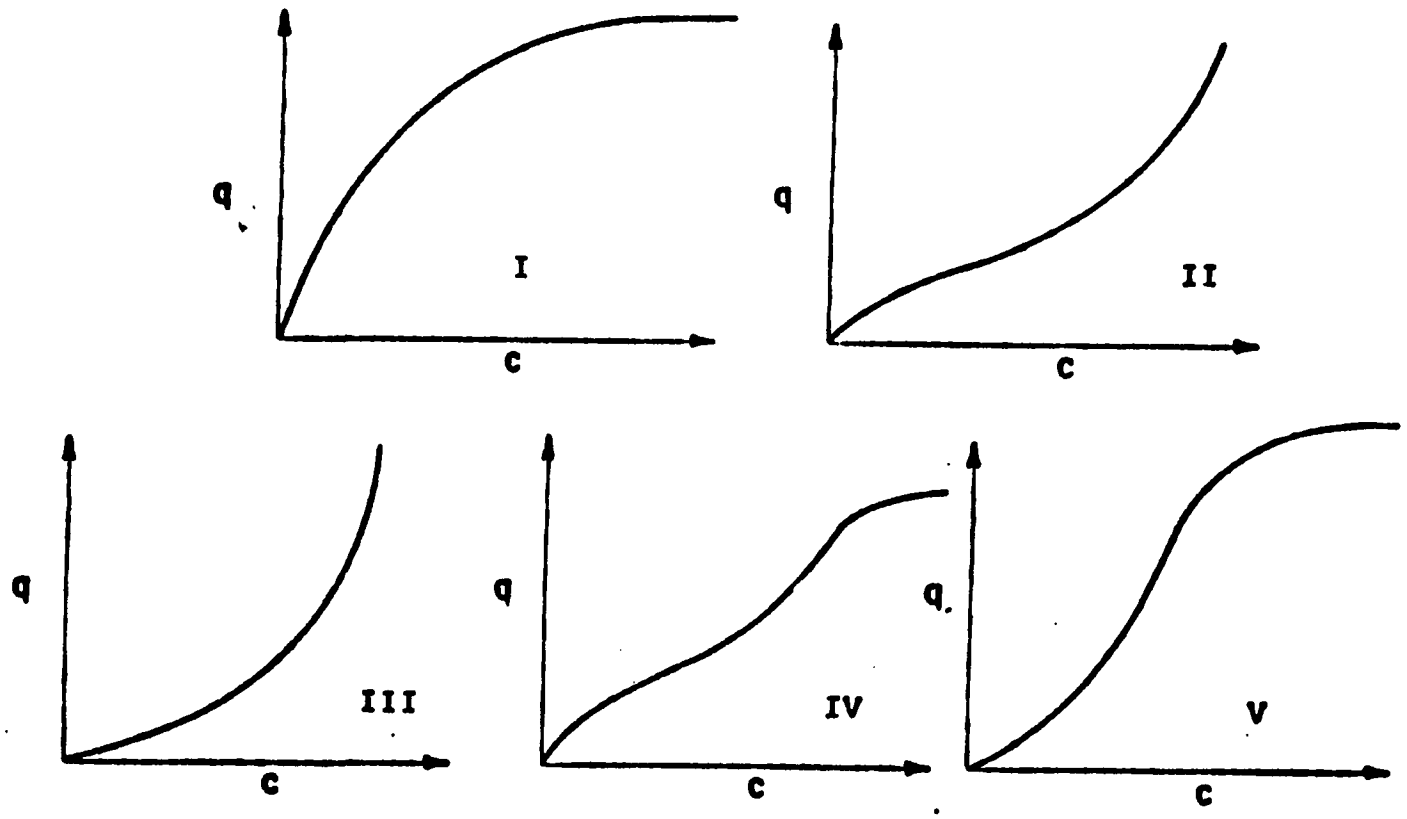

Fig.1 : Brunauer et al's Classification of Adsorption Equilibrium Isotherms.

q = uptake, the amount of adsorbate on the solid phase, and

C = the concentration of the solution

At very low concentration almost all isotherms yield a linear relationship between the uptake and the concentration. The proportionality constant is called the *Henry's constant*. More is said about the Henry's constant later.

3.1.2 Langmuir Isotherm(4)

In deriving this model,the following assumptions are used: 1) all sites of the adsorbent have the same activity for adsorption. 2) There is no interaction between the adsorbed molecules. 3)All the adsorption occurs by the same mechanism. 4) Each adsorbed complex has the same structure. 5) The extent of adsorption is restricted to a monolayer.

For the derivation of the Langmuir model, the rate of adsorption is taken to be proportional to the uncovered fraction of the surface and the gas pressure,or

$$r_a = k_1 P(1 - \theta) \qquad (3.2)$$

where

θ = fraction covered by adsorbed molecules

The desorption rate is equal to the fraction of covered surface, or

$$r_d = k_2 \theta \qquad (3.3)$$

At equilibrium, the rate of adsorption is equal to the rate of desorption, and the fraction covered is given by

$$\theta = \frac{bP}{1 + bP} \qquad (3.4)$$

$$b = k_1/k_2$$

The fraction covered can be replaced by V/V_m, where V_m is the volume of gas adsorbed per gram of solid at the monolayer point and V is the volume adsorbed. Thus

$$V=V_m bP/(1+bP) \qquad 3.5$$

For a system using different notation like C for the concentration, q for the uptake, Q_m for the maximum capacity of the solid and K' as the equilibrium constant, the Langmuir equation becomes

$$q = Q_m K'C/(1 + K'C) \qquad 3.6$$

At low pressure or concentration, the equation becomes linear

$$V=V_m bP \qquad \text{or} \qquad 3.7$$

$$q=Q_m K'C \qquad 3.8$$

At high pressure or concentration, V,q approach the limiting values V_m,Q_m respectively.

In testing the equilibrium data,the Langmuir equation can be linearized as follows,

$$P/V = 1/bV_m + P/V_m \qquad 3.9$$

$$C/q = 1/K'Q_m + C/Q_m \qquad 3.10$$

A plot of C/q versus C should give a straight line and the two constants Q_m and K' can be evaluated from the slope and the intercept.

3.1.3 BET Isotherm

Brunauer,Emmet and Teller(3) extended the Langmuir

approach to multilayer adsorption.The basic assumption for this isotherm is that the Langmuir equation applies to each layer with the exception that the heat of adsorption for the first layer may be different from that of the succeeding layers.The heat of adsorption for the succeeding layers is equal to the heat of condensation of the adsorbate.The B.E.T equation is written as

$$\frac{P}{V(P_0 - P)} = \frac{1}{V_m C'} + \frac{(C'-1)P}{C'V_m P_0} \qquad 3.11$$

where

P = pressure

V_m = volume of adsorbate at saturation point

V = volume of adsorbate

P_0 = saturation pressure

C' = constant for a particular gas-solid system

A plot of $P/V(P_0-P)$ vs. P/P_0 should give a straight line with a slope of

$$\text{slope} = \frac{C' - 1}{V_m C'} \qquad 3.12$$

and an intercept of

$$I = \frac{1}{V_m C'} \qquad 3.13$$

The volume of adsorbed gas corresponding to a monolayer can be readily obtained by using equations 3.12 and 3.13.The result is

$$V_m = \frac{1}{\text{slope} + I} \qquad 3.14$$

The volume V_m can be easily converted to the number of molecules adsorbed. The B.E.T equation is used mainly for surface area measurement. The advantage of the method lies in the fact that only two data points are enough to calculate the area. If the term $V_m C$ is large enough, only one data point is required.

3.1.4 Freundlich Isotherm

The use of this isotherm is limited to a small concentration range. The main objection to it is that the curve increases monotonously and no ultimate uptake value is reached. Also the equation does not

reduce to the Henry's Law equation unless for the special case when n is equal to one. The equation is

$$q = m\, C^{1/n} \qquad 3.15$$

where

q = amount adsorbed per unit weight of adsorbent.

C = adsorbate concentration.

m and n are experimental constants to be determined.

The Freundlich equation can be linearized as

$$\ln q = 1/n \ln C + \ln m \qquad 3.16$$

A plot of ln q versus ln C gives a straight line with a slope of 1/n and an intercept of ln m.

3.2 RATE LIMITING MECHANISMS

The rate of adsorption of a species onto an adsorbent is controlled by one or a combination of the following mechanisms:

(1) Mass-transfer through the external film surrounding the particle surface.

(2) Adsorption on the particle surface.

(3) Internal mass transfer through the fluid phase

occupying the pores of the adsorbent.

(4) Diffusion of the adsorbate molecules along the surfaces of the pores.

Usually the performance of a packed-bed adsorber is either described by empirical correlation of the data or through a mathematical analysis coupled with a reasonable rate controlling mechanism. Sometimes both techniques are used. However, the mechanistic approach assumptions are more frequently used.

3.2.1 EMPIRICAL APPROACH TO THE CORRELATION OF ADSORPTION DATA

Engell and Coull(5) measured the breakthrough curves for gaseous chloroform adsorbed on activated carbon.They approximated the shape of the breakthrough curves by the error function.Their empirical correlation is given as

$$\phi = 1 - 0.5\left(1 + \frac{2}{\sqrt{\pi}} \int_0^{\frac{t-a}{b}} e^{-Z^2}\, dZ\right) \qquad 3.17$$

where

$$a = C_1\left[\frac{C_o G}{A}\right]^n + C_2$$

$$b = C_3\left[\frac{C_o G}{A}\right]^m + C_4$$

$\phi = C/C_o$

C_o = inlet concentration

C = outlet concentration

t = time from the beginning of the run

z = bed height

C_1, C_2, C_3, C_4, n, m are constants characteristic to the adsorption system.

Another empirical approach is the Mass Transfer Zone (MTZ) technique described by Barry (6) who assumed the rate of adsorption on the surface limiting. Simply speaking, he declared that the length of the breakthrough curves is a measure of the rate of adsorption. The MTZ length is defined as

$$L_{MTZ} = Z \left[\frac{(t_S - t_B)}{t_S - (1-E)(t_S - t_B)} \right] \qquad 3.18$$

where

L_{MTZ} = length of the mass transfer zone

z = bed length

t_s = saturation time

t_B = breakpoint time, time at which the exit concentration reaches some defined measurable amount

E = fraction of the MTZ not loaded with adsorbate

The MTZ length is determined experimentally and is correlated as a function of the adsorption variables such as adsorbent size, composition of inlet fluid, flow rate, fluid properties, etc. This approach is restricted to 'constant pattern behaviour' systems.

3.3 USE OF MECHANISMS TO CORRELATE THE ADSORPTION DATA

In this approach, only one or more of the resistances are assumed to control the rate of adsorption. The equations describing the controlling resistance are formulated. The differential mass balance equation is then integrated with the rate equation to produce the breakthrough curves which can be compared with experimental data to test the validity of the model.

3.3.1 External diffusion controlling

Hougen and Marshall(7) in 1946 assumed that the

mass transfer rate was controlled by the diffusion through the film surrounding the particle. They also assumed a linear relationship for adsorption equilibrium for the system. This model will apply for cases where the fluid contents of the bed is small compared to the total volume of the fluid throughput. Klotz(8) also assumed the same limiting mechanism,and expressed the adsorption rate in terms of the bulk concentration.

3.3.2 Internal Mass Transfer Controlling

Antonson(9) dealt with the case where internal mass transfer was controlling the adsorption rate.He studied the adsorption of ethane in molecular sieves and assumed a non-linear equilibrium relationship. He solved the problem numerically using an explicit finite difference technique. He generated the breakthrough curves for several values of the intraparticle diffusion coefficient, and by superimposing the theoretical breakthrough curves to the experimental ones, obtained the best fit value of the diffusion coefficient. With this method reasonably accurate values of diffusivities can be predicted

provided that the equilibrium data can be fitted with a Langmuir-type isotherm.

Hasanain(10) extended the work of Antonson to cases where the equilibrium isotherm can be fitted by the more generalized three-parameter isotherm equation of Radke and Prausnitz(11). His approach, being more flexible, is a definite improvement over Antonson's approach.

3.3.3 Combination of Internal and External Mass Transfer Resistances

The combination of these two resistances was modelled by Eagleton and Bliss(12) who correlated the external and internal mass transfer coefficients for the adsorption of water vapor from air over packed-beds of alumina,florite and silica gel.

Shortly after,Rosen(13) published an analytical solution to the mass transfer equation for a packed-bed when both film resistance and intraparticle diffusion are controlling.He did not assume any mechanism a priori.The main restrictions to his model were the assumption of a linear relationship for adsorption at equilibrium and the use of spherical

adsorbents.

3.3.4 Combination of External, Internal and Surface Reaction Resistances

The difficult analysis of this combination was carried out by Masamune and Smith(14).They tabulated the solutions of all possible combination of these resistances.In a later paper(15) they studied the adsorption of ethyl alcohol on silica gel.They modelled for the case when the internal diffusion and surface reaction were the only controlling steps.They evaluated the reaction constants from the equilibrium data and used it to generate a number of breakthrough curves for the different values of diffusivity.The generated curves were then superimposed on the experimental data to calculate the diffusion coefficients from the best fits. Unfortunately, the model is only applicable to linear isotherms.

3.3.5 Effect of Axial Dispersion

Lambaret(16) investigated the effect of axial dispersion coupled with an external mass transfer resistance and linear surface reaction. His equilibrium data were best fitted by a linear

isotherm. He solved the model numerically to generate the breakthrough curves for the adsorption of hydrocarbons on a fixed bed of activated carbon.

3.3.6 The Second Order Adsorption Reaction Controlling

Another resistance to mass transfer is the adsorption reaction on the surface. Thomas(17) studied this limiting mechanism for cation-exchange on resin, and found an analytical solution from which breakthrough curves could be generated. More is said about this topic in Chapter Four.

3.4 HEAT OF ADSORPTION

One of the advantages of using the resin over activated carbon for the removal of organic compounds from waste waters is the relative ease of regeneration. The resin-adsorbate bonds are physical or weak chemical bonds. Chemical bonds are strong and the heat of chemisorption is high compared to the heat of physical adsorption. So the magnitude of heat effects is an important criterion to differentiate between physical adsorption and chemisorption. The heat of adsorption of small molecules (CO, N_2) are typically in the order of 3 to 6 Kcal/mol. The

heat of adsorption may be expected to increase with the molecular weight. For chemisorption the heat is comparable to that of chemical reation, and is about 30 to 60 Kcal/mol. Sometimes values as high as 150 Kcal/mol may be experienced. However, chemisorption can occur with release of almost negligible heat.

Physical adsorption is always exothermic. For gas-solid systems physical adsorption brings about the condensation of the gas, and very often the heat of adsorption is very close to the heat of condensation of the gas. For liquid-solid systems the fluid is already in the liquid phase, but thermodynamics explain the exothermic character of physical adsorption. For a spontaneous process like adsorption to occur the free energy of the system must decrease. From the relationship $\Delta H = \Delta G + T\Delta S$, it is evident that ΔH is always negative if ΔS is negative. And in physical adsorption this is always the case because the adsorption brings about a more ordered configuration of molecules.

The heat of adsorption is also a property to characterize the degree of heterogeneity of the surface. If the surface is homogeneous, the

differential heat of adsorption will be constant.But with a heterogeneous surface the molecules will tend to adsorb on the most active sites first , then on the less active ones.So it may be expected that in general the heat of adsorption will decrease with surface coverage.But sometimes a maxima with coverage is observed because of the lateral interaction of the adsorbed molecules.

The heat of adsorption is referred to by these three terms:

(1) The *isothermal integral heat of adsorption.* This is the total heat attributed to the adsorption process from zero adsorbate loading to some final adsorbate loading at constant temperature.

(2) The *differential heat of adsorption.* This is the change in the integral heat of adsorption with a change in adsorbate loading.It is a function of coverage, temperature and concentration.

(3) The *isosteric heat of adsorption* . This is defined as

$$\Delta H = R \, (d \ln C / d(1/T))_q \qquad 3.19$$

where R is the ideal gas constant, C and T are the concentration and temperature respectively. When ln C is plotted against 1/T a straight line should be obtained with a slope of $\Delta H/R$. The heat of adsorption can then be calculated.

3.5 HENRY'S CONSTANT

The Henry's constant is an equilibrium constant between the the adsorbed phase and the fluid phase. It is defined as

$$K = \lim_{C \to 0} (q/C) \qquad 3.20$$

At very low values of C a plot of q vs C should give a straight line with a slope of K.

The following Van't Hoff relation derived from thermodynamics represents the functionality of the Henry's constant with temperature.

$$K = K_0 \exp (q_0/RT) \qquad 3.21$$

where

q_0 = heat of adsorption at zero uptake

R = ideal gas constant

K_0 = preexponential constant

K_0 is primarily related to the change in entropy of adsorbate. A plot of ln K v/s 1/T gives a straight line with a slope q_0/R.

Barrer and Lee(18) proposed a virial isotherm in terms of osmotic pressure to describe the adsorption phenomena which may be written as

$$C = q/K * \exp (A_1 q + A_2 q^2 + ... + A_i q^i) \quad 3.22$$

where

K = Henry's constant

A plot of ln C/q v/s q will give ln 1/K as the intercept. This is true for low concentrations. The Henry's constant found can be used in equation 3.21 to calculate the heat of adsorption.

CHAPTER FOUR

THEORY

4.1 The Mathematical Model

In general, the fluid flow in a packed bed of adsorbent is described by the following equations:

1) Energy balances in solid and fluid phases

2) Equation of continuity

3) Equation of motion

4) Species balances for both solid and fluid phases

The following simplifying assumptions are made to reduce the number of equations:

1) Dilute adsorbate concentrations

2) Small pressure drops through the bed and plug flow velocity profiles

3) Cylindrical fixed bed with flow in the axial direction

4) Small amount of material is removed from the

fluid

5) One adsorbable compound in the fluid phase

6) Solid phase consists of spherical particles only

7) Negligible swelling or shrinking of the particle

The use of the first assumption eliminates the energy balance in both phases and thus the operation is considered isothermal. The equation of continuity and motion are eliminated via the use of the second and third assumptions, leaving only the material balance equations.

4.2 Fluid Phase Material Balance

To model the adsorption of a substance in a packed bed, a material balance is made over a differential element ΔZ in the fixed bed. The assumptions are: constant density, uniform velocity, and zero concentration of the adsorbate at the start of the experiment in the particles and the void spaces of the bed. Axial dispersion is assumed negligible. Then the material balance becomes

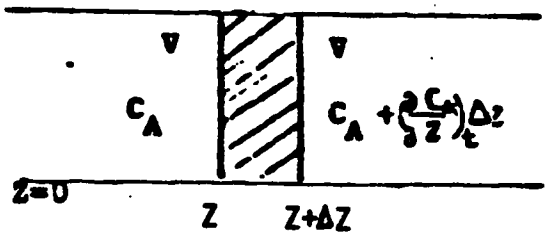

(A in) - (A out) = (A accumulated) 4.1

$$\text{Input} = S\,V\,C_A \qquad 4.2$$

$$\text{Output} = S\,V\left\{C_A + \left(\frac{\partial C_A}{\partial Z}\right)_t \Delta Z\right\} \qquad 4.3$$

$$\text{Accumulation} = S\,\rho_b\,\Delta Z\left(\frac{\partial q_A}{\partial t}\right)_Z + \varepsilon S\,\Delta Z\left(\frac{\partial C_A}{\partial t}\right)_Z \qquad 4.4$$

Substituting equations (4.2) to (4.4) into (4.1) gives

$$-S\,V\left(\frac{\partial C_A}{\partial Z}\right)_t \Delta Z = S\,\rho_b\,\Delta Z\left(\frac{\partial q_A}{\partial t}\right)_Z + \varepsilon S\,\Delta Z\left(\frac{\partial C_A}{\partial t}\right)_Z \qquad 4.5$$

Rearranging eq. (4.5) and dividing both sides by $S\,\rho_b\,\Delta Z$ gives

$$-\frac{V}{\rho_b}\left(\frac{\partial C_A}{\partial Z}\right)_t - \frac{\varepsilon}{\rho_b}\left(\frac{\partial C_A}{\partial t}\right)_Z = \left(\frac{\partial q_A}{\partial t}\right)_Z \qquad 4.6$$

As

$$F = S\,V = S\,\varepsilon\,v_Z \qquad 4.7$$

V may be substituted for in equation 4.6 to give

$$-\frac{F}{S\rho_b}\left(\frac{\partial C_A}{\partial Z}\right)_t - \frac{\varepsilon}{\rho_b}\left(\frac{\partial C_A}{\partial t}\right)_Z = \left(\frac{\partial q_A}{\partial t}\right)_Z \qquad 4.8$$

where

C_A = concentration of A in the fluid phase

q_A = concentration of A in the solid phase

S = cross-sectional area of the column

ρ_b = bulk density of the packed column

ε = porosity of the packed column

t = time

V = superficial velocity (flow velocity if column was empty)

F = flowrate

Equation 4.8 is the differential mass balance. It has to be coupled with an expression describing the rate of adsorption. The following briefly describes some of the adsorption rate expressions postulated in the literature.

4.3 Rate expressions for adsorption

The fact that the mass-transfer waves are S-shaped is evidence that there is mass transfer resistance. The greater the resistance, the longer is the wave. As the resistance to mass transfer decreases, the wave becomes shorter. The ideal case is when the

width of the breakthrough curve is zero(zero length). The following rate expressions have been postulated in the literature.

(a) The rate equation postulated by Klotz(8) is

$$r = \frac{K_k \varepsilon}{\rho_b} C \qquad 4.9$$

where

r = rate of adsorption, umoles/gm

K_K = mass transfer coefficient, hr^{-1}

C = fluid phase concentration

ρ_b = bulk density of the packed column

The primary assumption in the Klotz model is that the adsorbed phase will exert no "back pressure" against the bulk phase concentration and the component ceases to be removed when the adsorbate concentration on the solid reaches saturation.

(b) Overall fluid phase mass transfer rate expression,

$$r = \frac{K_F a_F \varepsilon}{\rho_b} (C-C^*) \qquad 4.10$$

where

$K_F a_F$ = overall mass transfer coefficient

C^* = equilibrium concentration at the solid surface

In this model the rate of adsorption is described as the result of a driving force between the bulk concentration and the equilibrium concentration of the adsorbed liquid phase. The difference in concentration between the bulk phase and the concentration at the surface is due to the resistance offered by the boundary layer surrounding the solid particle.

(c) Solid Glueckauf model(19)

The rate describes the resistance offered by the internal resistance.

$$r = K_p a_p (q^* - q) \qquad 4.11$$

where

$K_p a_p$ = internal mass transfer coefficient

q^* = adsorbate composition at the solid surface in equilibrium with the bulk concentration.

q = average adsorbate composition on the solid.

In this model the rate of adsorption is related to the driving force between the adsorbate composition at the solid surface in equilibrium with the bulk concentration and the average adsorbate composition.

(d) Solid phase Vermeulen model(20)

The rate expression is

$$r = K_V \left(\frac{q^{*2} - q^2}{2q} \right) \qquad 4.12$$

where

K_V = Overall mass transfer coefficient

q^* = adsorbate composition at the solid surface in equilibrium with the bulk concentration.

q = average adsorbate composition on the solid.

In this model the rate of adsorption is related to a non-linear driving force between the adsorbate composition at the solid surface in equilibrium with

the bulk concentration and the average adsorbate composition.

(e) Geser and Kostecki model(21)

The rate expression is

$$r = K_{GE} (Q_m - q) \qquad 4.13$$

where

K_{GE} = Overall mass transfer coefficient

Q_m = maximum capacity of the adsorbent.

In this model the rate of adsorption is related to the difference in the maximum capacity of the adsorbent and the adsorbate composition at the particle surface.

(f) Reversible Second Order Surface reaction model(17)

In this model the rate of adsorption is assumed to be proportional to the concentration in the bulk phase and to the maximum amount of adsorbate the solid can take. The rate of desorption is

proportional to the amount of adsorbate on the solid. The rate is defined as

$$r = k_a|C(Q_m - q) - q/K'| \qquad 4.14$$

where

k_a = adsorption rate constant, lit/umoles-hr

K' = adsorption equilibrium constant

Q_m = concentration corresponding to a complete monolayer on the solid.

(g) Irreversible second order surface reaction model

The rate is given as

$$r = K_I C\ (Q_m - q) \qquad 4.15$$

In this model the rate of adsorption is proportional to the Kinetic driving force and K_I is the corresponding 'kinetic coefficient', lit/umoles-hr.

4.4 Prediction of the breakthrough curves

The column concentration profiles can be predicted by the Thomas method(17) and the equilibrium data for the adsorbate-adsorbent system. In adsorption the

rate may be controlled by more than one mechanisms. But then, the solution becomes complicated. Thomas assumed only one limiting mechanism and that was the surface kinetics. His model was derived originally for ion-exchange, but Hiester and Vermeulen(22) showed it to be useful for cases where the rate-controlling steps other than surface kinetics applied. In this method, the differential mass balance equation along with the assumed rate expression for adsorption is normalized after transformation through appropriate dimensionless parameters. The following is a description of the procedure.

Beginning with eq. (4.8)

$$-\frac{F}{S\rho_b}\left(\frac{\partial C_A}{\partial Z}\right)_t - \frac{\varepsilon}{\rho_B}\left(\frac{\partial C_A}{\partial t}\right)_Z = \left(\frac{\partial q_A}{\partial t}\right)_Z$$

and rewriting it in terms of the following variables

$$\xi = \frac{k_a Z \rho_b Q_m}{\varepsilon V_Z} = \frac{k_a v \rho_b Q_m}{F} \quad \text{(bed length parameter)} \qquad 4.16$$

$$\tau = k_a\left(\frac{1}{K'} + C_{A0}\right)\left(t - \frac{Z}{V_Z}\right) \quad \text{(dimensioless time parameter)}$$

$$\bar{X} = \frac{C_A}{C_{A0}} \qquad 4.17$$

$$\bar{Q} = \frac{q_A}{q_{Am}} \qquad 4.18$$

$$4.19$$

Thus

$$Z, t \longrightarrow \xi, \tau$$

$$\left(\frac{\partial C_A}{\partial t}\right) = k_a\left(\frac{1}{K'} + C_{A0}\right)\left(\frac{\partial C_A}{\partial \tau}\right)_\xi \qquad 4.20$$

$$\left(\frac{\partial C_A}{\partial Z}\right) = \frac{k_a \rho_b Q_m}{\varepsilon V_Z}\left(\frac{\partial C_A}{\partial \xi}\right)_\tau - \frac{k_a}{V_Z}\left(\frac{1}{K'} + C_{A0}\right)\left(\frac{\partial C_A}{\partial \tau}\right)_\xi \qquad 4.21$$

$$\left(\frac{\partial q_A}{\partial t}\right) = k_a \left(\frac{1}{K'} + C_{A0}\right)\left(\frac{\partial q_A}{\partial t}\right) \qquad 4.22$$

where q_{A_∞} is the saturation capacity of the bed when the concentration of the solute is C_{AO}, and v is the volume of the packed bed. Upon substituting Q_m from the Langmuir equation(3.6)

$$q_{A_\infty} = \frac{K'Q_m C_{A0}}{1 + K'C_{A0}} \qquad 4.23$$

Equation (4.8) can be written in terms of the new dimensionless variables as

$$\left(\frac{\partial \bar{Q}}{\partial \bar{z}}\right)_\xi = -\left(\frac{\partial \bar{X}}{\partial \xi}\right)_\tau \qquad 4.24$$

The *Second-Order Surface Kinetics* is assumed to be the limiting mechanism. The rate of adsorption is given as

$$\left(\frac{\partial q_A}{\partial t}\right)_Z = k_a \left[C_A (Q_m - q_A) - \frac{1}{K'} q_A \right] \qquad 4.25$$

where

k_a is the rate constant for adsorption

C_A is the concentration of the adsorbate in the fluid

q_A is the concentration of adsorbate in the adsorbent

K' is the adsorption equilibrium constant, and

Q_m is the maximum capacity of the adsorbent Substitution of Q_m from the Langmuir equation into 4.25 gives

$$\frac{\partial (q_A/q_{A_\infty})}{\partial t} = k_a\left(\frac{1 + K'C_{A0}}{K'}\right)\left[\frac{C_A}{C_{A0}}\left(1 - \frac{q_A}{q_{A_\infty}}\right) - \frac{1}{1 + K'C_{A0}}\frac{q_A}{q_{A_\infty}}\left(1 - \frac{C_A}{C_{A_0}}\right)\right] \qquad 4.26$$

Dividing both sides by $k_a\left(\frac{1 + K'C_{A0}}{K'}\right)$ and defining

$$r^* = \frac{1}{1 + K'C_{A0}} \qquad 4.27$$

equation (4.26) becomes

$$\left(\frac{\partial \bar{Q}}{\partial \tau}\right)_\xi = \bar{X}\left(1 - \bar{Q}\right) - r^* \bar{Q}\left(1 - \bar{X}\right) \qquad 4.28$$

combining eqs. (4.24) and (4.28) gives

$$\left(\frac{\partial \bar{X}}{\partial \xi}\right)_\tau = -\bar{X}\left(1 - \bar{Q}\right) + r^* \bar{Q}\left(1 - \bar{X}\right) \qquad 4.29$$

When the bed is initially free of adsorbate, the boundary conditions are

$\bar{X} = 1$ at $\xi = 0$ for all τ 4.30

$\bar{Q} = 0$ at $\tau = 0$ for all ξ 4.31

A solution of the above set of equations of the fluid and solid phases was obtained by Thomas by using the methods of the Riemann function. The resulting solutions are

$$\bar{X} = \frac{C_A}{C_{A0}} = \frac{J(r^*\xi, \tau)}{J(r^*\xi, \tau) + [1 - J(\xi, r^*\tau)] \exp[(r^* - 1)(\tau - \xi)]} \quad 4.32$$

$$\bar{Q} = \frac{q_A}{q_{A0}} = \frac{1 - J(\tau, r^*\xi)}{J(r^*\xi, \tau) + [1 - J(\xi, r^*\tau)] \exp[(r^* - 1)(\tau - \xi)]} \quad 4.33$$

where the J function has been presented in graphical or tabulated forms in several references(22,23)

If the approach taken by Thomas is to be of general use, then other rate controlling mechanisms must be related to the above solution. When the *External Film Resistance* is controlling

$$\frac{\partial q}{\partial t} = \frac{k_f a_p \varepsilon}{\rho_b}(C_A - C_A^*) \quad 4.34$$

where C_A^* is the concentration of the fluid in equilibrium with the solid phase of concentration q_A. These are related by the equilibrium isotherm. At equilibrium the rate of adsorption is equal to zero, and

$$C_A = C_A^* \qquad 4.35$$

By substituting into eq.(4.26)

$$C_A^* = \frac{q_A}{q_{A\infty}}\left[\frac{r^* C_{A0}}{1 + (q_A/q_{A\infty})(r^* - 1)}\right] \qquad 4.36$$

Thus, upon writing eq.(4.34) and using the definition of C_A given by eq. (4.36), gives

$$\frac{\partial(q_A/q_{A\infty})}{\partial t} = \frac{K_F a_F C_{A0}\varepsilon}{\rho_b q_{A\infty}[1 + q_A/q_{A\infty}(r^* - 1)]}\left[\frac{C_A}{C_{A0}}(1 - q_A/q_{A\infty}) - r^* q_A/q_{A\infty}(1 - C_A/C_{A0})\right] \qquad 4.37$$

The above equation can be written in dimensionless form by using the variables

$$\xi = \frac{K_F a_F \varepsilon V}{F} \quad \text{(bed length parameter)} \qquad 4.38$$

$$\tau_E = \frac{K_F a_F C_{A0}\varepsilon}{\rho_b q_{A\infty}[1 + q_A/q_{A\infty}(r^* - 1)]}\left(t - \frac{z}{v_z}\right) \quad \text{(dimensionless time parameter)}$$

$$\bar{Q} = \frac{q_A}{q_{A\infty}} \qquad 4.39$$

$$\bar{X} = C/C_0 \qquad 4.40$$

$$4.41$$

Although τ_E contains the variable $q_A/q_{A\infty}$, Hiester and Vermeulen suggested that when the complete adsorption wave curves are fitted an average value can be used.

For r^* less than 1, $(q_A/q_{A\infty}) = 0.5$ 4.42

For r^* greater than 1, $q_A/q_{A\infty} = 1/(r^* + 1)$ 4.43

After normalising eq.(4.37), we obtain eqs. (4.28) and (4.29) and the boundary conditions given by (4.30) and (4.31). Thus the solutions are given by eqs (4.32) and (4.33), but with the dimensionless variables defined in equations 4.38 to 4.31.

The preceding approach can be extended to the case where the *Internal Particle Resistance* within the adsorbent is controlling. The rate of adsorbate uptake is expressed as

$$\frac{\partial q_A}{\partial t} = k_p a_p (q_A^* - q_A) \qquad 4.44$$

where q_A^* is the concentration of the solid in equilibrium with the coexisting fluid phase of concentration C_A, and is related to the fluid concentration by the equilibrium isotherm. According to the above equation, when the rate of adsorption is equal to zero, $q_A = q_A^*$. Substituting eq. (4.44) into eq. (4.26) gives

$$q_A^* = \frac{q_A C_A}{(1 - r^*) C_A + r^* C_{A0}} \qquad 4.45$$

To reduce the above expression to the form given by eqs. (4.28) and (4.29) the dimensionless parameters are defined as

$$\xi = \frac{K_p a_p \rho_b q_{A_-} v}{F C_{AO}} \qquad 4.46$$

$$\tau = \frac{K_p a_p}{\left[r^* + (C_R/C_{AO})(1 - r^*)\right]}\left(t - \frac{v\varepsilon_i}{F}\right) \qquad 4.47$$

$$\bar{Q} = \frac{q_A}{q_{A_-}} \qquad 4.48$$

$$\bar{X} = \frac{C_A}{C_{AO}} \qquad 4.49$$

Hiester and Vermeulen suggested that an average value can be used for the variable C_A/C_{AO}:

For r^* less than 1, $(C_A/C_{AO}) = 0.5$ 4.50

For r^* greater than 1, $C_A/C_{AO} = 1/(r^* + 1)$. 4.51

Again the solution is represented by eqs. (4.32) and (4.33).

CHAPTER FIVE

EQUIPMENT AND PROCEDURE

5.1 Equipment

In order to measure the concentration of the solutions, a Beckman DG-BT ultraviolet spectrophotometer was used. Use of a gas chromatograph was first suggested, but then was rejected due to vaporisation of the samples. The DPCA acid decomposes above 150 degrees centigrade at atmospheric pressure.

For the batch equilibrium studies, the solutions have to be shaken to eliminate the external diffusion limitations. For this purpose a Kolb (West Germany) shaker-bath was used. The shaker-bath is equipped with a temperature controller which can be set to a range of temperatures above room temperature. The controller allows the bath temperature to be controlled to within one degree centigrade. The intensity of the shaking can also be controlled.

To conduct the continuous-flow adsorption studies, four steel tubes of 1.1 cm. I.D. were connected together. T connections at the junctions of the tubes

allowed samples to be taken for analysis by means of a syringe. The experimental set-up is shown in Fig 2. To pass the solution through the packed bed, a peristaltic pump (Harvard Instrument, Model 1203) was used. The pump allowed reasonable control of the flow rate.The flow rate was calculated by measuring the volume of liquid pumped during a known time.

5.2 PROCEDURE

5.2.1 Calibration curves

Fixed quantities of DPCA acid and phenol were dissolved in known volumes of distilled water. The absorbance was read and plotted against the known concentrations. It should be noted that care must be taken that the cell used in the spectrophotometer does not adsorb the organics on its wall. Otherwise erroneous concentration readings may result. In our case we had to change the cells until a suitable one was found. The type used was a one centimeter plastic cell manufactured by Sargent Scientific Co. (USA). Different types of cells will give different absorbance readings for the same concentration. So the same cell has to be used throughout the experiment.

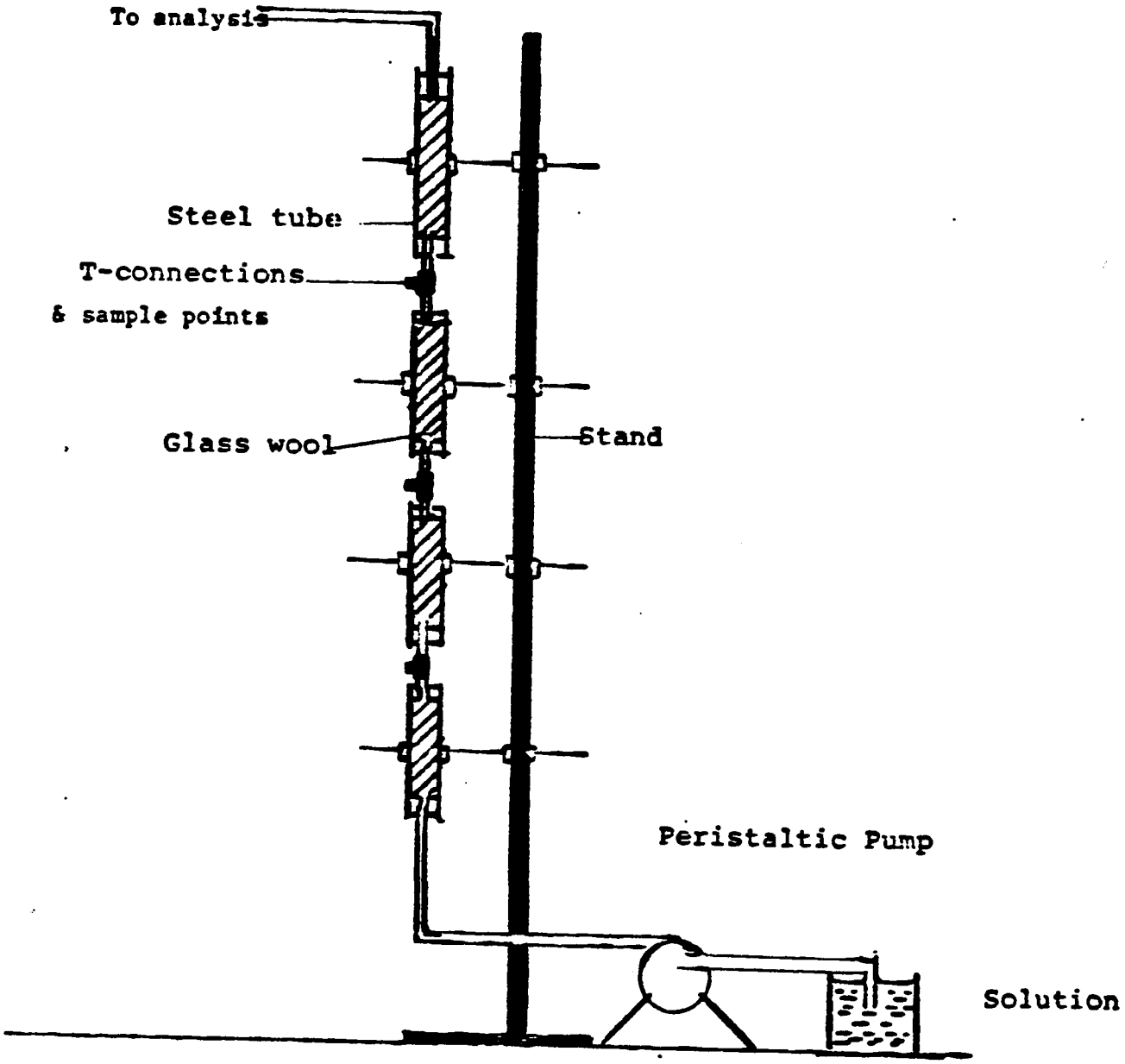

Fig 2 : Diagram of Experimental Set-up for the Column Experiments.

5.2.2 Batch Studies

The equilibrium isotherms were obtained by plotting the equilibrium vs the uptake of the resin. To this end, a small amount of resin (usually one gram) was contacted with a measured volume of known concentration (about 25 to 100 c.c) in a conical flask. The flask was placed in the shaker-bath heated to the desired temperature. The flask had to be firmly stoppered to prevent any spilling out of the solution. The mixture was then shaken for 24 hours with moderate shaking intensity. Then it was allowed to settle for another 24 hours. This time interval was considered sufficient for equilibrium to be established. Preliminary studies indicated that there was a negligible difference between the concentration of the solution measured three hours after contact and the concentration of the solution measured after a 24-hour contact. From the absorbance of the solution at equilibrium, the amount of organic compound in the solution could be calculated and, hence, the amount adsorbed by the resin.The uptake per unit weight of resin was then calculated.

5.2.3 Breakthrough Curves

The packed bed experiments were performed at room temperature. There was only a slight variation of about one degree due to the air-conditioning system. The four lengths of each bed were carefully filled with the resin so as to have a uniform density bed. Glass wool was inserted at the inlet and outlet of each length to eliminate end effects and to prevent entrainment of the resin out of the bed length. In order to find the lag time at each sample point, the volume between the pump inlet and the points at which samples were taken for analysis was measured. So knowing the flowrate, the lag time could be calculated.

The data were obtained by taking samples from four different points of the bed at different time intervals for analysis. By plotting the concentration of the solution vs time the breakthrough curves were obtained.

The bed was regenerated at saturation, i.e, when the inlet concentration equalled the outlet concentration. The regeneration curves were obtained

by passing pure water at the same rate as for adsorption and measuring the concentration along the bed length as described above.

5.2.4 Laboratory preparation of the Resin

In order to prepare the resin surface for the experimental work, it was necessary to remove the impurities from the resin surface. To accomplish this a suitable organic solvent had to be used. Since ethanol was abundantly available in the laboratory, it was used to wash the resin. The recommended procedure is to wash the resin, first in four times its volume of water then in four times its volume of methanol and last in four volumes of water again. In this experiment, ten times the volume of the resin was used in all cases. The resin was then dried in a fanned oven for about 48 hours at 200 degrees C,after which it was kept in stoppered flasks.

This procedure was followed to regenerate the resin after each use to ensure the complete removal of organic material from the resin.

CHAPTER SIX

RESULTS AND DISCUSSIONS

6.1 CALIBRATION CURVES

In order to determine the concentration of the components in a solution, a Beckman ultra-violet spectrophotometer was used. DCPA acid and phenol absorb U.V rays at 282 μm and 271 μm respectively. Standard solutions of both compounds were prepared and the absorbance read at these wavelengths.The absorbance was then plotted versus the concentration to obtain the calibration curves. The plots are shown in Fig 3 and Fig 4 for phenol and DPCA acid respectively. The relationship between the concentration of the pure components and the absorbance could be written down as

$$C_{acid} = 560 * \text{absorbance at } 282\ \mu m \qquad (6.1)$$

$$C_{phenol} = 656 * \text{absorbance at } 271\ \mu m \qquad (6.2)$$

The curves are valid for a range of 0 to about 1000 micromoles per liter, but for this study only a

range of 0 to 300 micromoles per liter, corresponding to the usual concentrations in waste waters is used.

For the mixtures, the concentration of the individual components has to be found. If one assumes that over the low concentration range the absorbance of phenol and the acid are additive ,the following relationships can be established:

$$A_{271} = C_{acid}(S_{acid})_{271} + C_{phenol}(S_{phenol})_{271} \quad (6.3)$$

$$A_{282} = C_{acid}(S_{acid})_{282} + C_{phenol}(S_{phenol})_{282} \quad (6.4)$$

where

A_{271} = absorbance at 271 μm

A_{282} = absorbance at 282 μm

$(S_{acid})_{271}$ = slope of calibration curve of acid at 271 μm

$(S_{acid})_{282}$ = slope of calibration curve of acid at 282 μm

$(S_{phenol})_{271}$ = slope of calibration curve of phenol at 271 μm

$(S_{phenol})_{282}$ = slope of calibration curve of phenol at 282 μm

The slopes of the curves can be evaluated from Figs 3 and 4. They have been found to be

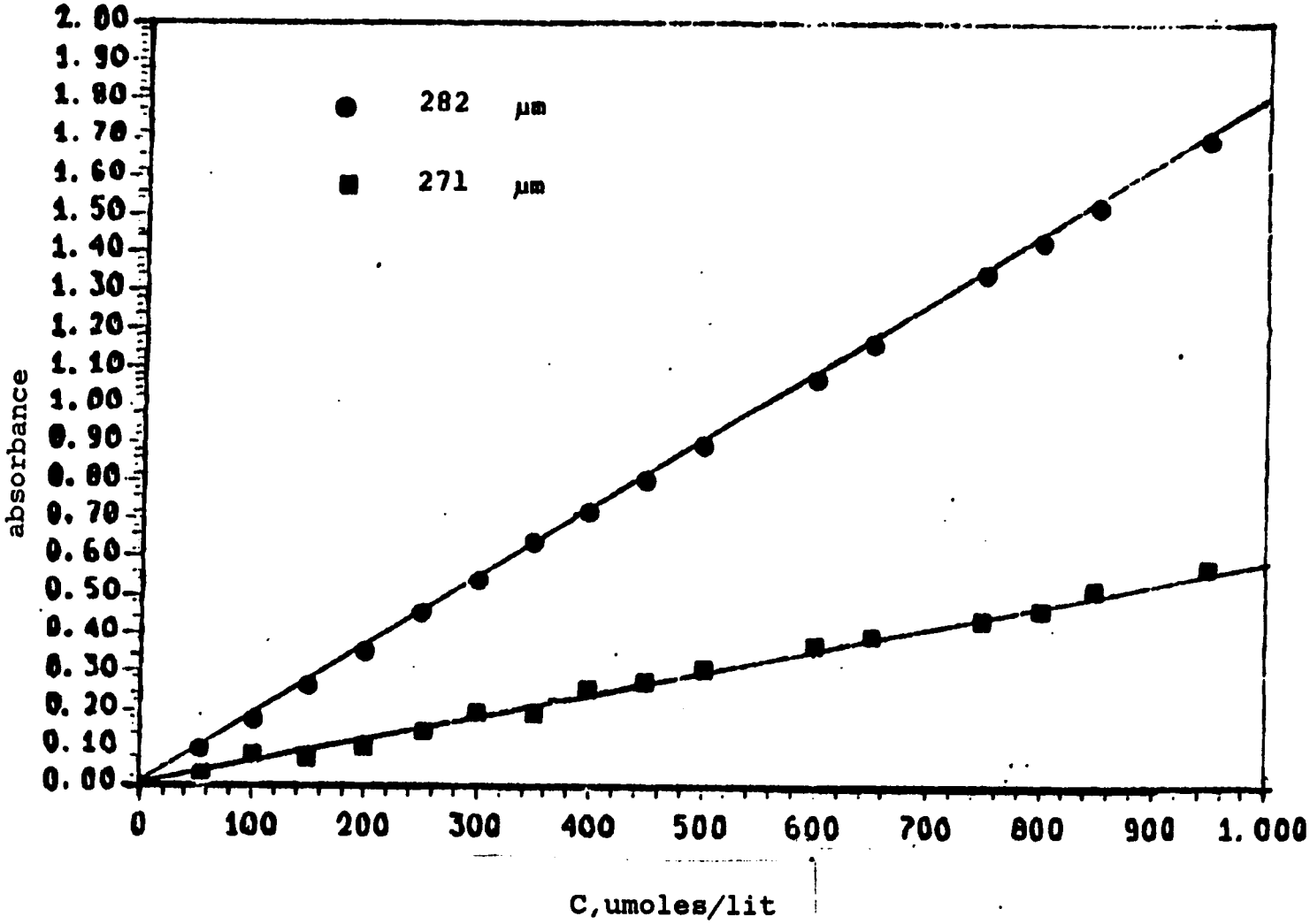

Fig 3 : Calibration Curve: Absorbance vs DPCA Acid concentration.

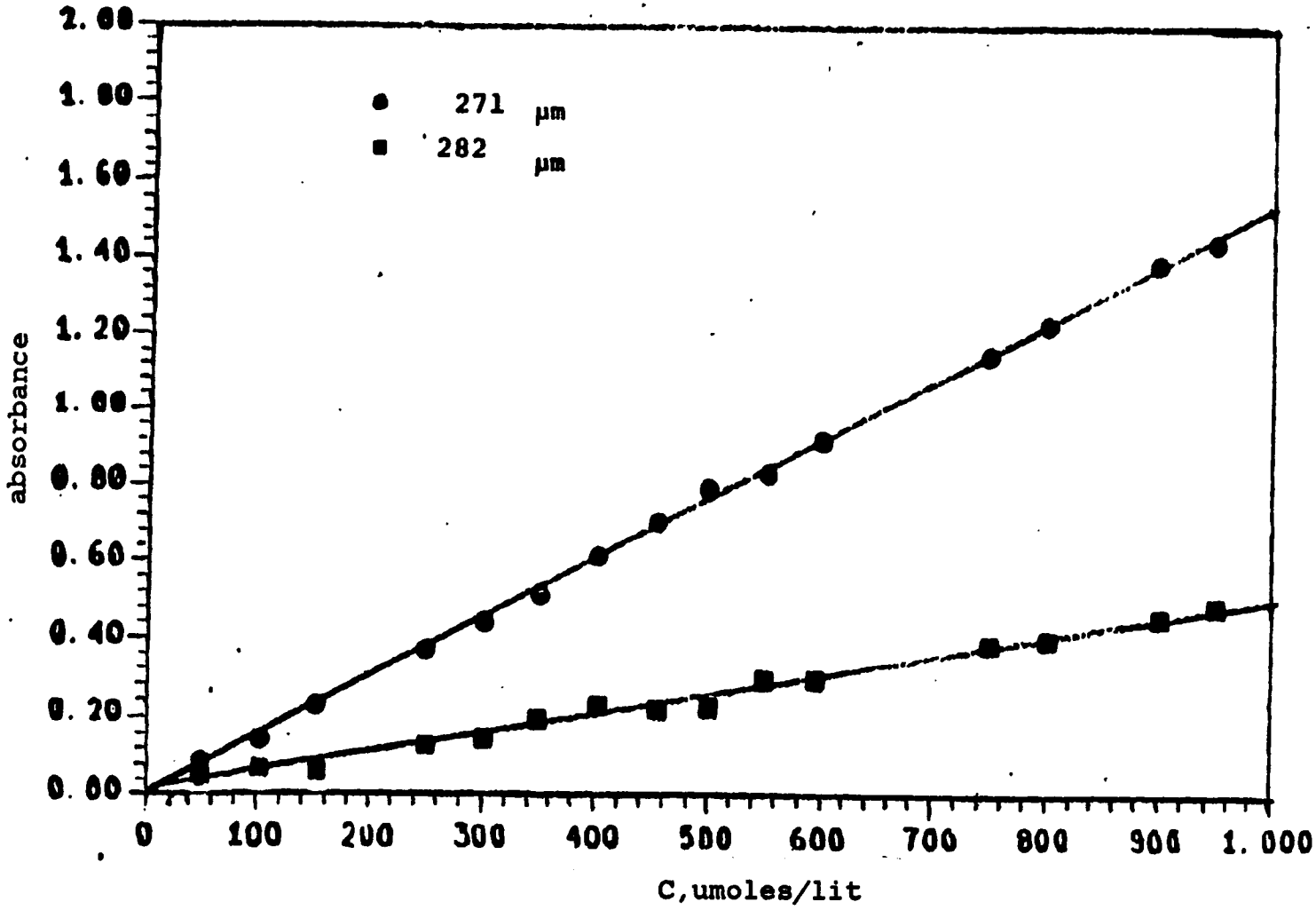

Fig 4 : Calibration Curve: Absorbance vs phenol concentration.

$(S_{acid})_{271}$ = 0.000588 (lit/umoles)

$(S_{acid})_{282}$ = 0.001786 (lit/umoles)

$(S_{phenol})_{271}$ = 0.001524 (lit/umoles)

$(S_{phenol})_{282}$ = 0.000501 (lit/umoles)

The individual concentration of C_{acid} and C_{phenol} are obtained by solving the above equations.

6.2 EQUILIBRIUM ISOTHERMS

Equilibrium isotherms for phenol and DPCA acid were measured at 298, 313 and 323 degrees Kelvin. The following procedure was followed. Known amounts of the XAD-7 resin were shaken in measured volumes of standard solutions for 48 hours.The solutions were analysed and the equilibrium concentration read.The uptake of adsorbate in equilibrium with the solution can be easily calculated. A sample of the calculations is shown in Appendix A, Sec A.1.

It should be noted that for the case under study, equilibrium was reached very quickly.Samples analysed

after a three-hour contact gave the same results 48 hours later. Long contact and too severe shaking may cause spalling of the resin.Thus, a sort of colloidal solution may form and higher absorbance readings may result. However, moderate shaking for 24 hours followed by settling for another 24 hours resolved the problem.

6.2.1 Phenol Equilibrium Adsorption

Table 1 shows the data obtained for the batch equilibrium adsorption of phenol on XAD-7 at three different temperatures. The data are plotted as phenol uptake versus concentration for the three temperatures in Fig. 5. The data are correlated with the Langmuir and the Freundlich models. The Langmuir constants are determined from a plot of 1/q vs 1/C as discussed in Sec. 3.1.1.

Table 2 shows the values of the Langmuir constants at the three temperatures.

Table 1: Data for equilibrium adsorption of phenol on XAD-7 resin at 25,40,50°C

25 °C		40 °C		50°C	
C	q	C	q	C	q
25	5.6	35	4	40	2.8
33	7.6	50	6	60	4
42	8.8	63	8	100	7
52	12.8	77	9.8	120	8
58	16.2	85	12	150	10.8
67	18	98	11.8	163	12
72	20	105	14	180	12.4
73	20.5	118	16	210	16
77	20	120	16.2	250	18
78	21.5	150	20.4	260	18.2
79	21	170	23.6		
87	24.8	180	12.4		
93	26	220	27.4		
98	26	260	28		
103	29.8				
105	30.6				
128	35				
150	38				
165	38.2				
177	50				
197	51.8				
212	54				

C in μmoles/liter

q in μmoles/gram

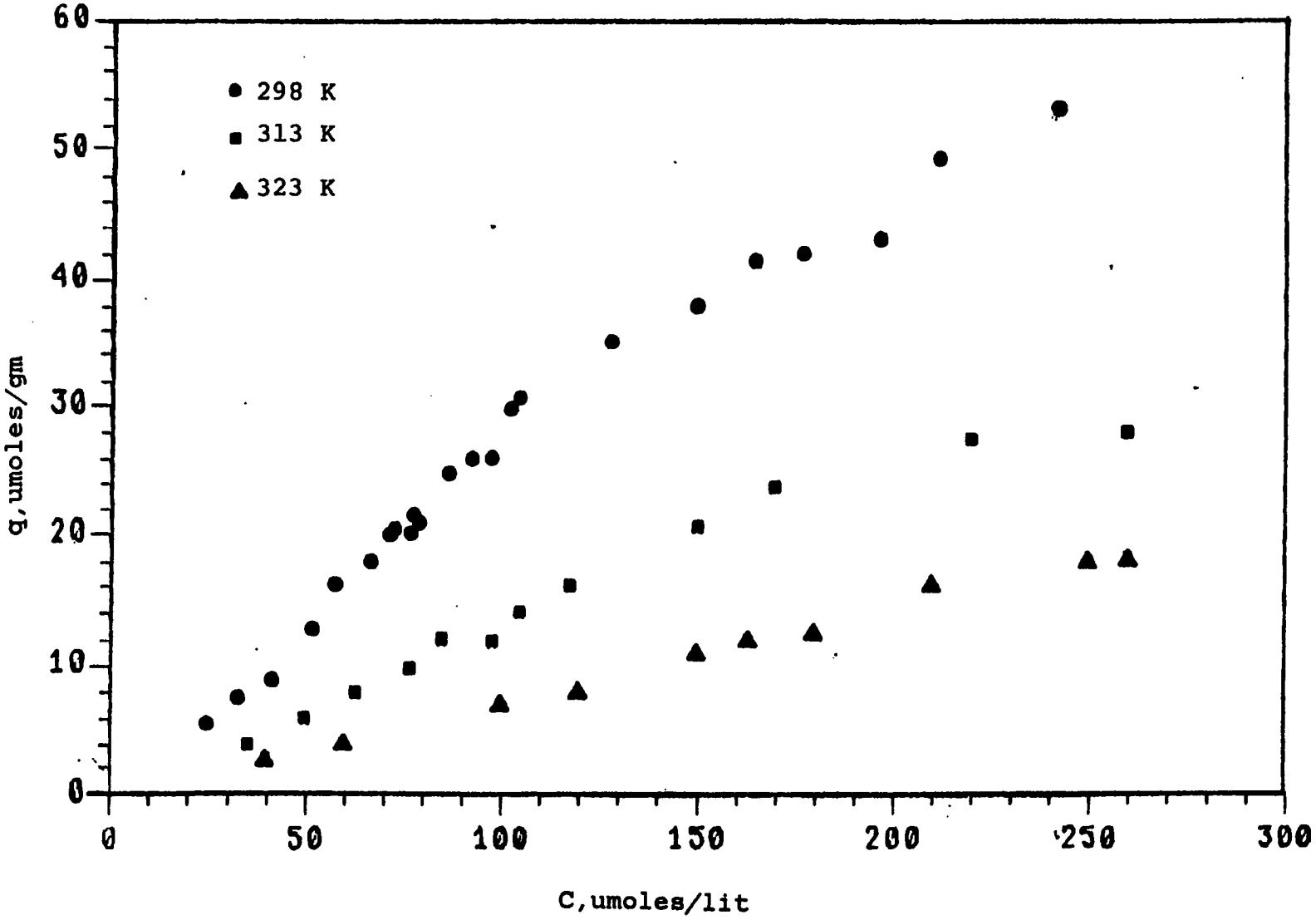

Fig 5 : Equilibrium Isotherms of Phenol at 298,313 and 323 K.

Table 2: Langmuir constants for adsorption of phenol

T(K)	Q_m	$K'*10^5$	$K=K'Q_m$
298	170	186.5	0.317
313	155	100.0	0.155
323	150	50.0	0.075

Q_m in micromoles/gram

K' in lit/μmole

Temperature T in degree Kelvin

K is the Henry's constant.

It must be emphasized, however, that obtaining a straight line is a necessary, but not a sufficient condition for the applicability of Langmuir theory to the data in question. The Langmuir model is compared to the equilibrium data at 298,313 and 323 degrees Kelvin in Figs 6, 7 and 8.

The data are also modelled using the Freundlich Isotherm and reasonable fits are obtained.

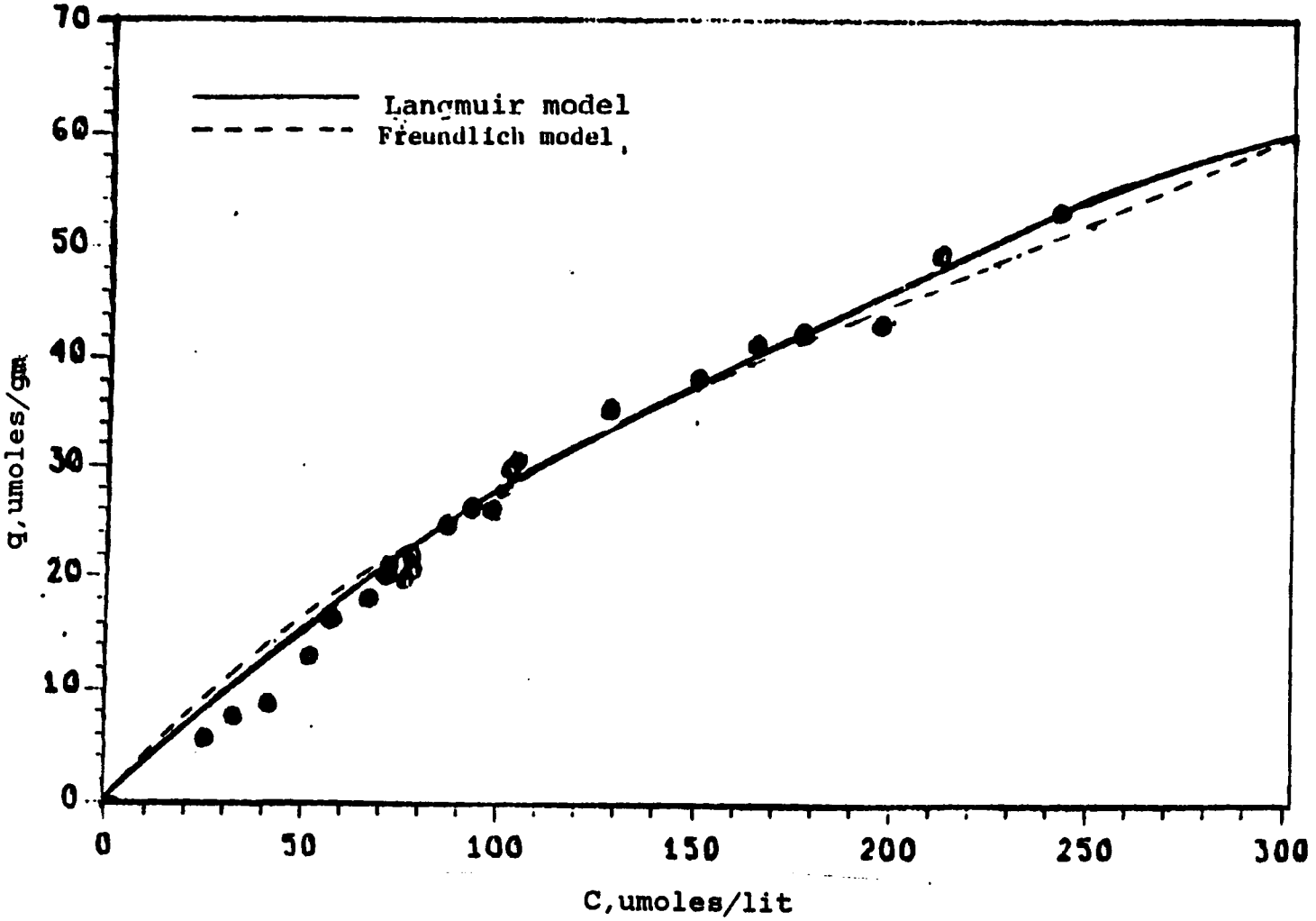

Fig 6 : Phenol Equilibrium Isotherm at 298 K.

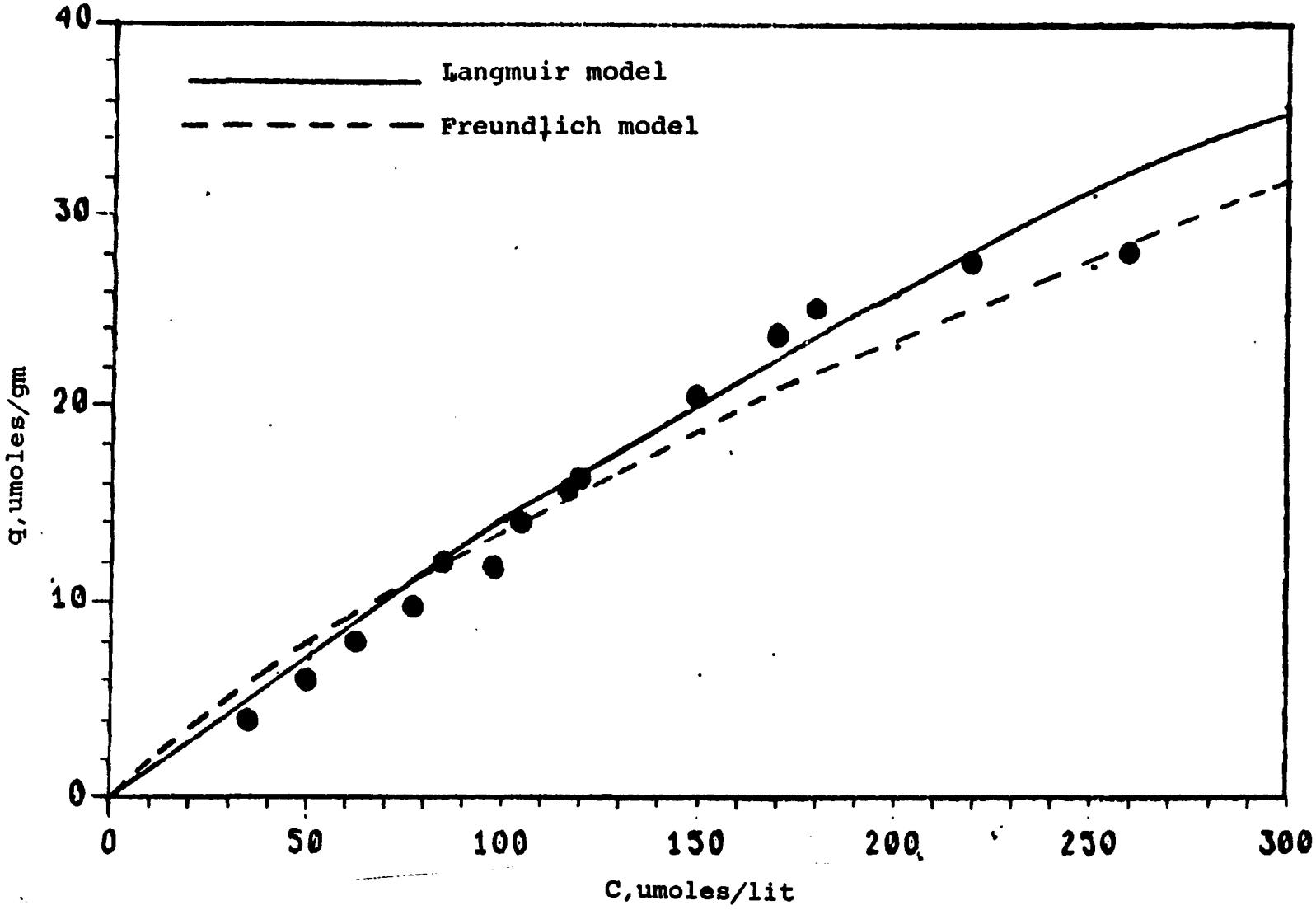

Fig 7 : Phenol Equilibrium Isotherm at 313 K.

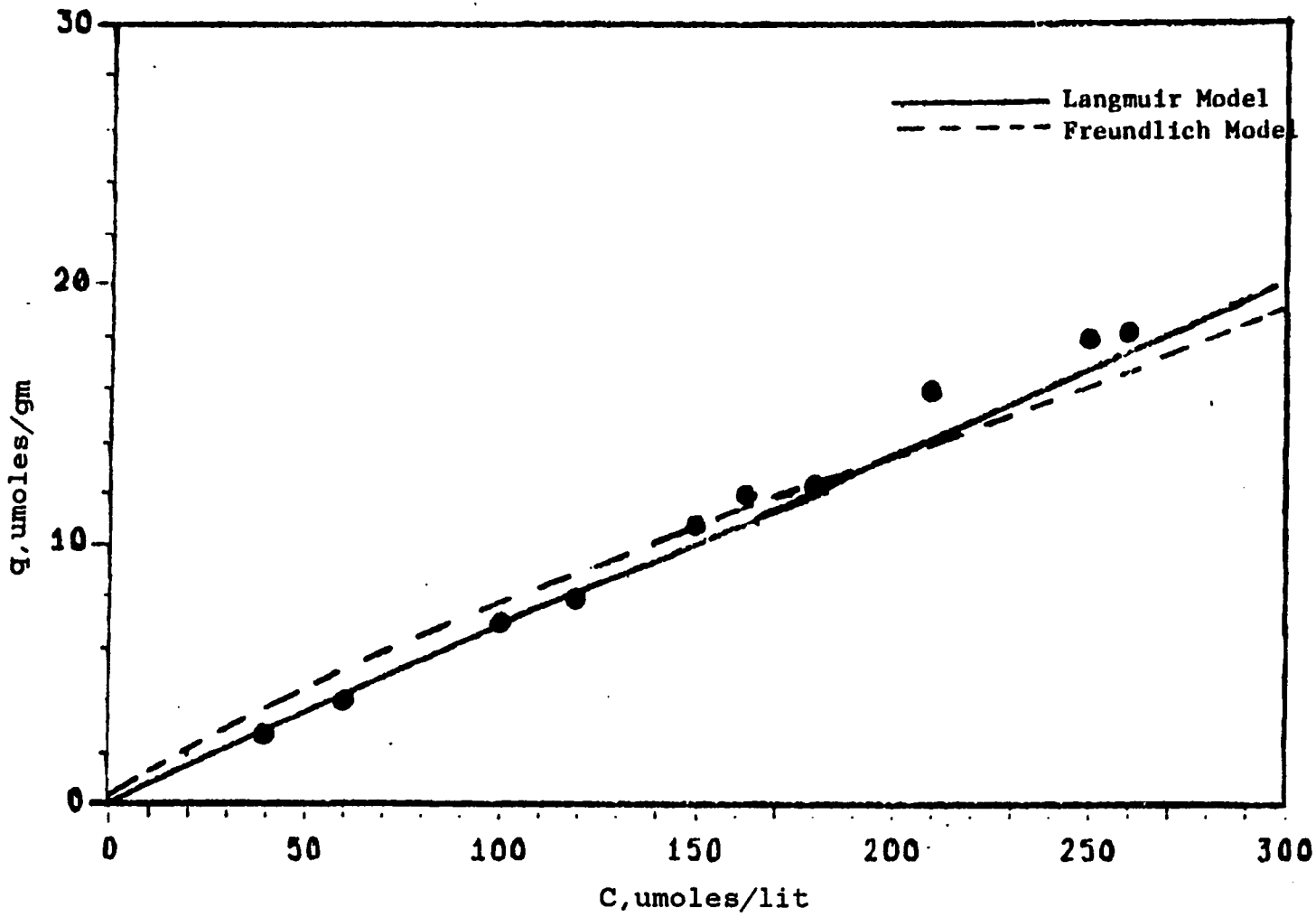

Fig 8 : Phenol Equilibrium Isotherm at 323 K.

Following the discussion in Sec 3.1.2, the constants of the Freundlich model are calculated from the intercept and the slope of the straight line obtained from plotting ln q vs ln C. The constants are given in Table 3 for the three different temperatures. The Freundlich model is compared to the equilibrium data at 298,313 and 323 degrees Kelvin as shown in Figs 6,7 and 8.

Table 3: Freundlich constants

T (K)	m	n
298	0.625	1.25
313	0.380	1.29
323	0.375	1.47

6.2.2 2,4 Dichlorophenoxyacetic Acid Equilibrium Adsorption

The data for the equilibrium adsorption of the DPCA acid show a linear relation between the

concentration and the acid uptake. The data are shown in Table 4. A plot of q, the uptake, vs. the concentration at the three temperatures is shown on Fig 9.

Because of the linear relationship between the uptake of the resin and the concentration, it is desirable to find the Henry's constant for the system and see how close the data fit the line q =K * C, where K is the Henry's constant. The Henry's constant can be caculated from the Virial equation (3.22). For low concentrations, only the first term in the exponential is important so that the equation reduces to

$$C = q/K \exp (A_1 q) \qquad 6.5$$

Therefore a plot of ln C/q vs q should give ln 1/K as the intercept. The results are shown in Table 5.

Table 4: Data for equilibrium adsorption of DPCA acid on XAD-7 resin at 25,40,50 °C

25 °C		40 °C		50°C	
C	q	C	q	C	q
60	1.8	100	2.7	90	1.2
72	2.8	110	2.6	110	2.0
80	3	129	2.9	114	2.1
84	3.3	158	4.3	140	2.6
90	3.4	159	4.4	160	3
100	3.6	162	4.6	180	3
110	4.5	166	4.5	182	3.3
120	4.8	210	5.8	228	4.0
133	5.6	236	5.4	280	5
150	5.3	240	6.2	300	4.7
162	5.7	250	6.8	316	5.7
180	7.4	294	7.3	346	6
204	7.6	308	7.3	360	7
246	8.6	342	8	370	7.6
254	9.4	356	8.6	400	7
290	9.6	423	10.4	440	7.8
308	11	450	10.8	460	8.3
320	11.8	455	11	500	8.7
331	11.6	460	10.8	522	9.3
348	12.1	500	11.4		
358	12.4	562	12.8		
370	12.8				
402	14				
408	14.5				
426	15.3				
436	15.2				
442	16				

C in μmoles/liter

q in μmoles/gram

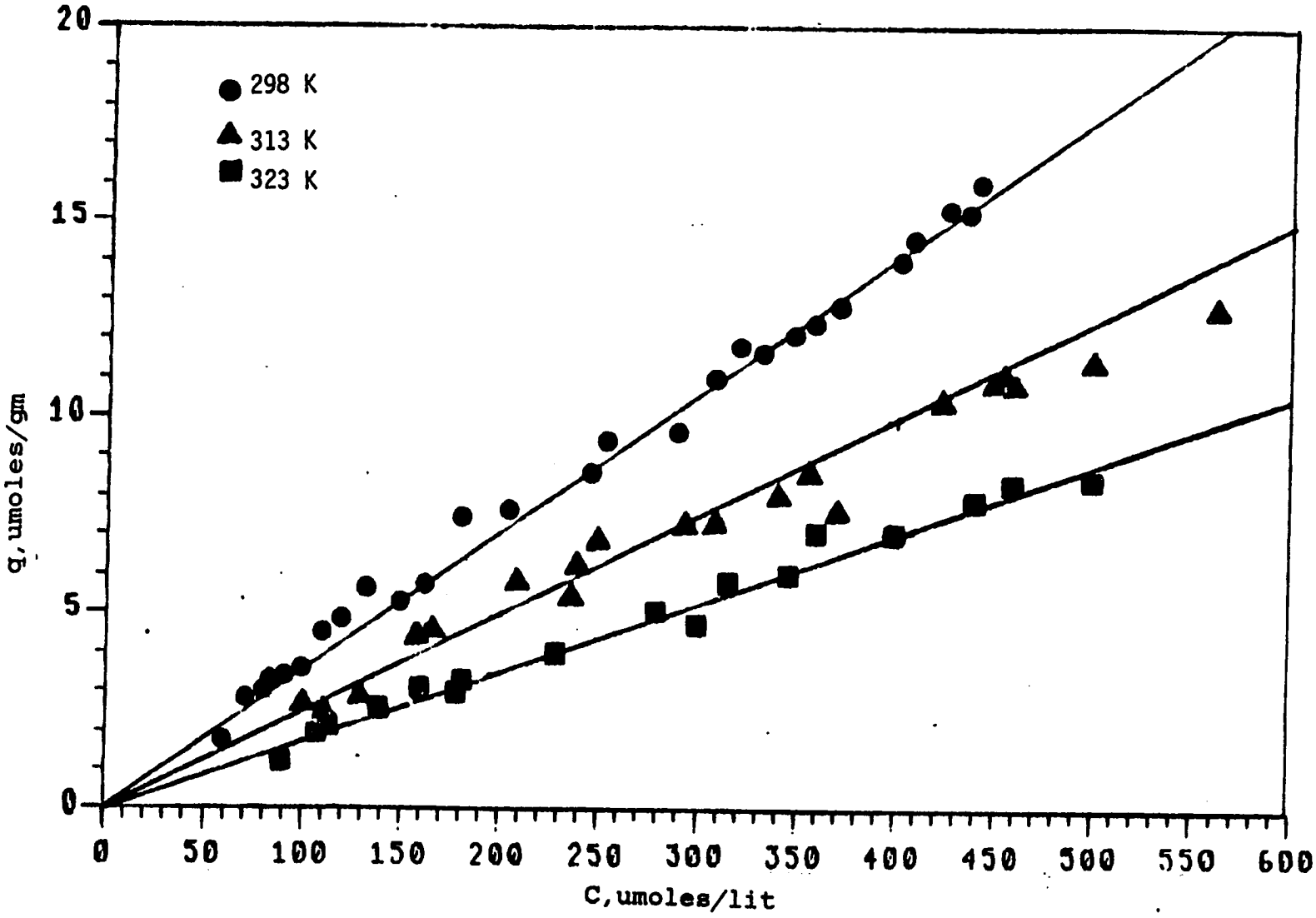

Fig 9 : Equilibrium Isotherms of DPCA Acid at 298,313 and 323 K.

Table 5

Henry's constants for 2,4 dichlorophenoxyacetic acid

T(K)	-ln K	K
298	3.350	0.035
313	3.709	0.0245
323	4.051	0.0174

K = Henry's constant, lit/g m .

The linear isotherm represented by q = K* C is fitted to the equilibrium data on Fig 9. These isotherms seem to fit the data quite well.

It is also apparent that the resin has a greater affinity for the phenol than for the acid. This may be explained partly by the difference in the acidity of the two compounds. This matter is discussed in more detail later.

6.2.3 EQUILIBRIUM ISOTHERMS FOR MIXTURES OF DPCA ACID & PHENOL

Equilibrium adsorption studies were carried out for mixtures of DPCA acid and phenol at 25 degrees centigrade. The same procedure as in the case of the binary solutions was adopted. A sample of the calculations is shown in Sec A.2. The data are given in Table 6 and these points are plotted in Fig 10.

It is apparent, despite the greater scattering of the data, that the uptake of each component in the mixture is almost equal to that of the single component. In other words, it seems that the adsorption at equilibrium of each component has not been markedly affected by the presence of the other one.

In an attempt to find an explanation to this phenomenon a comparison between the maximum capacity of the resin for each component is made. This is the term Q_m calculated from the Langmuir model (Table 2). The data for the DPCA acid are adapted to a Langmuir

Table 6: Data for equilibrium adsorption of mixture solutions of Phenol and DPCA acid on XAD-7 resin at 25 C

ACID		PHENOL	
C	q	C	q
45	1.57	40	11
46	1.54	42	12
70	2.40	44	12
71	2.38	44	13
74	2.42	70	20
130	4.60	72	20.9
132	4.61	76	21
132	4.70	98	26.2
182	6.32	100	26
199	6.41	105	29
220	7.60	150	35.2
222	7.80	150	38
230	8.00	152	37.1
270	9.30	154	36
270	9.41	154	41
272	9.30	179	41.5
275	9.51	185	41
326	11.10	207	45
350	11.75	210	44.1
353	13.09	247	46

C in μmoles/lit.

q in μmoles/gm.

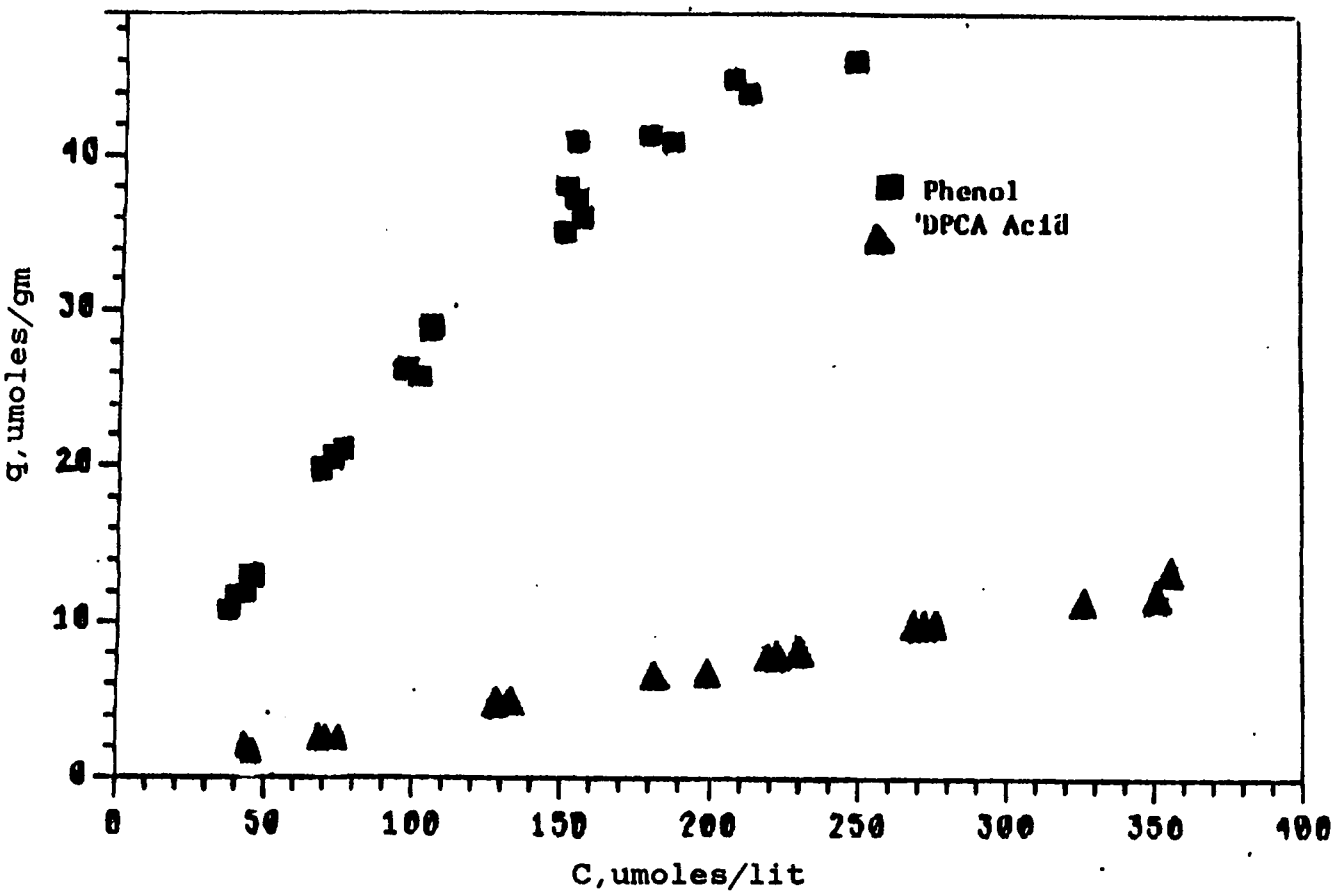

Fig 10 :Equilibrium Isotherms of DPCA Acid and Phenol Mixtures at 298 K.

model and Q_m calculated. It is found that for the acid, Q_m = 1000 umoles/gm. For the phenol the maximum capacity is 170 umoles/gm. This fact, together with the difference in acidity of the components leads to the possible conclusion that the acid and the phenol are adsorbing on different sites and are not competing with each other for adsorption sites. The adsorption on different sites may explain the unchanged nature of the equilibrium isotherms.

6.3 DETERMINATION OF THE HEAT OF ADSORPTION

The heat of adsorption of phenol and 2,4 DPCA acid on XAD-7 is calculated in two ways. First, the isosteric heat of adsorption is found by the Hersch equation(3.19). According to this equation, the natural log of the concentration is plotted against the inverse of the absolute temperature at constant loadings. The slope of the straight line obtained is equal to $\Delta H/R$. The second method uses the Van't Hoff equation (3.21) as described in section 3.5.

6.3.1 *Isosteric Heat of Adsorption*

Horizontal lines corresponding to constant loadings are drawn on the isotherms plotted on Figs 5 and 9 to produce the concentration vs temperature data. The logarithm of concentration is plotted against the inverse of the absolute temperature. The data for the acid and phenol are shown in Tables 7 and 8. Figs 11 and 12 show the plot of ln C vs 1/T for the DPCA acid and phenol respectively. The calculated heat of adsorption at different loadings are given in Tables 9 and 10. Since the isosteric heat of adsorption is defined as the heat given off, the positive sign indicates that the adsorption of phenol and DPCA acid on the resin is an exothermic process.

Table 7 Data for calculation of isosteric heat of adsorption of DPCA acid

loading (μm/gm)	$1/T*10^3$ (1/K)	$C*10^6$ moles	slope $(*10^{-3})$ (K)
2	3.356 3.195 3.096	51 80 110	-2.962
4	3.356 3.195 3.096	108 160 226	-2.769
6	3.356 3.195 3.096	164 265 344	-2.615
8	3.356 3.195 3.096	220 328 460	-2.844

Table 8 : Data for calculation of isosteric heat of adsorption of phenol

loading (μm/gm)	$1/T*10^3$ (1/K)	$C*10^6$ moles/lit	slope ($*10^{-3}$) (K)
4	3.356 3.195 3.096	16 21 65.5	-5.115
8	3.356 3.195 3.096	31 62 108.5	-4.577
12	3.356 3.195 3.096	44.5 90 166	-4.846
16	3.356 3.195 3.096	59 114 203	-4.615

Table 9: Values of the Isosteric heat of adsorption of DPCA acid

Loading (umoles/gm)	ΔH (Kcal/gmole)
2	5.9
4	5.5
6	5.2
8	5.6

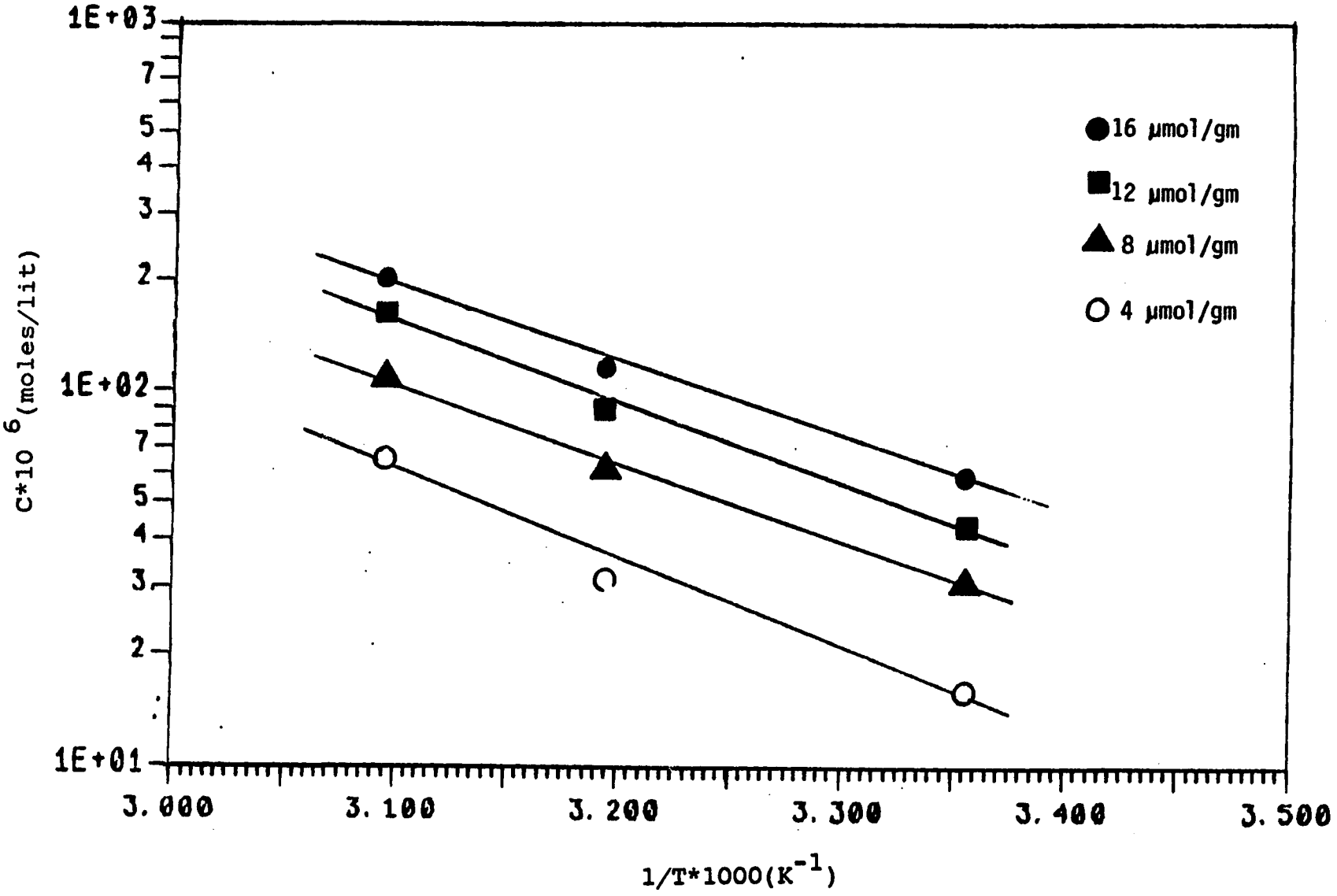

Fig 11: ln C vs 1/T for Phenol.

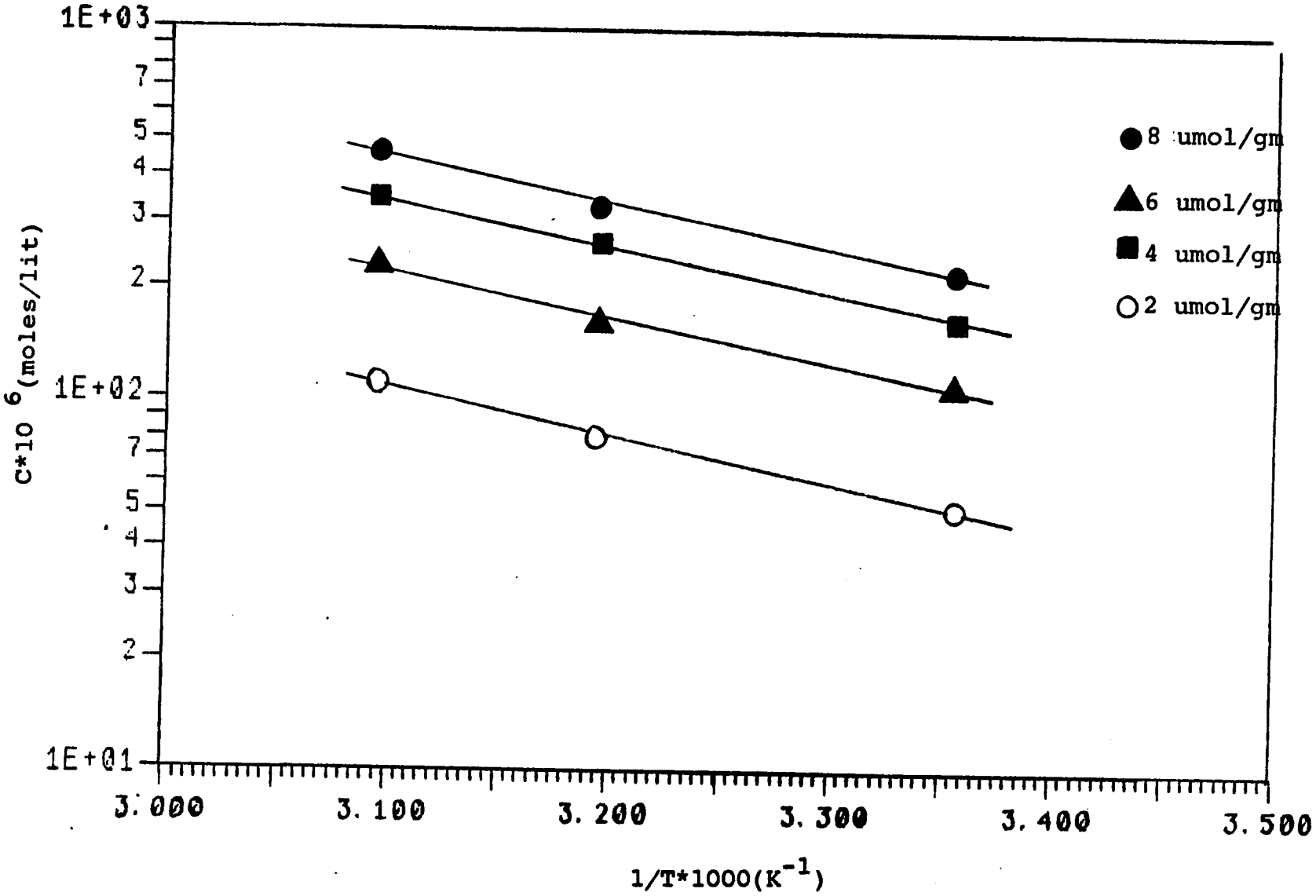

Fig 12 : ln C vs 1/T for DPCA Acid.

Table 10: Values of the isosteric heat of adsorption of phenol

loading (umoles/gm)	ΔH (Kcal/gmole)
4	10.2
8	9.1
12	9.6
16	9.2

6.3.2 Heat of adsorption calculated from Van't Hoff equation

The second method used involves the calculation of the Henry's constants according to the Virial equation (3.22) of Barrer and Lee. When ln C/q vs q at different temperatures for both compounds is plotted, straight horizontal lines are obtained as shown in Figs 13 and 14. From the intercept (equal to ln 1/K) with the ln C/q axis, the values of 1/K are obtained. The Henry's constants for DPCA acid and phenol adsorption on the resin are given in Table 11. The Henry's constants calculated by this method are mostly consistent with those calculated before (see Table 2)

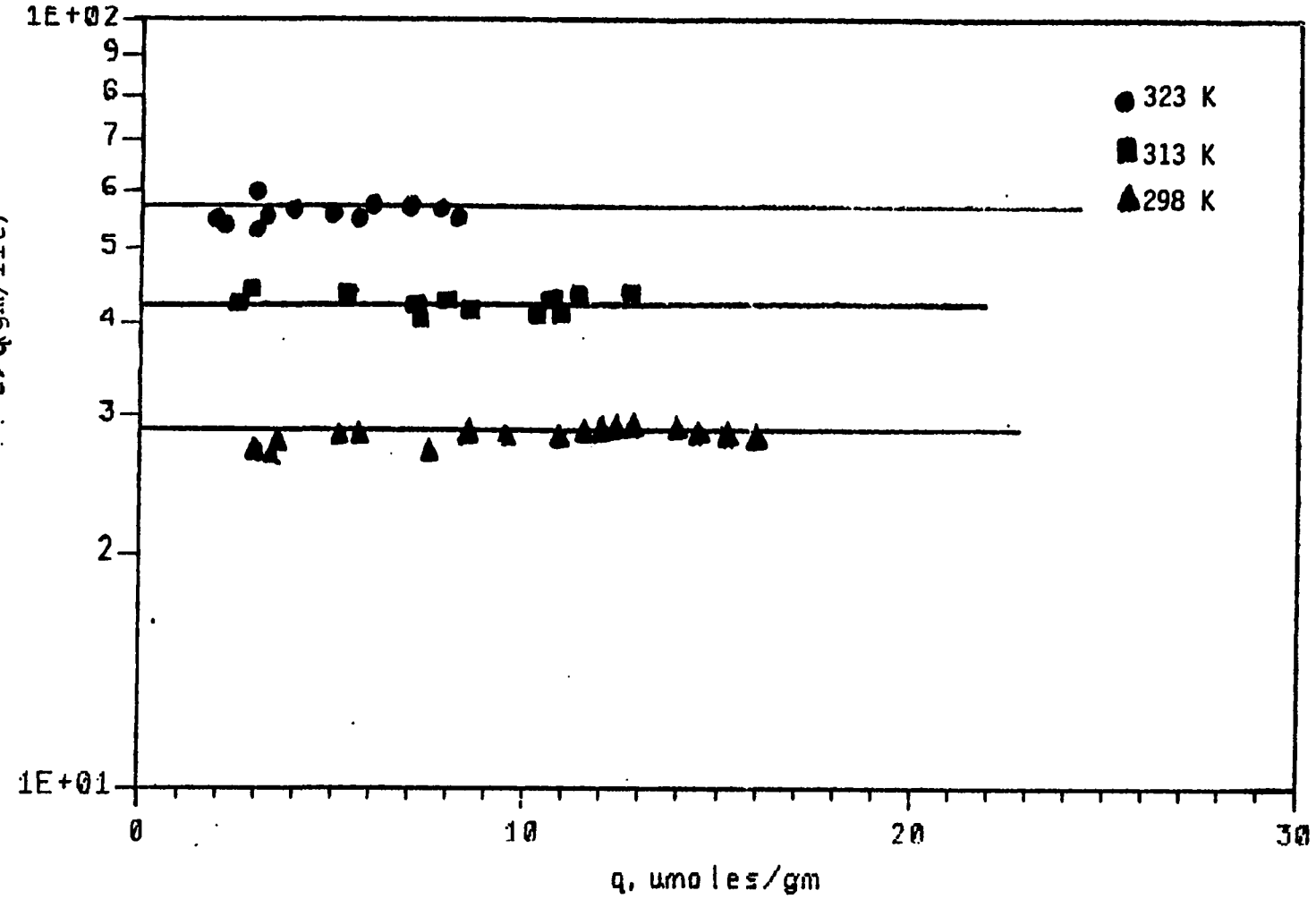

Fig 13 : C/q vs q for Phenol at 298,313 & 323 K.

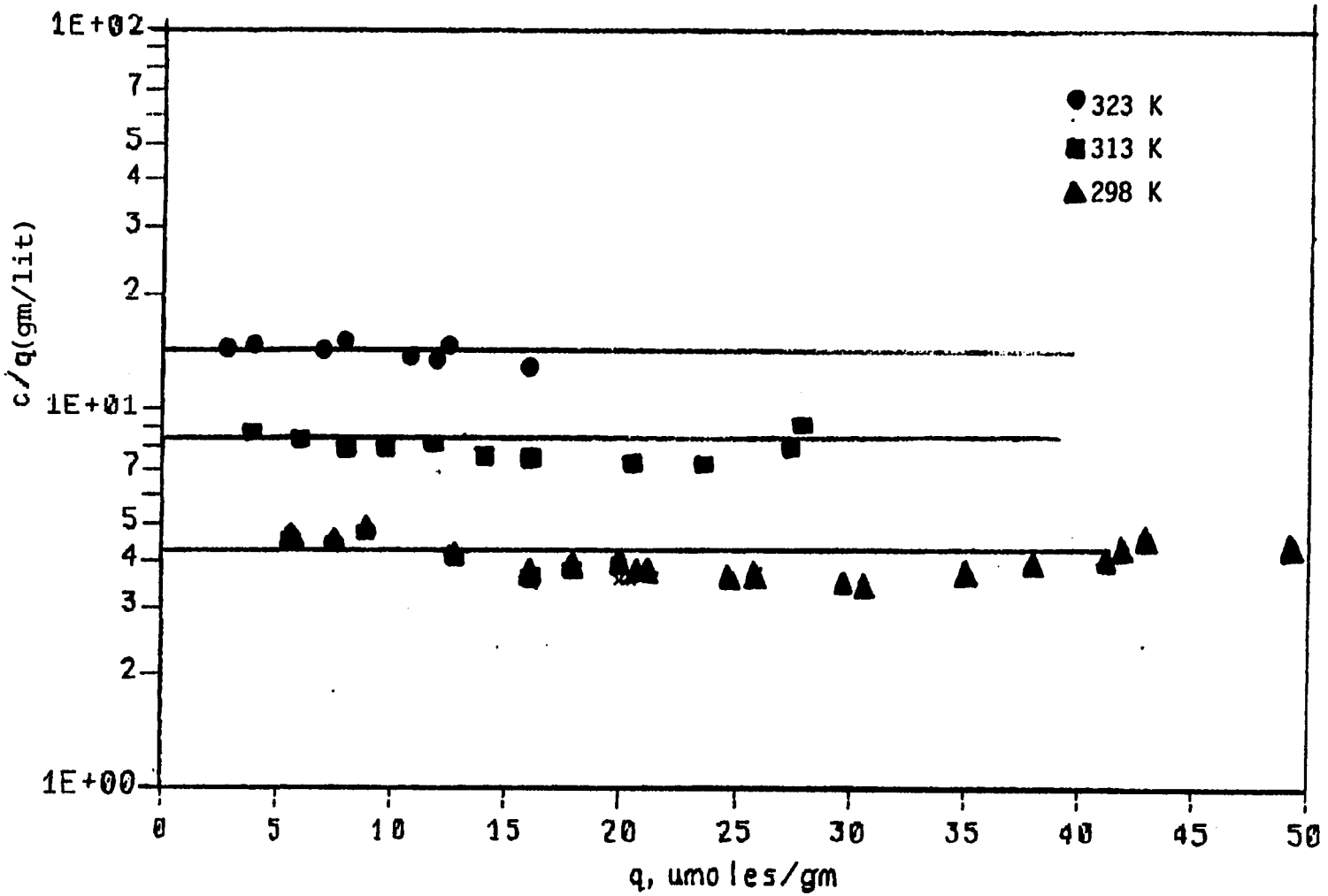

Fig 14 : C/q vs q for DPCA Acid 298,313 & 323 K.

Table 11: Henry's constants

temperature K	Henry's constant acid	phenol
298	0.0351	0.278
313	0.0245	0.128
323	0.0174	0.076

K in lit/gm.

Plots of ln K vs 1/T are shown in Fig 15. According to the Van't Hoff equation these plots should produce straight lines of slopes equal to Q_0/R, and hence, the heat of adsorption was calculated. The results are given below.

Table 11a:Heat of adsorption calculated by the Van't Hoff equation

compound	slope	ΔH(Kcal/gmole)
acid	2.78	5.52
phenol	5.00	9.94

The heats of adsorption calculated by both methods are in close agreement

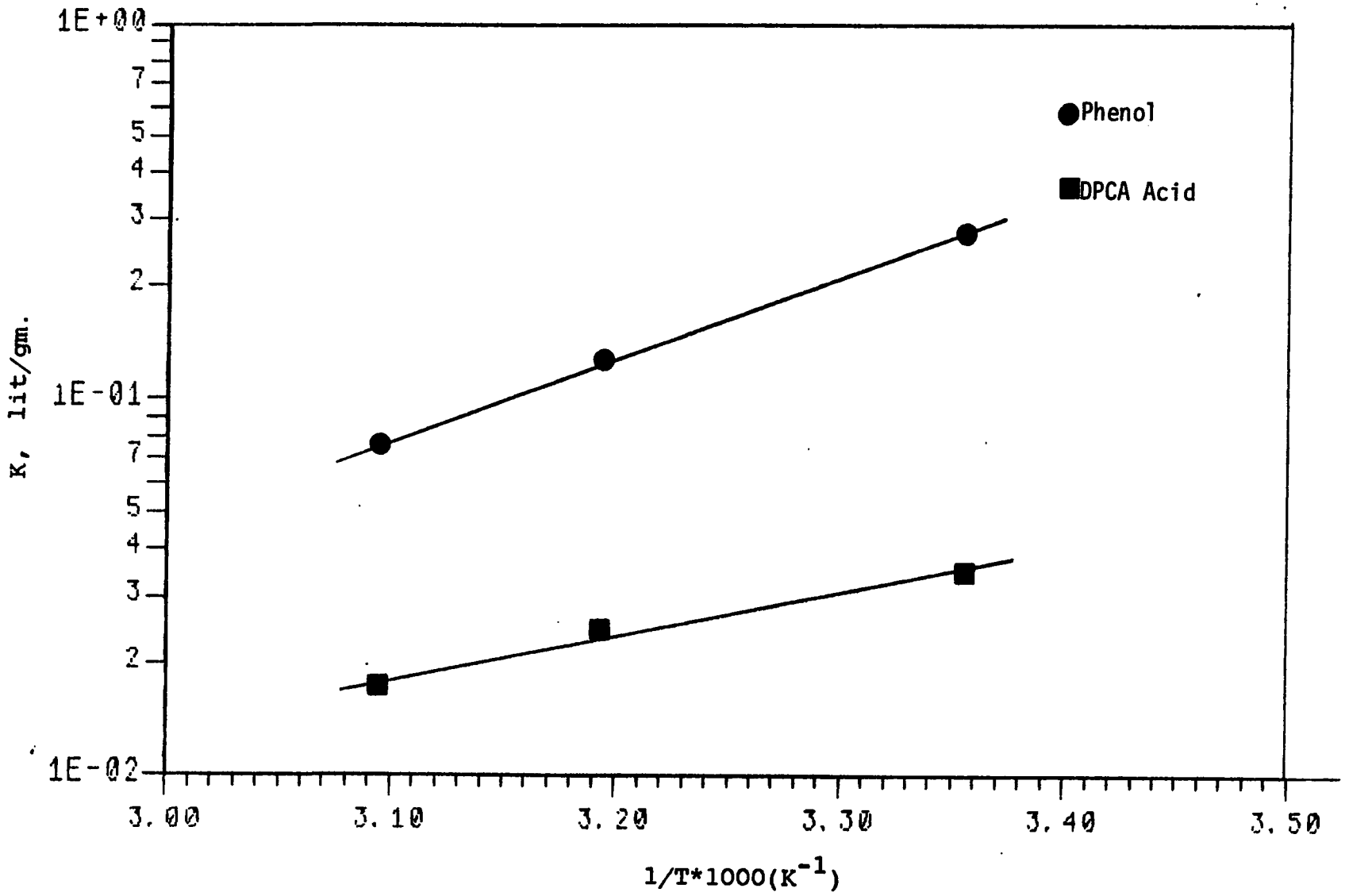

Fig 15 : ln K vs 1/T for Phenol and DPCA Acid.

with each other. The order of magnitude of the heat of adsorption may suggest that the adsorption of both compounds on XAD-7 occurs under the influence of the Van der Waals forces or by weak chemisorption. This supports the claim that the resin is easily regenerable.

Research done by Hasanain et al(24) on adsorption of acetic acid on the same type of amberlite resin, but of a different grade (XAD-2), yielded a heat of adsorption of 3.5 Kcal/gmol. The results of the present research are of the same order of magnitude.

The relative constant heat of adsorption of the compounds on the XAD-7 may be attributed to the fact that the resin is an artificial one. In artificial resins the surface is usually more homogeneous than the surfaces of naturally occurring resin.

6.4 Breakthrough Curves

The column experiments are conducted as described before in chapter 5. Samples are taken at 4 different points to give the concentration variation with time

and length of bed. The flow rates are kept constant as far as possible, but there is a very slight variation from the set flow rate every now and then due to the fluctuation in the electric current in the laboratory. But since the variaton is slight an average value of the flow rate is used. The operating conditions of the runs for both adsorption and regeneration are given in Table 12. The experimental data are shown in Tables 13 to 19 and the experimental breakthrough curves are presented in Figs 16 to 22.

As expected, the breakpoints occur earlier for larger flowrates, but having the same initial concentration. For the same flowrates but shorter length of tube, the breakpoint occurs earlier. Since the size distribution of the resin was originally very narrow, sufficient amount of resin of different sizes was not available to conduct the experiment with different sizes of adsorbent. So the behaviour of the breakthrough curves with different particle sizes has not been studied.

Table 12: Operating conditions of column experiments

RUN	component	density	flowrate	inlet conc	L1	L2	L3	L4
1	acid	610	8	274.4	14.9	30.7	49.7	88.3
2	acid	550	6	274.4	14.9	37.4	50.0	80.1
3	phenol	573	7	164	20.0	30.9	49.7	78.1
4	phenol	570	9	164	14.9	30.5	47.3	77.0
5	acid	584	10	224	14.7	30.0	49.0	72.0
6	phenol	540	10	203	14.9	31.0	51.0	74.0
7	phenol	540	8	203	16.1	30.0	54.1	78.1
8	acid	520	8	274	14.8	30.2		
9	phenol	550	8	203	16.0	30.1		

Density of bed in grams/liter

Flowrate in cc/minute

Inlet concentration in μmoles/liter

Length of bed in centimeters

Table 13: Experimental data for Run # 1

L1		L2		L3		L4	
t	C/C_0	t	C/C_0	t	C/C_0	t	C/C_0
10	.02	20	0	64	.01	160	.05
18	.20	33	.06	85	.13	196	.28
40	.45	60	.31	101	.25	220	.38
55	.52	106	.63	146	.58	254	.60
80	.60	142	.83	178	.78	280	.71
99	.66	180	.95	200	.90	321	.84
120	.85	202	.99	231	1.0	340	.89
149	.93	250	1.0			370	.96
170	.98					383	.99
200	1.0						

t in minutes

Table 14: Experimental data for Run # 2

L1		L2		L3		L4	
t	C/C_0	t	C/C_0	t	C/C_0	t	C/C_0
24	.02	52	.09	83	.03	210	0.07
31	.09	72	.16	120	.21	239	0.21
39	.19	84	.26	162	.43	271	0.32
54	.32	102	.479	178	.52	300	0.39
71	.41	118	.51	184	.56	340	0.47
83	.51	140	.60	198	.64	401	0.55
101	.70	157	.71	222	.77		
119	.81	162	.78	246	.91		
140	.93	178	.85	247	1.0		
150	1.0	186	.90				
		196	.94				
		207	.97				
		235	1.0				

t in minutes

Table 1 5: Experimental data for Run # 3

L1		L2		L3		L4	
t	C/C_0	t	C/C_0	t	C/C_0	t	C/C_0
75	.04	50	0	300	.01	675	0.07
105	.08	90	0	345	.02	745	0.21
125	.11	105	0	360	.03	810	0.32
158	.17	150	.009	430	.07	845	0.39
223	.30	235	.1	485	.2	855	0.47
310	.51	315	.23	565	.4	900	0.55
375	.72	440	.49	635	.52	940	0.65
425	.86	465	.59	675	.64	1025	0.84
455	.94	505	.72	700	.69	1130	0.91
505	.99	565	.83	780	.83		
615	1.0	600	.91	865	.92		
		650	.97	950	.99		
		730	1.0	1015	1.0		

t in minutes

Table 16: Experimental data for Run # 4

L1		L2		L3		L4	
t	C/C_0	t	C/C_0	t	C/C_0	t	C/C_0
10	0	140	.02	330	.06	710	.13
20	.01	160	.03	390	.16	790	.25
60	.03	221	.08	450	.24	856	.36
115	.11	291	.18	630	.48	910	.46
150	.20	342	.29	730	.63	1010	.58
185	.26	400	.39	830	.75	1060	.67
250	.43	429	.44	995	.90	1218	.85
310	.60	455	.51	1103	.99	1341	.99
340	69	500	.60	1181	1.0		
415	.80	550	.73				
487	.91	616	.81				
555	.98	654	.88				
630	1.0	702	.94				
		761	.99				
		851	1.0				

t in minutes

Table 17: Experimental data for Run # 5

L1		L2		L3		L4	
t	C/C_0	t	C/C_0	t	C/C_0	t	C/C_0
9	.09	25	.14	43	.04	80	.05
15	.22	31	.27	53	.15	96	.14
22	.35	38	.39	67	.33	108	.26
27	.47	45	.51	78	.55	139	.52
33	.59	52	.61	98	.73	158	.68
40	.68	65	.75	108	.81	170	.80
47	.76	85	.93	126	.93	181	.90
57	.84	96	1.0	140	1.0		
65	.90						
71	.99						

t in minutes

Table 18: Experimental data for Run # 6

L1		L2		L3		L4	
t	C/C_0	t	C/C_0	t	C/C_0	t	C/C_0
45	.04	145	.10	228	.04	450	.07
85	.17	205	.24	304	.14	526	.19
102	.30	265	.44	363	.27	690	.60
131	.40	300	.55	459	.51	801	.84
164	.48	355	.73	508	.64	902	.97
230	.65	403	.87	621	.80		
275	.78	441	.95	650	.87		
316	.89	499	1.0	732	.97		
394	1.0			811	1.0		

t in minutes

Table 19: Experimental data for Run # 7

L1		L2		L3		L4	
t	C/C_0	t	C/C_0	t	C/C_0	t	C/C_0
101	.06	235	.10	360	.03	575	.00
151	.18	264	.19	490	.30	640	.10
196	.30	310	.30	585	.55	760	.31
246	.44	401	.52	698	.77	826	.42
299	.57	498	.77	751	.89	910	.61
385	.80	580	.95	810	.96		
447	.91	652	1	911	1		
500	.97						
543	1						

t in minutes

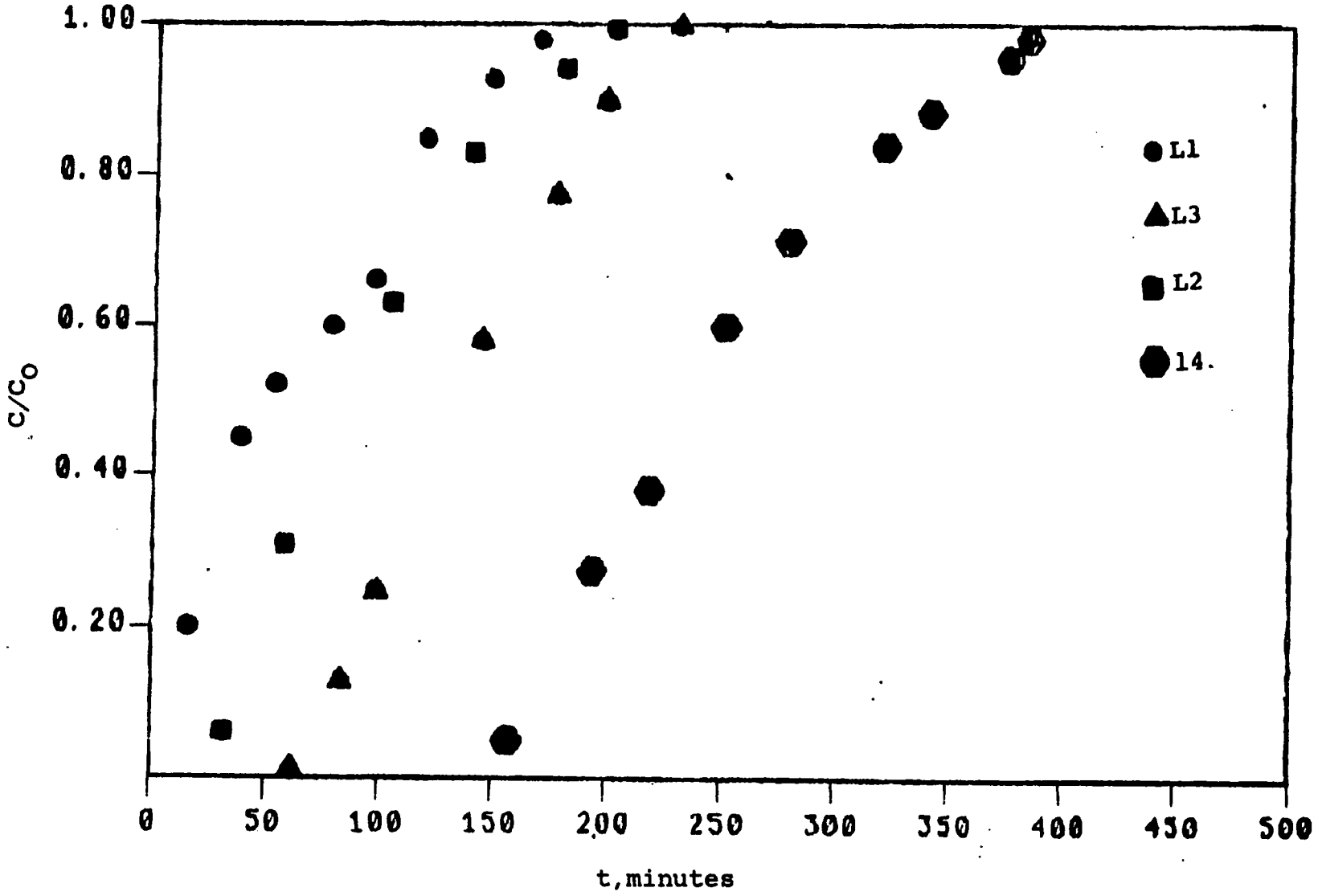

Fig 16 : Experimental Breakthrough Curves- RUN 1.

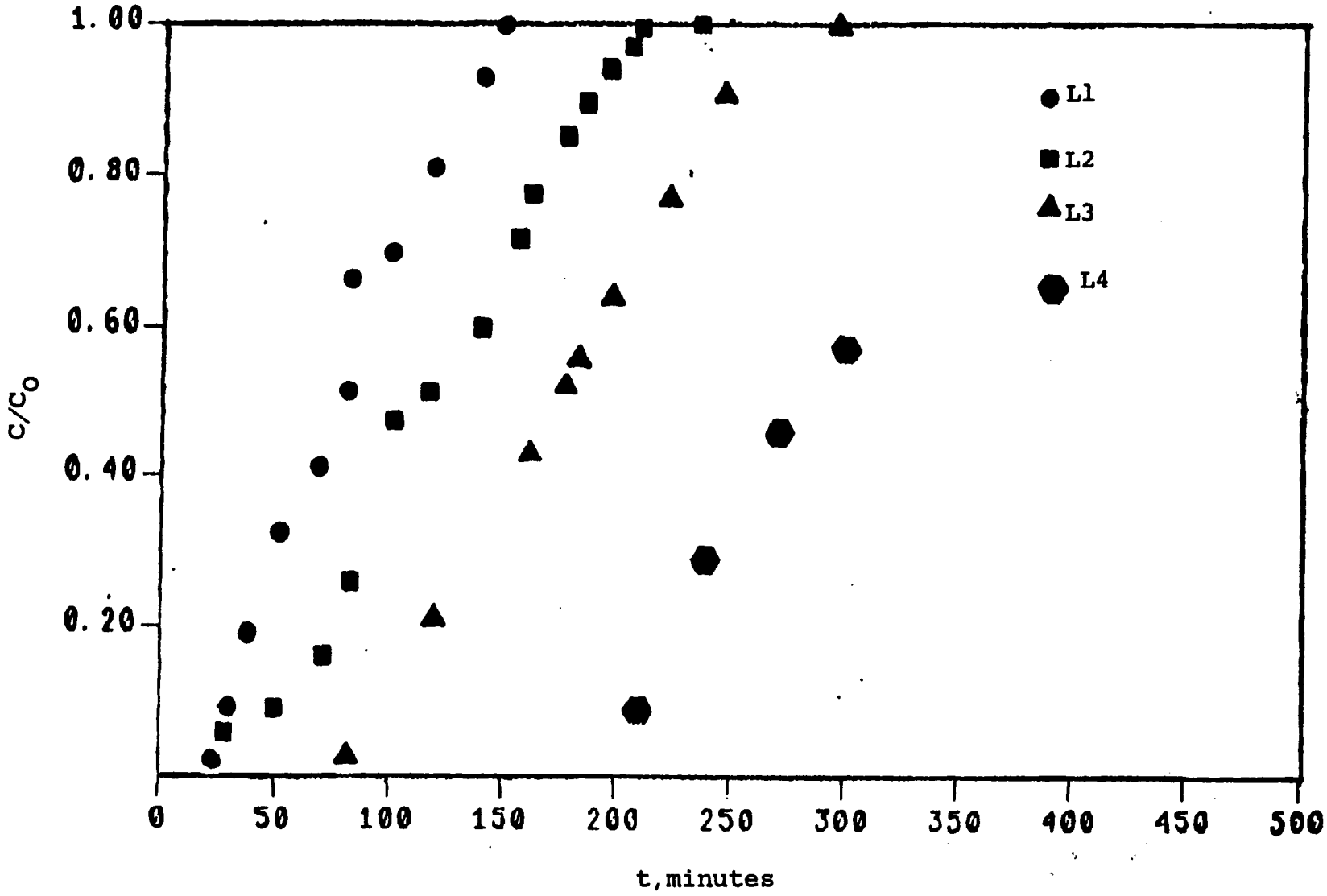

Fig 17 : Experimental Breakthrough Curves- RUN 2.

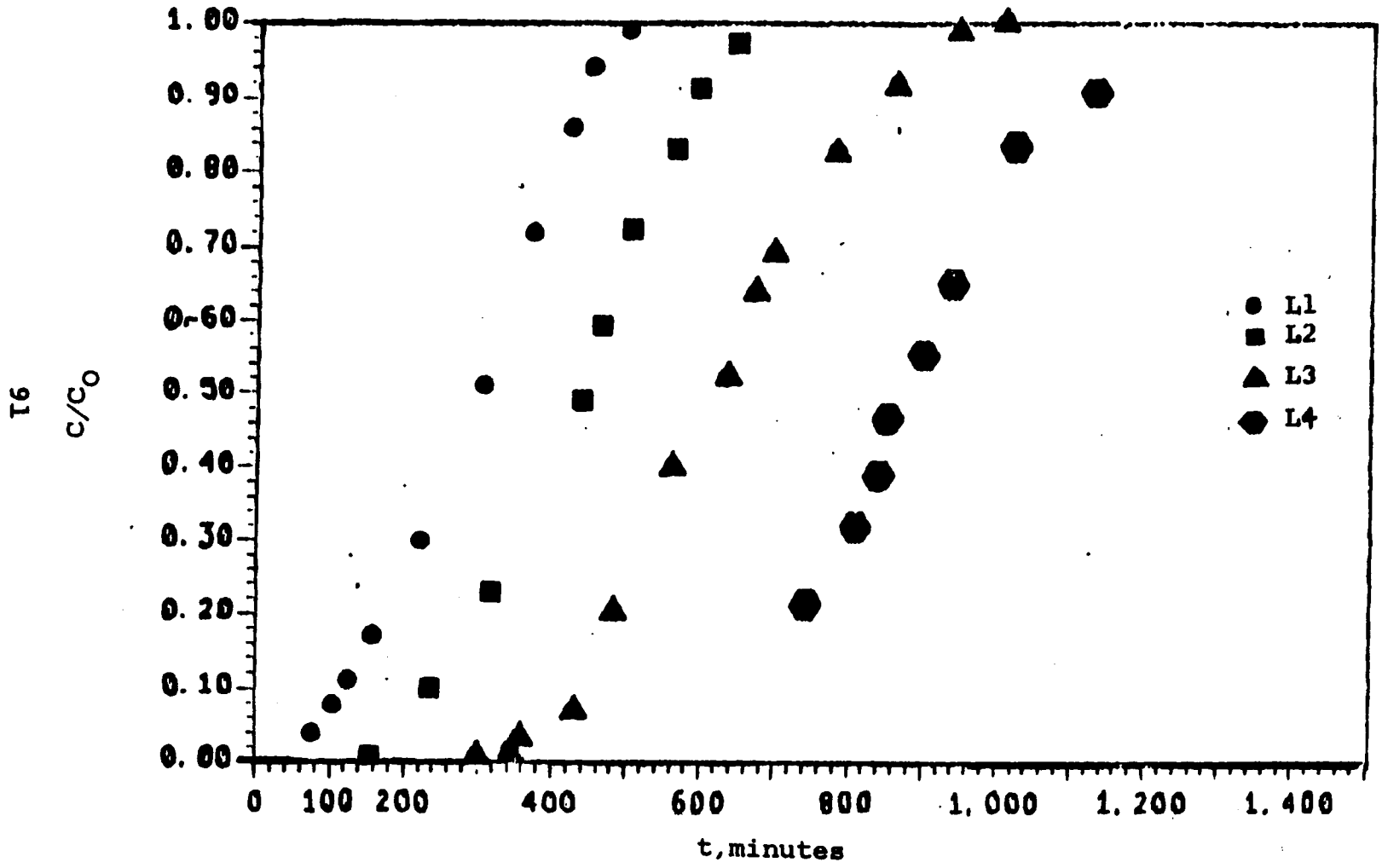

Fig 18 : Experimental Breakthrough Curves- RUN 3.

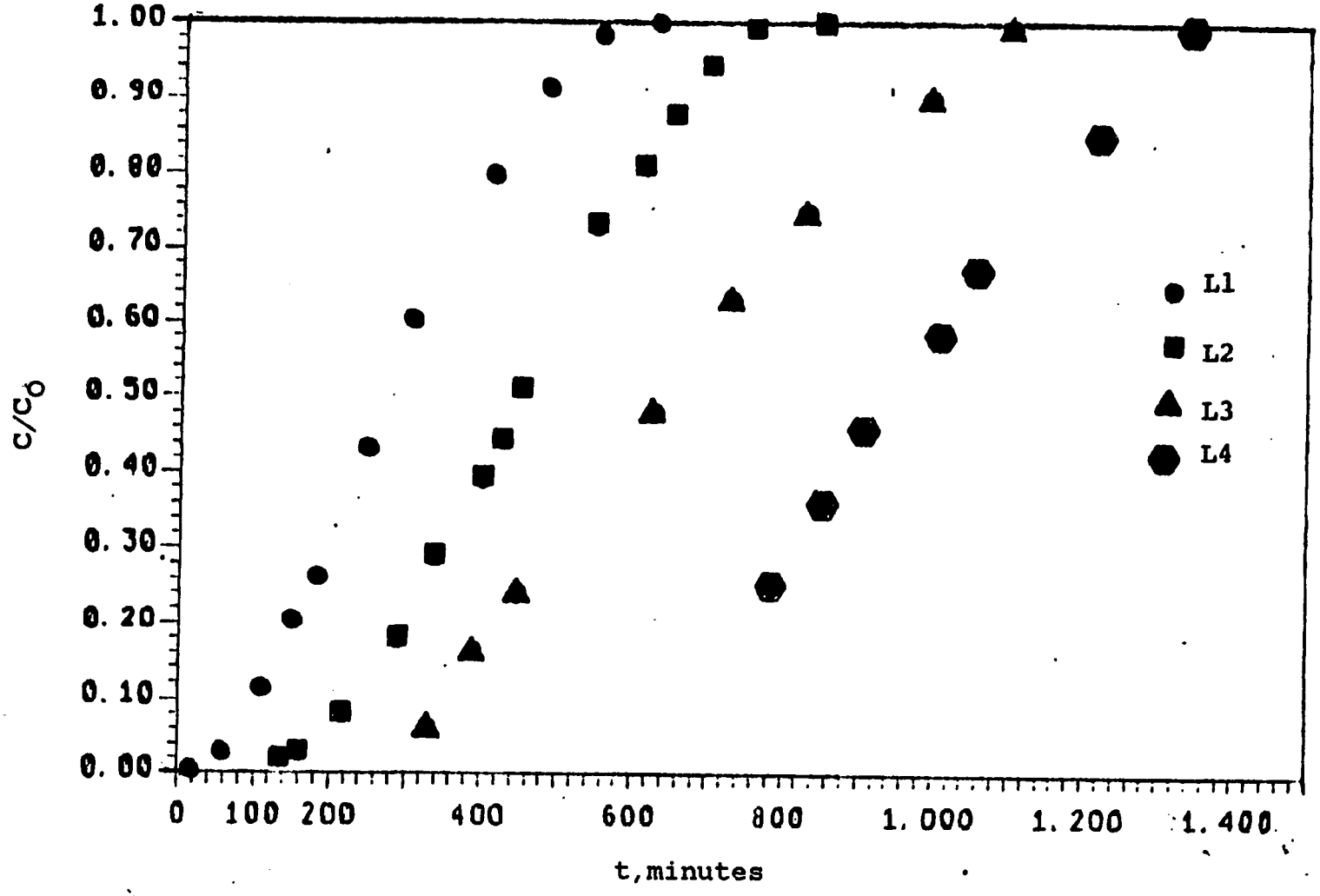

Fig 19 : Experimental Breakthrough Curves- RUN 4.

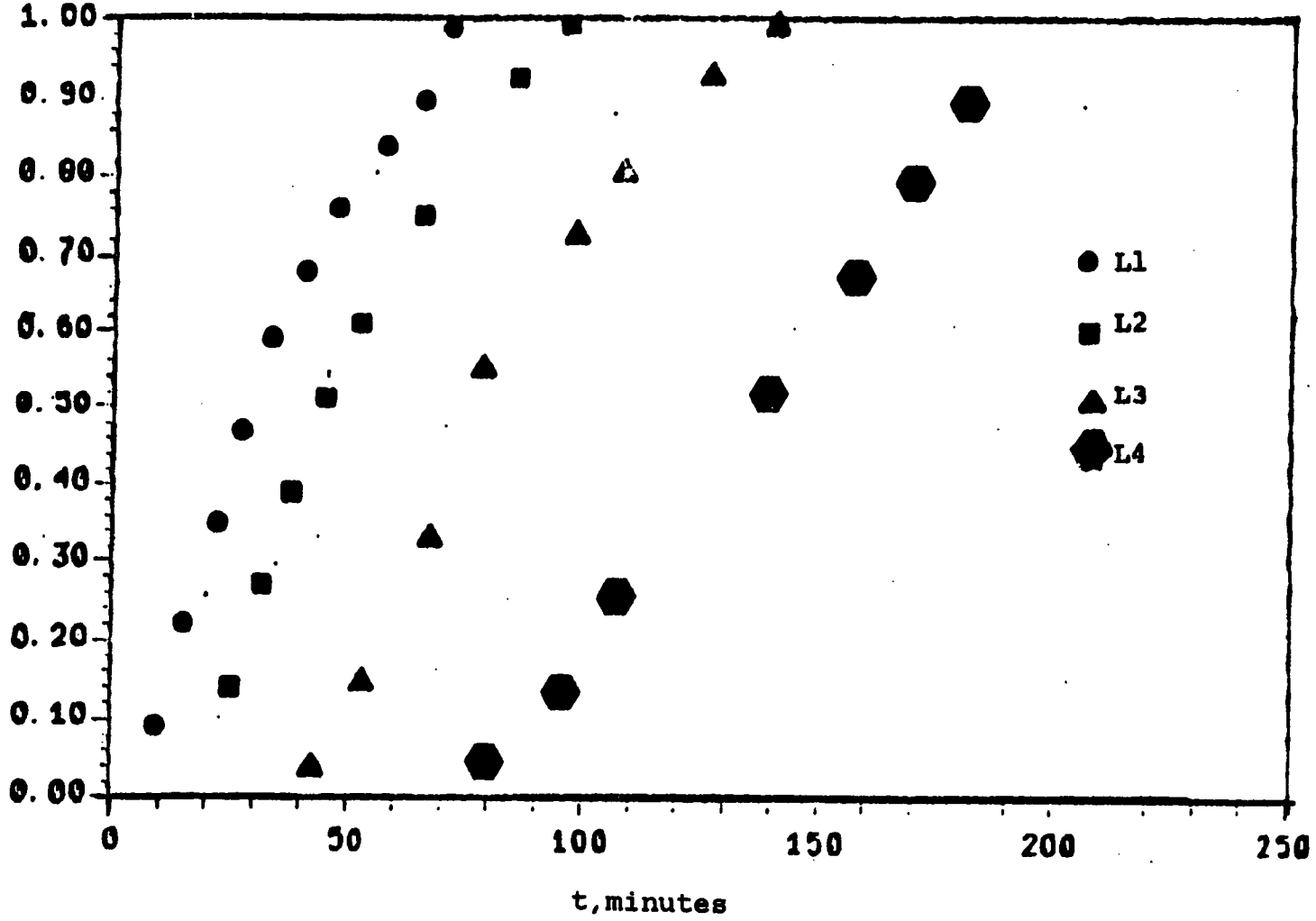

Fig 20 : Experimental Breakthrough Curves- RUN 5.

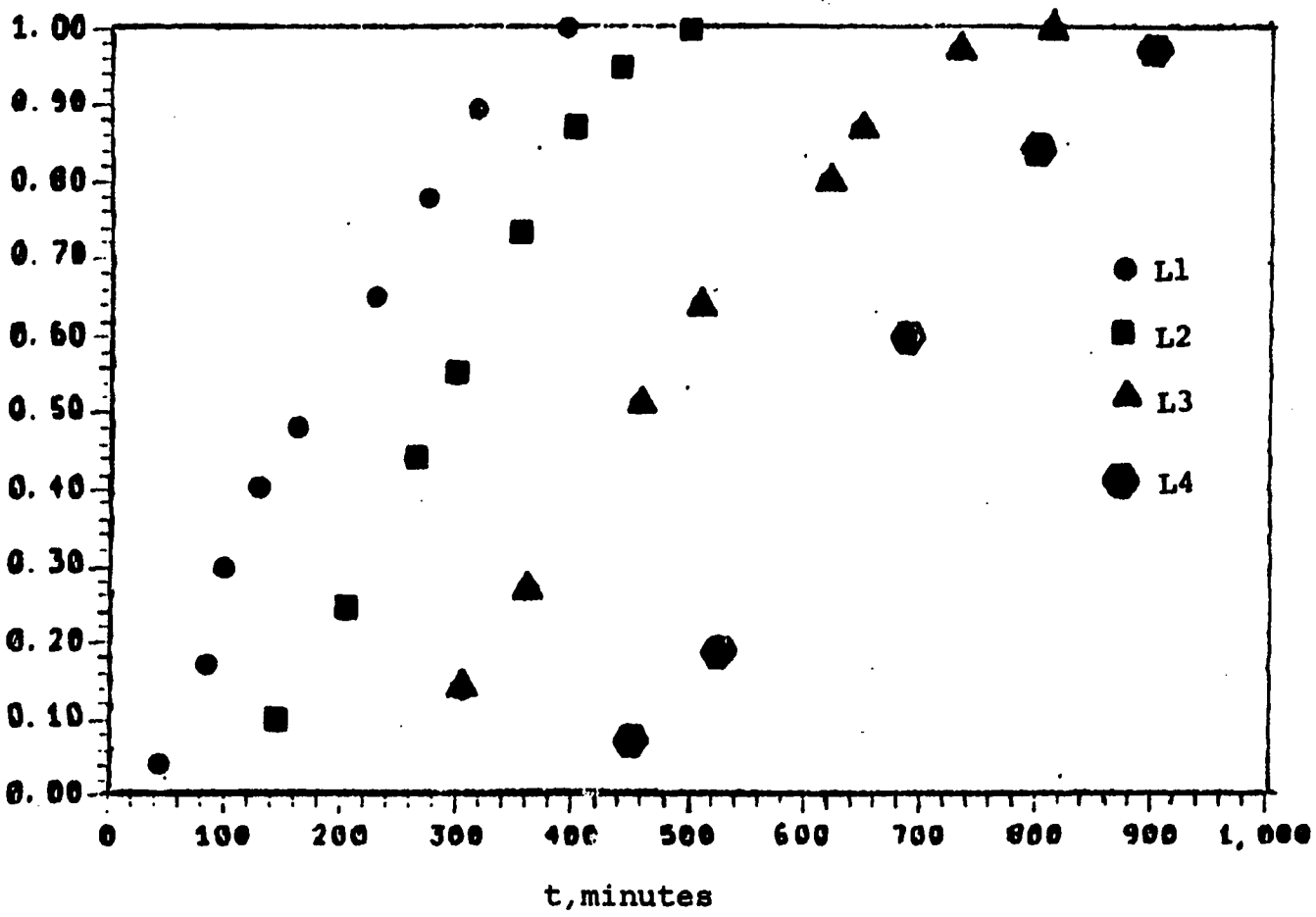

Fig 21 : Experimental Breakthrough Curves- RUN 6.

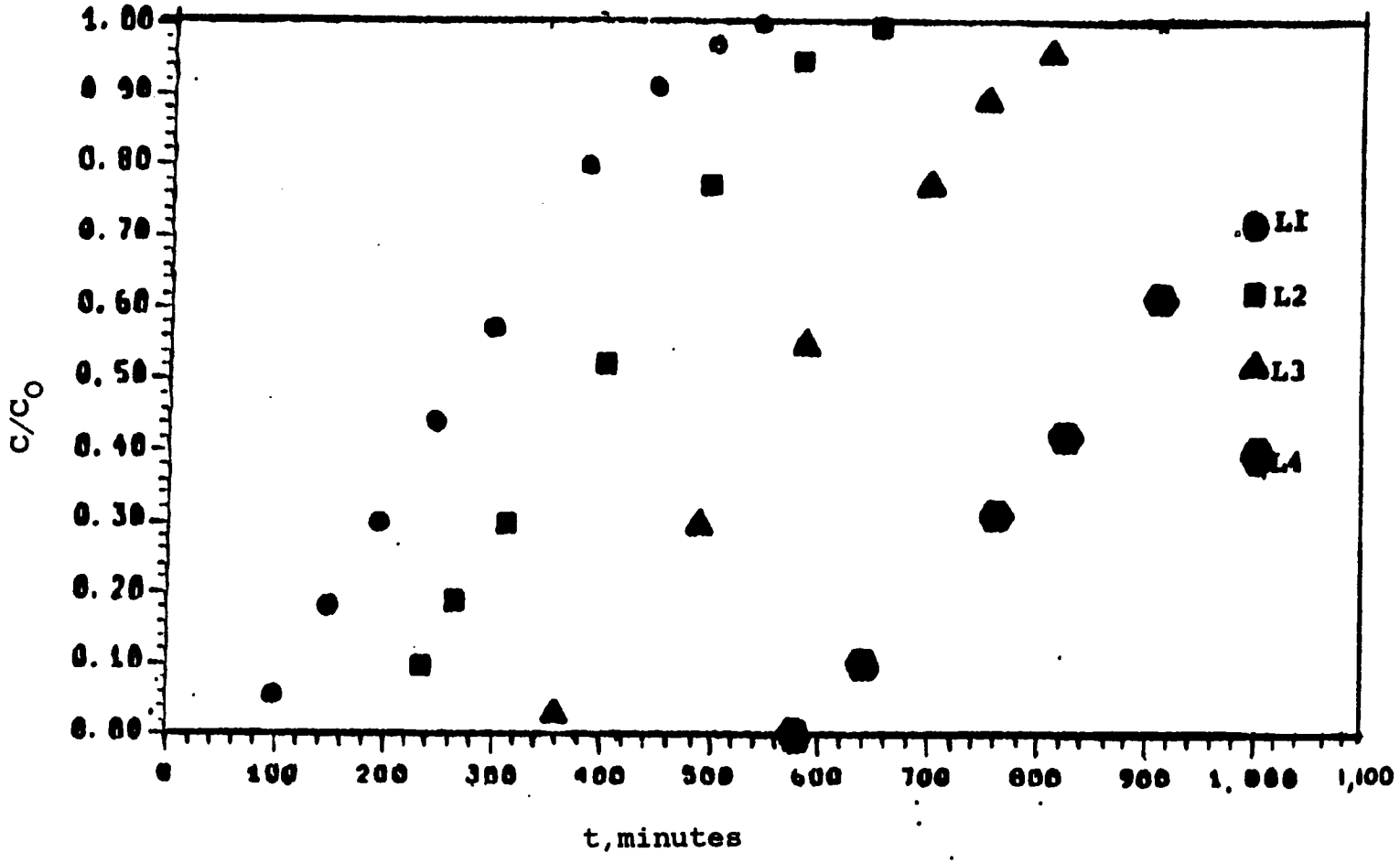

Fig 22 : Experimental Breakthrough Curves- RUN 7.

6.4.1 Mass-Transfer Coefficients

The mass transfer coefficients according to the different models discusssed in Sec 4.3 have been calculated, and the results are shown in Table 20. The calculations were performed by drawing the plots of C/C_0 vs the length and taking the slope at a constant time to get$(\partial C/\partial Z)_t$. The term $(\partial C/\partial t)_Z$ in the differential mass-balance is calculated from the slope of the plots of C/C_0 vs time at a constant length. A sample of these calculations is shown in Appendix A.3. In most calculations, the coefficients are measured at about $C/C_0 = 0.6$ because preliminary calculations have shown that the rate measured at this point represent an average value. Substitution of the values of $(\partial C/\partial t)_z$ and $(\partial C/\partial z)_t$ in the mass balance equation (eq. 4.8), along with the values of S,F,V and the bulk density, allows the term $(\partial q/\partial t)_Z$ to be calculated. From graphical integration of the $\partial q/\partial t$ vs t curve, the parameter q is calculated.

It is apparent that the mass transfer coefficients are almost constant throughout the length. The curves are of the 'constant-pattern' types. For the DPCA

Table 20: Mass transfer coefficients calculated by the differential method for adsorption of phenol and DPCA acid.

	($*10^6$)					($*10^4$)	($*10^5$)			
RUN	$K_F a_F$	K_a	$K_p a_p$	K_K	K_V	K_{GE}	K_I	F	C_0	Compdund
1	264	227	6.12	14.00	5.2	41.6	2.9	10	274.4	DPCA Acid
2	254	190	5.14	11.36	4.8	34.2	2.1	8	274.4	DPCA Acid
3	284	993	0.61	19.00	0.53	198.0	25.1	7	164	Phenol
4	506	1880	1.18	34.00	0.49	227.0	23.1	9	164	Phenol
5	592	349	11.0	18.50	9.10	35.6	3.2	10	224	DPCA Acid
6	282	1422	0.83	46.10	0.63	570.1	56.2	10	203	Phenol
7	227	2640	1.74	19.95	1.64	439.1	35.8	8	203	Phenol

$K_F a_F, K_K, K_p a_p, K_V$ and K_{GE} in hr^{-1}

K_a, K_l in $\frac{lit}{hr \cdot \mu mol}$

F = flowrate, cc/min

C_0 = initial concentration, μmol/lit

acid it was found that the coefficients vary slightly with the length. The average values of these coefficients are tabulated. For the phenol, it is observed that the external mass-transfer coefficients increase with the flowrate for same inlet concentration. It is too early to suggest a controlling mechanism from this behaviour.

The theoretical external mass transfer coefficients were calculated by the Gaffney and Drew (29) method for phenol. A sample of the calculations are shown in Sec. A.6. A particle diameter of 100 microns was used for the calculations. Below are the theoretical external mass transfer coefficients compared to the experimental ones.

Table 20a: Comparison of Theoretical and Experimental mass Transfer Coefficients

RUN	F	C_o	hr^{-1} Experimental External MTC	hr^{-1} Theoretical External MTC
3	7	164	284	173
4	9	164	506	190
6	10	203	287	207
7	8	203	227	192

F = flowrate, cc/min.
C_o = initial concentration, umoles/lit.

The experimental external mass transfer coefficients are higher than those of the theoretical ones. The reason is probably due to the fact that the diameter used in the calculations of the theoretical mass transfer coefficients was fixed, whereas in reality the particle sizes range from above 175 microns to 20 microns and below. Presented in Table 20b is the size distribution resin from a sample quantity of 8.6 grams sieved for 30 minutes. An examination of the particle on the pan revealed the presence of particles smaller than 20 microns. Since the mass transfer coefficients theoretically calculated is inversely proportional to the particle diameter raised to the power of 1.5, the discrepancy between the theoretical and experimental mass transfer coefficients may be explained by the size distribution of the particle.

Table 20b:Size Distribution of the Resin XAD-7

above 175 mic	150 mic	106 mic	75 mic	53 mic	below 53 mic
2.0 gm	1.0 gm	2.1 gm	1.2 gm	0.7gm	1.6 gm

Similarly for the DPCA acid the second order kinetics coefficients show an increase with higher flowrates. An analysis on the different controlling mechanisms is presented in the next section.

6.4.2 Search for a controlling mechanism.

According to the Thomas model, prediction of breakthrough curves requires prior knowledge of the mass-transfer controlling mechanism in the adsorption bed. One purpose of this research was to find such a controlling mechanism. The procedure is as follows:

(1) Calculate the mass-transfer rate at certain points of the bed.

(2) Calculate the mass-transfer coefficients

(3) Use the Thomas equations to calculate the breakthrough curves for the three cases discussed in Chapter 4.

(4) Compare the generated curves with the experimental data. The theoretical curves that most closely matches the experimental data will indicate the limiting resistance if there is one.

This procedure was followed for a number of runs and for some selected bed lengths. Sections A.4 and A.5 show sample calculations of the breakthrough curves for the acid and phenol respectively. In Tables 21 to 50 some of the results of the calculations for the prediction of the breakthrough curves under the influence of the different controlling mechanisms are presented. In Figs 23 to 32 the theoretical breakthrough curves for the three rate limiting mechanisms are compared to the experimental data. It is apparent that the theoretical curve which represents the influence of the Second Order Kinetics curve fits the experimental data better than the two other theoretical curves in case of the DPCA acid. The previously mentionned curves were calculated by the Thomas method for cases where the internal and the external diffusion were the controlling mechanisms. For the phenol the external diffusion rate-limiting theoretical breakthrough curve is closer to the data points than

Table 21 : C/C_0 vs t profile calculated by the Thomas Method

Second Order Kinetics Model

Run One

L2, Z = 30.7 cms

$r^* = 1$

$$\xi = \frac{k_a Q_m^- \rho_b v}{F} = 10.3$$

$$\tau = k_a \left(\frac{1}{K^r} + C_0 \right)\left(t - \frac{Vc}{F} \right) = 8.2(t-0.02)$$

$t = 7.3\,\tau + 1.2$

τ	ξ	$X = \frac{C}{C_0}$	t
6	10.3	0.18	45
9	10.3	0.39	67
15	10.3	0.72	111
21	10.3	0.97	154
30	10.3	1	220

t in minutes

Table 22 : C/C_0 vs t profile calculated by the Thomas Method

Internal Diffusion Model

Run One

L2, Z = 30.7 cms

$r^*_s = 1$

$$\xi = \frac{K_P a_P \rho_b q_e v}{F C_0} = 9.7$$

$$\tau = \frac{K_P a_P}{[r^* + (C/C_0)(1 - r^*)]} \left(t - \frac{v \varepsilon}{F} \right) = 9.68(t-0.02)$$

$t = 6.2 \tau + 1.2$

τ	ξ	$X = \frac{C}{C_0}$	t
5	9.7	0.13	33
10	9.7	0.55	64
15	9.7	0.85	95
20	9.7	0.97	126
25	9.7	1	157

t in minutes

Table 23 : C/C_0 vs t profile calculated by the Thomas Method

External Diffusion Model

Run One

L2, Z = 31 cms

$r^* = 1$

$$\xi = \frac{K_F a_F \epsilon v}{F} = 16.4$$

$$\tau = \frac{K_F a_F \epsilon C_0}{\rho_b q_\infty [\, 1 + (q/q_\infty)(r^* - 1)]} \left(t - \frac{v\,\xi}{F} \right) = 12.68(t-0.02)$$

$t = 4.73\tau + 1.2$

τ	ξ	$X = \frac{C}{C_0}$	t
10	16.4	0.19	48
15	16.4	0.50	72
18	16.4	0.75	86
20	16.4	0.82	93
30	16.4	1	142

t in minutes

Table 24 : C/C_0 vs t profile calculated by the Thomas Method

Second Order Kinetics Model

Run Two

L2, Z = 37.4 cms

$r^* = 1$

$\xi = \frac{k_a Q_m^- \rho_b v}{F} = 10$

$\tau = k_a \left(\frac{1}{K'} + C_0 \right)\left(t - \frac{Ve}{F} \right) = 5.31(t-0.03)$

$t = 11.3\,\tau + 1.8$

τ	ξ	$X = \frac{C}{C_0}$	t
3	10	0.02	35
5	10	0.10	60
7	10	0.17	79
10	10	0.48	115
15	10	0.82	172
20	10	0.95	228

t in minutes

Table 25 : C/C_0 vs t profile calculated by the Thomas Method

Internal Diffusion Model

Run Two

L2, Z = 37.4 cms

$r^* = 1$

$$\xi = \frac{K_P a_P \rho_b q_\infty v}{F C_0} = 9.4$$

$$\tau = \frac{K_P a_P}{[r^* + (C/C_0)(1 - r^*)]} \left(t - \frac{v \varepsilon}{F} \right) = 5(t-0.03)$$

$t = 12\tau + 1.8$

τ	ξ	$X = \frac{C}{C_0}$	t
3	9.4	0.05	38
5	9.4	0.17	62
7	9.4	0.49	86
10	9.4	0.65	122
13	9.4	0.84	158
15	9.4	0.92	182
18	9.4	0.96	218

t in minutes

Table 26 : C/C_0 vs t profile calculated by the Thomas Method

External Diffusion Model

Run Two

L2, Z = 37.4 cms

$r^* = 1$

$$\xi = \frac{K_F a_F \varepsilon v}{F} = 9.4$$

$$\tau = \frac{K_F a_F \varepsilon C_0}{\rho_b q_\infty [\, 1 + (q/q_\infty)(r^* - 1)]} \left(t - \frac{v\,\varepsilon}{F} \right) = 5(t-0.03)$$

$$t = 12\,\tau + 1.8$$

τ	ξ	$X = \frac{C}{C_0}$	t
3	9.4	0.05	38
5	9.4	0.17	62
7	9.4	0.49	86
10	9.4	0.65	122
13	9.4	0.84	158
15	9.4	0.92	182
18	9.4	0.96	218

t in minutes

Table 27 : C/C_0 vs t profile calculated by the Thomas Method

Second Order Kinetics Model

Run Two

L3, Z = 50 cms

$r^* = 1$

$$\xi = \frac{k_a Q_m \rho_b v}{F} = 14$$

$$\tau = k_a \left(\frac{1}{K^T} + C_0\right)\left(t - \frac{Vt}{F}\right) = 5.45(t-0.05)$$

$t = 11\tau + 3$

τ	ξ	$X = \frac{C}{C_0}$	t
5	14	0.01	58
7	14	0.09	80
10	14	0.21	113
15	14	0.51	168
20	14	0.81	223
25	14	0.98	278

t in minutes

Table 28 : C/C_0 vs t profile calculated by the Thomas Method

Internal Diffusion Model

Run Two

L3, Z = 50 cms

$r^* = 1$

$$\xi = \frac{K_P a_P \rho_b q_\infty v}{F C_0} = 13$$

$$\tau = \frac{K_P a_P}{[r^* + (C/C_0)(1 - r^*)]} \left(t - \frac{v \varepsilon}{F} \right) = 5.14(t-0.05)$$

$t = 11.67\ \tau + 3$

τ	ξ	$X = \frac{C}{C_0}$	t
7	13	0.18	85
10	13	0.32	120
15	13	0.72	178
20	13	0.90	237
25	13	0.99	295

t in minutes

Table 29 : C/C_0 vs t profile calculated by the Thomas Method

External Diffusion Model

Run Two

L3, Z = 50 cms

$r^* = 1$

$$\xi = \frac{K_F a_F \varepsilon v}{F} = 13$$

$$\tau = \frac{K_F a_F \varepsilon C_0}{\rho_b q_\infty [\, 1 + (q/q_\infty)(r^* - 1)]} \left(t - \frac{v\,\xi}{F} \right) = 5.13(t-0.05)$$

$$t = 11.7\tau + 3$$

τ	ξ	$X = \frac{C}{C_0}$	t
7	13	0.18	86
10	13	0.32	120
15	13	0.72	178
20	13	0.90	237
25	13	0.99	295

t in minutes

Table 30 : C/C_0 vs t profile calculated by the Thomas Method

Internal Diffusion Model

Run Four

L2, Z = 30.5 cms

$r^* = 0.766$

$$\xi = \frac{K_P a_P \rho_b q_\infty v}{F C_0} = 9.06$$

$$\tau = \frac{K_P a_P}{[r^* + (C/C_0)(1 - r^*)]} \left(t - \frac{v \epsilon}{F} \right) = 1.34(t-0.03)$$

$t = 44.9\tau + 1.8$

τ	$r^* \xi$	$J(r^*\xi, \tau)$	ξ	$r^* \tau$	$J(\xi, r^*\tau)$	$X=C/C_0$	t
5	6.9	0.37	9.06	3.8	0.10	0.14	227
7	6.9	0.69	9.06	5.4	0.27	0.37	316
10	6.9	0.83	9.06	7.7	0.57	0.71	451
12	6.9	0.93	9.06	9.2	0.62	0.83	541
15	6.9	0.98	9.06	11.5	0.83	0.96	675

t in minutes

Table 31 : C/C_0 vs t profile calculated by the Thomas Method

Second Order Kinetics Model

Run Four

L2, Z = 30.5 cms

$r^* = 0.766$

$\xi = \frac{k_a Q_m \rho_b v}{F} = 9.87$

$\tau = k_a \left(\frac{1}{K^T} + C_0 \right)\left(t - \frac{Vc}{F} \right) = 1.316(t-0.03)$

$t = 45.6\tau + 1.8$

τ	$r^* \xi$	$J(r^*\xi, \tau)$	ξ	$r^* \tau$	$J(\xi, r^*\tau)$	$X=C/C_0$	t
5	7.56	0.33	9.87	3.8	0.07	0.10	230
7	7.56	0.60	9.87	5.4	0.21	0.28	321
10	7.56	0.80	9.87	7.7	0.46	0.60	456
12	7.56	0.90	9.87	9.2	0.59	0.78	549
15	7.56	0.96	9.87	11.5	0.73	0.92	686

t in minutes

Table 32 : C/C_0 vs t profile calculated by the Thomas Method

External Diffusion Model

Run Four

L2, Z = 30.5 cms

$r^* = 0.766$

$$\xi = \frac{K_F a_F \varepsilon v}{F} = 10.1$$

$$\tau = \frac{K_F a_F \varepsilon C_0}{\rho_b q_\infty [\, 1 + (q/q_\infty)(r^* - 1)]} \left(t - \frac{v\,\varepsilon}{F} \right) = 1.463(t-0.03)$$

$t = 41\tau + 1.8$

τ	$r^*\xi$	$J(r^*\xi, \tau)$	ξ	$r^*\tau$	$J(\xi, r^*\tau)$	$X=C/C_0$	t
5	7.77	0.27	10.1	3.83	0.05	0.08	207
7	7.77	0.50	10.1	5.36	0.11	0.21	289
10	7.77	0.73	10.1	7.67	0.31	0.50	412
12	7.77	0.85	10.1	9.19	0.42	0.70	494
15	7.77	0.94	10.1	11.5	0.59	0.88	617

Table 33 : C/C_0 vs t profile calculated by the Thomas Method

Internal Diffusion Model

Run Five

L2, Z = 30 cms

$r^* = 1$

$$\xi = \frac{K_P a_P \rho_b q_e v}{F C_0} = 9.9$$

$$\tau = \frac{K_P a_P}{[r^* + (C/C_0)(1 - r^*)]} \left(t - \frac{v \varepsilon}{F} \right) = 9.6(t-0.02)$$

$t = 6.25\xi + 1.2$

τ	ξ	$X = \frac{C}{C_0}$	t
5	9.9	0.18	32
7	9.9	0.44	44
10	9.9	0.61	63
15	9.9	0.90	95
20	9.9	0.98	126

t in minutes

Table 34 : C/C_0 vs t profile calculated by the Thomas Method

External Diffusion Model

Run Five

L2, Z = 30 cms

$r^* = 1$

$$\xi = \frac{K_F a_F \varepsilon v}{F} = 10$$

$$\tau = \frac{K_F a_F \varepsilon C_0}{\rho_b q_\infty [\, 1 + (q/q_\infty)(r^* - 1)]} \left(t - \frac{v\,\varepsilon}{F} \right) = 10(t-0.02)$$

$$t = 6\tau + 1.2$$

τ	ξ	$X = \frac{C}{C_0}$	t
5	10	0.12	31
7	10	0.33	43
10	10	0.54	61
15	10	0.83	91
20	10	0.98	121

t in minutes

Table 35 : C/C_0 vs t profile calculated by the Thomas Method

Second Order Kinetics Model

Run Five

L2, Z = 30 cms

$r^* = 1$

$$\xi = \frac{k_a Q_m \rho_b v}{F} = 8.9$$

$$\tau = k_a \left(\frac{1}{K'} + C_0 \right)\left(t - \frac{V\varepsilon}{F} \right) = 10(t-0.02)$$

$t = 6\tau + 1.2$

τ	ξ	$X = \frac{C}{C_0}$	t
5	8.9	0.20	31
7	8.9	0.47	43
10	8.9	0.64	61
15	8.9	0.92	90
20	8.9	0.99	121

t in minutes

Table 36 : C/C_0 vs t profile calculated by the Thomas Method

Internal Diffusion Model

Run Five

L5, Z = 72 cms

$r^* = 1$

$$\xi = \frac{K_P a_P \rho_b q_\infty v}{F C_0} = 24$$

$$\tau = \frac{K_P a_P}{[r^* + (C/C_0)(1 - r^*)]} \left(t - \frac{v \varepsilon}{F} \right) = 9.6(t-0.05)$$

$t = 6.25\tau + 3$

τ	ξ	$X = \frac{C}{C_0}$	t
20	24	0.25	128
25	24	0.48	160
30	24	0.76	191
35	24	0.94	222

t in minutes

Table 37 : C/C_0 vs t profile calculated by the Thomas Method

External Diffusion Model

Run Five

L4, Z = 72 cms

$r^* = 1$

$$\xi = \frac{K_F a_F \varepsilon v}{F} = 24$$

$$\tau = \frac{K_F a_F \varepsilon C_0}{\rho_b q_\infty [\, 1 + (q/q_\infty)(r^* - 1)]} \left(t - \frac{v\,\varepsilon}{F} \right) = 10(t-0.05)$$

$$t = 6\,\tau + 3$$

τ	ξ	$X = \frac{C}{C_0}$	t
20	24	0.25	123
25	24	0.48	153
30	24	0.76	183
25	24	0.94	213

t in minutes

Table 38 : C/C_0 vs t profile calculated by the Thomas Method

Second Order Kinetics Model

Run Five

L4, Z = 72 cms

$r^* = 1$

$\xi = \frac{k_a Q_m \rho_b v}{F} = 23$

$\tau = k_a \left(\frac{1}{K^T} + C_0 \right)\left(t - \frac{Ve}{F} \right) = 10(t-0.05)$

$t = 6\tau + 3$

τ	ξ	$X = \frac{C}{C_0}$	t
20	23	0.29	123
25	23	0.50	153
30	23	0.78	183
35	23	0.95	213

t in minutes

Table 39 : C/C_0 vs t profile calculated by the Thomas Method

Second Order Kinetics Model

Run six

L2, Z = 31 cms

$r^* = 0.725$

$\xi = \frac{k_a Q_m \rho_b v}{F} = 6.4$

$\tau = k_a \left(\frac{1}{K'} + C_0\right)\left(t - \frac{Vt}{F}\right) = 1.05(t-0.03)$

$t = 57\tau + 1.8$

τ	$r^*\xi$	$J(r^*\xi, \tau)$	ξ	$r^*\tau$	$J(\xi, r^*\tau)$	$X=C/C_0$	t
2	4.6	0.23	6.4	1.5	0.06	0.07	115
4	4.6	0.50	6.4	2.9	0.18	0.24	229
6	4.6	0.70	6.4	4.4	0.30	0.47	343
8	4.6	0.84	6.4	5.8	0.50	0.72	457
9	4.6	0.92	6.4	6.5	0.59	0.82	514
10	4.6	0.94	6.4	7.3	0.65	0.88	571

t in minutes

Table 40 : C/C_0 vs t profile calculated by the Thomas Method

Internal Diffusion Model

Run six

L2, Z = 31 cms

$r^* = 0.725$

$\xi = \frac{K_P a_P \rho_b q_e v}{F C_0 K_P a_P} = 5$

$\tau = \frac{K_P a_P}{[r^* + (C/C_0)(1 - r^*)]} \left(t - \frac{v \varepsilon}{F} \right) = 0.967(t-0.02^{\prime})$

$t = 62 \tau + 1.2$

τ	$r^* \xi$	$J(r^*\xi, \tau)$	ξ	$r^* \tau$	$J(\xi, r^*\tau)$	$X=C/C_0$	t
2	3.6	0.33	5	1.5	0.13	0.14	125
3	3.6	0.49	5	2.2	0.21	0.26	187
4	3.6	0.62	5	2.9	0.31	0.40	249
5	3.6	0.62	5	3.6	0.40	0.52	311
6	3.6	0.84	5	4.4	0.50	0.69	373
7	3.6	0.91	5	5.1	0.58	0.79	435
8	3.6	0.96	5	5.8	0.69	0.88	497

t, minutes

Table 41 : C/C_0 vs t profile calculated by the Thomas Method

External Diffusion Model

Run six

L2, Z = 31 cms

$r^* = 0.725$

$$\xi = \frac{K_F a_F \epsilon v}{F} = 5.55$$

$$\tau = \frac{K_F a_F \epsilon C_0}{\rho_b q_\infty [\, 1 + (q/q_\infty)(r^* - 1)]} \left(t - \frac{v\,\epsilon}{F} \right) = 1.149(t-0.02)$$

$t = 52.2\tau + 1.2$

τ	$r^*\xi$	$J(r^*\xi, \tau)$	ξ	$r^*\tau$	$J(\xi, r^*\tau)$	$X=C/C_0$	t
1	4	0.14	5.55	0.7	0.05	0.04	75
2	4	0.29	5.55	1.5	0.08	0.11	113
3	4	0.45	5.55	2.2	0.16	0.20	170
4	4	0.60	5.55	2.9	0.24	0.34	226
5	4	0.69	5.55	3.6	0.33	0.47	282
6	4	0.85	5.55	4.4	0.44	0.64	338
7	4	0.90	5.55	5.1	0.52	0.78	395

t in minutes

Table 42 : C/C_0 vs t profile calculated by the Thomas Method

Second Order Kinetics Model

Run six

L3, Z = 51 cms

$r^* = 0.725$

$\xi = \frac{k_a Q_m \rho_b V}{F} = 10.5$

$\tau = k_a \left(\frac{1}{K'} + C_0\right)\left(t - \frac{Vc}{F}\right) = \left(t - \frac{V\xi}{F}\right) = 0.95(t-0.03)$

$t = 63.2\tau + 1.8$

τ	$r^*\xi$	$J(r^*\xi, \tau)$	ξ	$r^*\tau$	$J(\xi, r^*\tau)$	$X=C/C_0$	t
3	7.6	0.10	10.5	2.2	0.01	0.01	191
5	7.6	0.28	10.5	3.6	0.10	0.06	318
7	7.6	0.53	10.5	5.5	0.31	0.23	444
10	7.6	0.78	10.5	7.3	0.52	0.59	634
12	7.6	0.85	10.5	8.7	0.72	0.85	760
15	7.6	0.95	10.5	10.9	0.81	0.95	950

t in minutes

Table 43 : C/C_0 vs t profile calculated by the Thomas Method

Internal Diffusion Model

Run six

L3, Z = 51 cms

$r^* = 0.725$

$$\xi = \frac{K_P a_P \rho_b q_- v}{F C_0 K_P a_P} = 8.7$$

$$\tau = \frac{}{[r^* + (C/C_0)(1 - r^*)]} \left(t - \frac{v \epsilon}{F} \right) = 0.967 \, (t - 0.02)$$

$t = 62\tau + 1.2$

τ	$r^* \xi$	$J(r^*\xi, \tau)$	ξ	$r^* \tau$	$J(\xi, r^*\tau)$	$X=C/C_0$	t
2	6.3	0.09	8.7	1.5	0.01	0.0	126
5	6.3	0.37	8.7	3.6	0.09	0.14	312
7	6.3	0.70	8.7	5.1	0.27	0.36	436
10	6.3	0.85	8.7	7.3	0.49	0.71	622
11	6.3	0.91	8.7	8.0	0.58	0.81	884

t in minutes

Table 44 : C/C_0 vs t profile calculated by the Thomas Method

External Diffusion Model

Run Six

L3, Z = 51 cms

$r^* = 0.725$

$$\xi = \frac{K_F a_F \epsilon v}{F} = \frac{K_F a_F \epsilon C_0}{\rho_b q_\infty [\, 1 + (q/q_\infty)(r^* - 1)]} \left(t - \frac{v\,\epsilon}{F} \right) = 1.149(t-0.03)$$

$$t = 52.2\,\tau + 1.8$$

τ	$r^*\xi$	$J(r^*\xi, \tau)$	ξ	$r^*\tau$	$J(\xi, r^*\tau)$	$X=C/C_0$	t
2	6.6	0.07	9.13	1.5	0.01	0.0	106
5	6.6	0.40	9.13	3.6	0.07	0.13	263
7	6.6	0.65	9.13	5.1	0.16	0.28	367
9	6.6	0.80	9.13	6.5	0.32	0.53	472
10	6.6	0.82	9.13	7.3	0.35	0.62	524
11	6.6	0.84	9.13	8.0	0.46	0.72	576

t in minutes

Table 45 : C/C_0 vs t profile calculated by the Thomas Method

Internal Diffusion Model

Run Three

L1, Z = 20 cms

$r^* = 0.766$

$$\xi = \frac{K_P a_P \rho_b q_\infty v}{F C_0} = 8.3$$

$$\tau = \frac{K_P a_P}{[r^* + (C/C_0)(1 - r^*)]} \left(t - \frac{v \varepsilon}{F} \right) = 1.5(t-0.02)$$

$t = 40\tau + 1.2$

τ	$r^* \xi$	$J(r^*\xi, \tau)$	ξ	$r^* \tau$	$J(\xi, r^*\tau)$	$X=C/C_0$	t
4	6.38	0.22	8.3	2.3	0.03	0.08	161
5	6.38	0.37	8.3	3.8	0.10	0.16	201
7	6.38	0.60	8.3	5.4	0.23	0.38	281
8	6.38	0.70	8.3	6.1	0.39	0.52	321
10	6.38	0.80	8.3	7.7	0.51	0.71	401
12	6.38	0.90	8.3	9.2	0.63	0.85	481
15	6.38	0.98	8.3	11.5	0.78	0.95	601

t in minutes

Table 46 : C/C_0 vs t profile calculated by the Thomas Method

External Diffusion Model

Run Three

L1, Z = 20 cms

$r^* = 0.766$

$$\xi = \frac{K_F a_F \epsilon v}{F} = 8.3$$

$$\tau = \frac{K_F a_F \epsilon C_0}{\rho_b q_\infty [\, 1 + (q/q_\infty)(r^* - 1)]} \left(t - \frac{v \xi}{F} \right) = 2.245(t - 0.02)$$

$$t = 26.73\tau + 1.2$$

τ	$r^* \xi$	$J(r^*\xi, \tau)$	ξ	$r^* \tau$	$J(\xi, r^*\tau)$	$X = C/C_0$	t
5	6.99	0.31	8.3	3.8	0.06	0.11	135
8	6.99	0.61	8.3	6.1	0.31	0.32	215
10	6.99	0.78	8.3	7.7	0.42	0.48	269
15	6.99	0.94	8.3	11.5	0.71	0.93	402

t in minutes

Table 47 : C/C_0 vs t profile calculated by the Thomas Method

Second Order Kinetics Model

Run Three

L1, Z = 20 cms

$r^* = 0.766$

$\xi = \frac{k_a Q_a \rho_b \Psi}{F} = 7.3$

$\tau = k_a \left(\frac{1}{K^T} + C_0 \right)\left(t - \frac{Vc}{F} \right) = 1.5(t-0.02)$

$t = 40\tau + 1.2$

τ	$r^* \xi$	$J(r^*\xi, \tau)$	ξ	$r^* \tau$	$J(\xi, r^*\tau)$	$X=C/C_0$	t
4	6.38	0.48	7.3	2.3	0.10	0.20	161
5	6.38	0.55	7.3	3.8	0.20	0.29	201
7	6.38	0.80	7.3	5.4	0.40	0.56	281
8	6.38	0.85	7.3	6.1	0.58	0.71	321
10	6.38	0.91	7.3	7.7	0.70	0.85	401
12	6.38	0.95	7.3	9.2	0.78	0.93	481
15	6.38	0.99	7.3	11.5	0.86	0.98	601

t in minutes

Table 48 : C/C_0 vs t profile calculated by the Thomas Method

Internal Diffusion Model

Run Three

L3, Z = 49.7 cms

$r^* = 0.766$

$$\xi = \frac{K_p a_p \rho_b q_\infty v}{F C_0} = 6.1$$

$$\tau = \frac{K_p a_p}{[r^* + (C/C_0)(1 - r^*)]} \left(t - \frac{v \varepsilon}{F} \right) = 1.5(t-0.05)$$

$t = 40 \tau + 3$

τ	$r^* \xi$	$J(r^*\xi, \tau)$	ξ	$r^* \tau$	$J(\xi, r^*\tau)$	$X=C/C_0$	t
6	15.1	0.05	19.7	4.6	0.00	0.00	243
8	15.1	0.17	19.7	6.1	0.00	0.01	323
10	15.1	0.20	19.7	7.7	0.02	0.02	403
12	15.1	0.35	19.7	9.1	0.04	0.06	483
15	15.1	0.55	19.7	11.5	0.10	0.17	603
20	15.1	0.84	19.7	15.3	0.29	0.56	803
25	15.1	0.97	19.7	19.2	0.57	0.89	1003

t in minutes

Table 49 : C/C_0 vs t profile calculated by the Thomas Method

Second Order Kinetics Model

Run Three

L3, Z = 49.7 cms

$r^* = 0.766$

$\xi = \frac{k_a Q_e \rho_b Y}{F} = 17.2$

$\tau = k_a \left(\frac{1}{K'} + C_0 \right)\left(t - \frac{Ve}{F} \right) = 1.5(t-0.05)$

$t = 40\tau + 3$

τ	$r^*\xi$	$J(r^*\xi, \tau)$	ξ	$r^*\tau$	$J(\xi, r^*\tau)$	$X=C/C_0$	t
10	13.2	0.20	17.2	7.7	0.04	0.04	403
12	13.2	0.40	17.2	9.2	0.05	0.08	483
15	13.2	0.56	17.2	11.5	0.12	0.20	603
20	13.2	0.86	17.2	15.3	0.30	0.60	803
25	13.2	0.98	17.2	19.2	0.58	0.93	1002

t in minutes

Table 50 : C/C_0 vs t profile calculated by the Thomas Method

External Diffusion Model

Run Three

L1, Z = 49.7 cms

$r^* = 0.766$

$$\xi = \frac{K_F a_F \epsilon v}{F} = 21.6$$

$$\tau = \frac{K_F a_F \epsilon C_0}{\rho_b q_\infty [\, 1 + (q/q_\infty)(r^* - 1)]} \left(t - \frac{v\,\epsilon}{F} \right) = 2.245(t - 0.05)$$

$$t = 26.73\tau + 3$$

τ	$r^*\xi$	$J(r^*\xi, \tau)$	ξ	$r^*\tau$	$J(\xi, r^*\tau)$	$X = C/C_0$	t
10	16.6	0.10	21.6	7.7	0.00	0.00	270
15	16.6	0.32	21.6	11.5	0.03	0.07	403
17	16.6	0.42	21.6	13.0	0.05	0.13	456
20	16.6	0.69	21.6	15.3	0.10	0.35	537
23	16.6	0.81	21.6	17.6	0.20	0.58	617
25	16.6	0.84	21.6	19.2	0.28	0.72	670
30	16.6	0.96	21.6	23.0	0.51	0.93	804

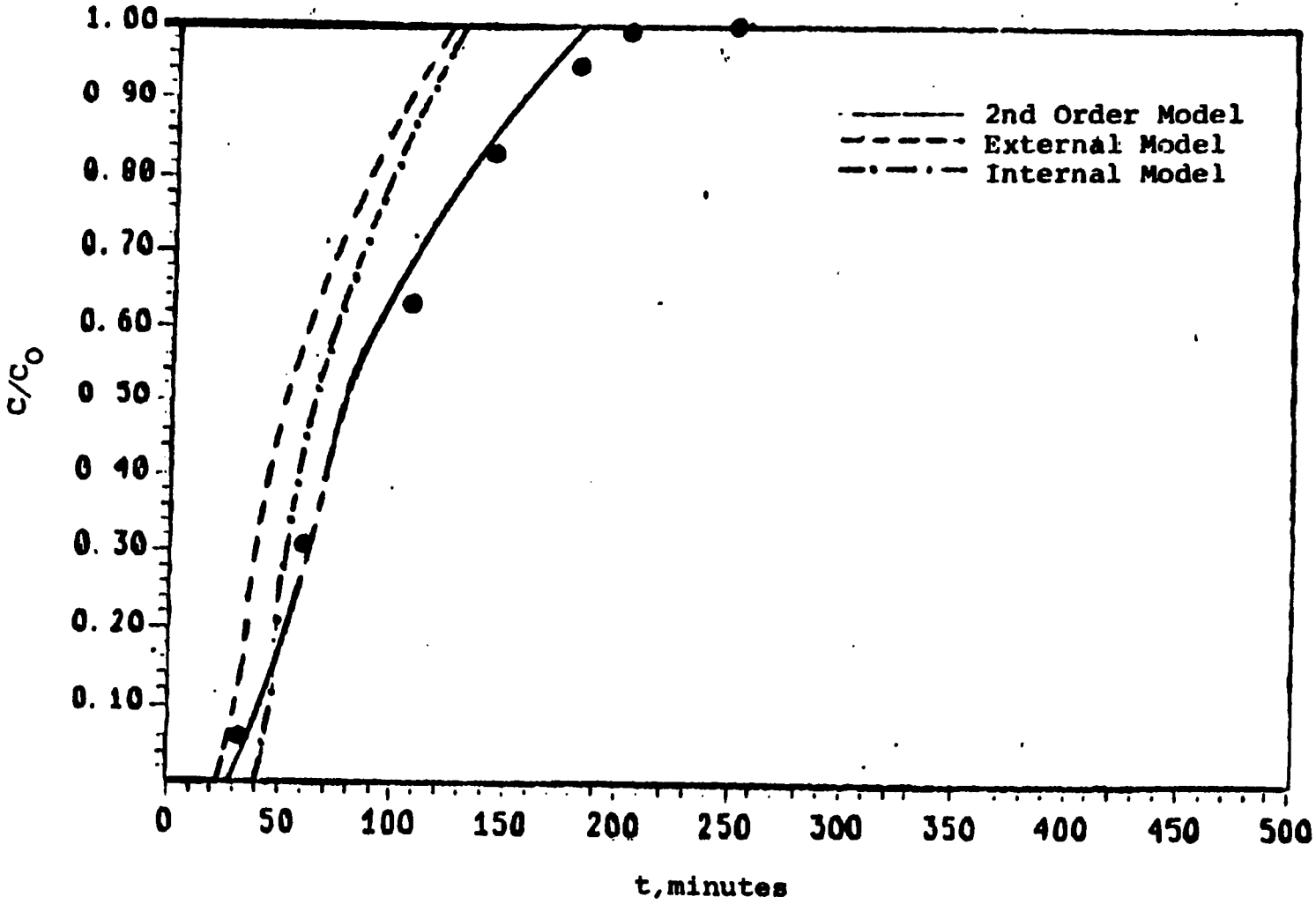

Fig 23 : Predicted Curves Compared to the Experimental data-RUN 1,L2.

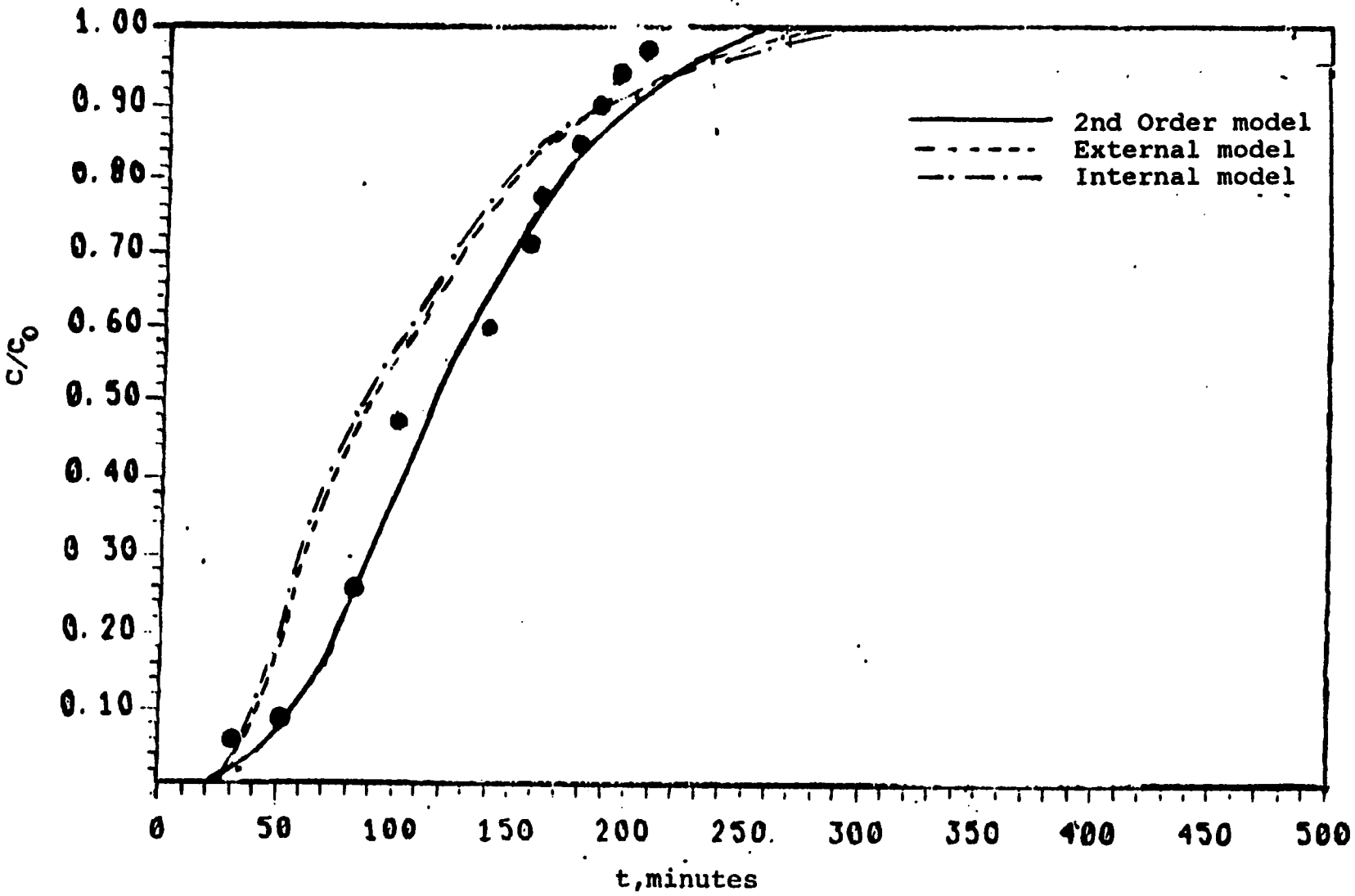

Fig 24 : Predicted Curves Compared to the Experimental data-RUN 2,L2.

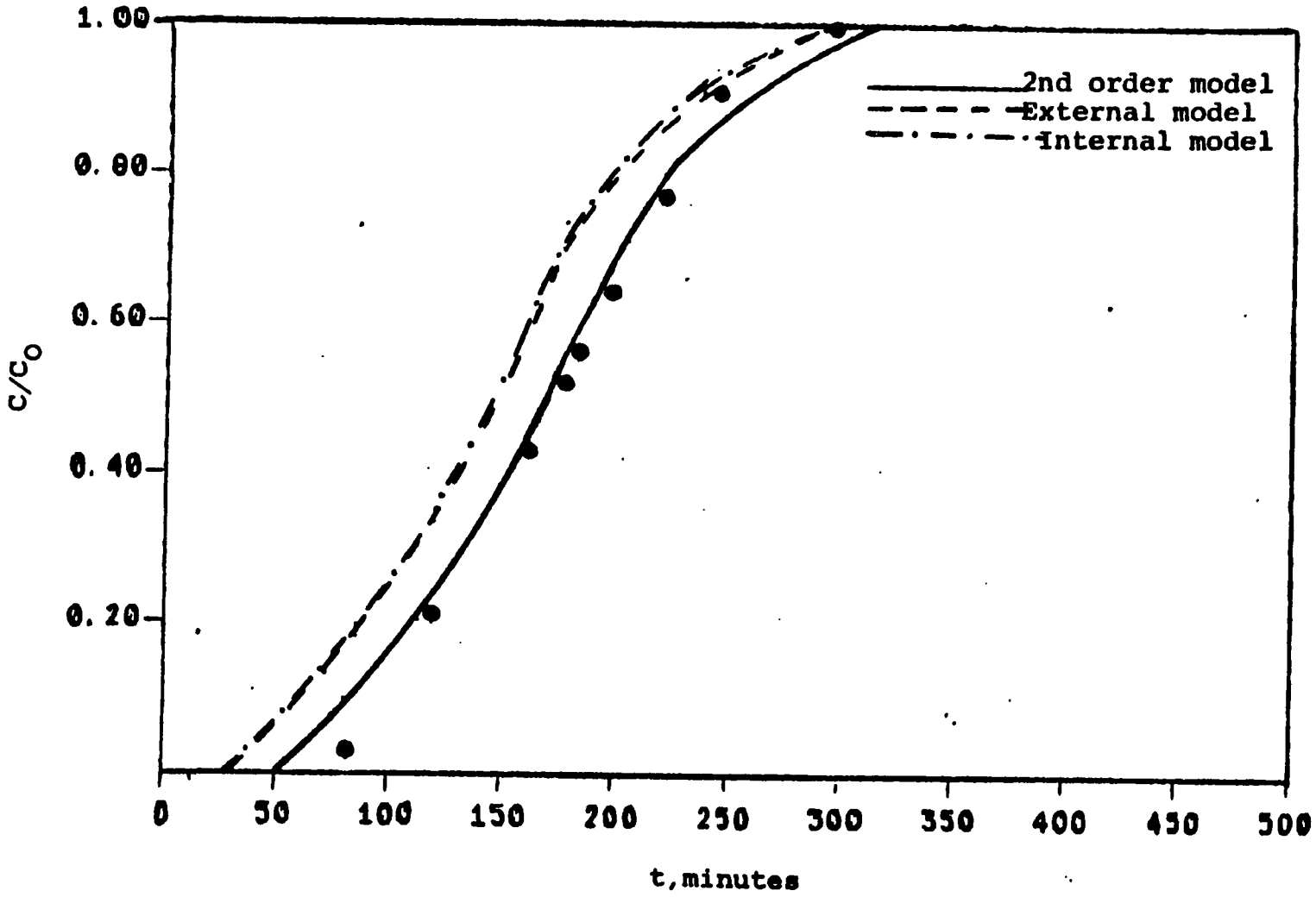

Fig 25 : Predicted Curves Compared to the Experimental data-RUN 2,L3

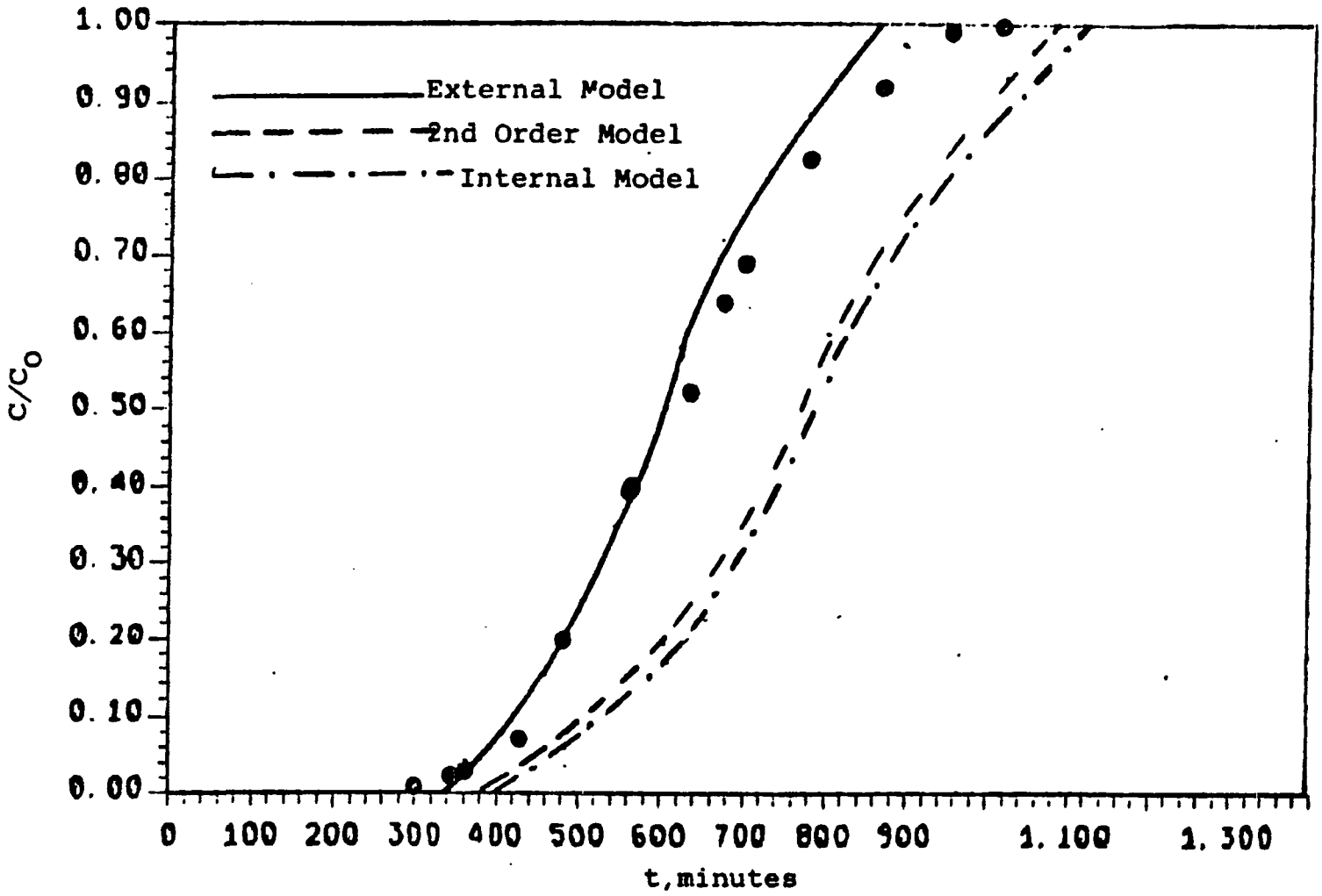

Figure 26: predicted curves compared to the experimental data -Run 3,L

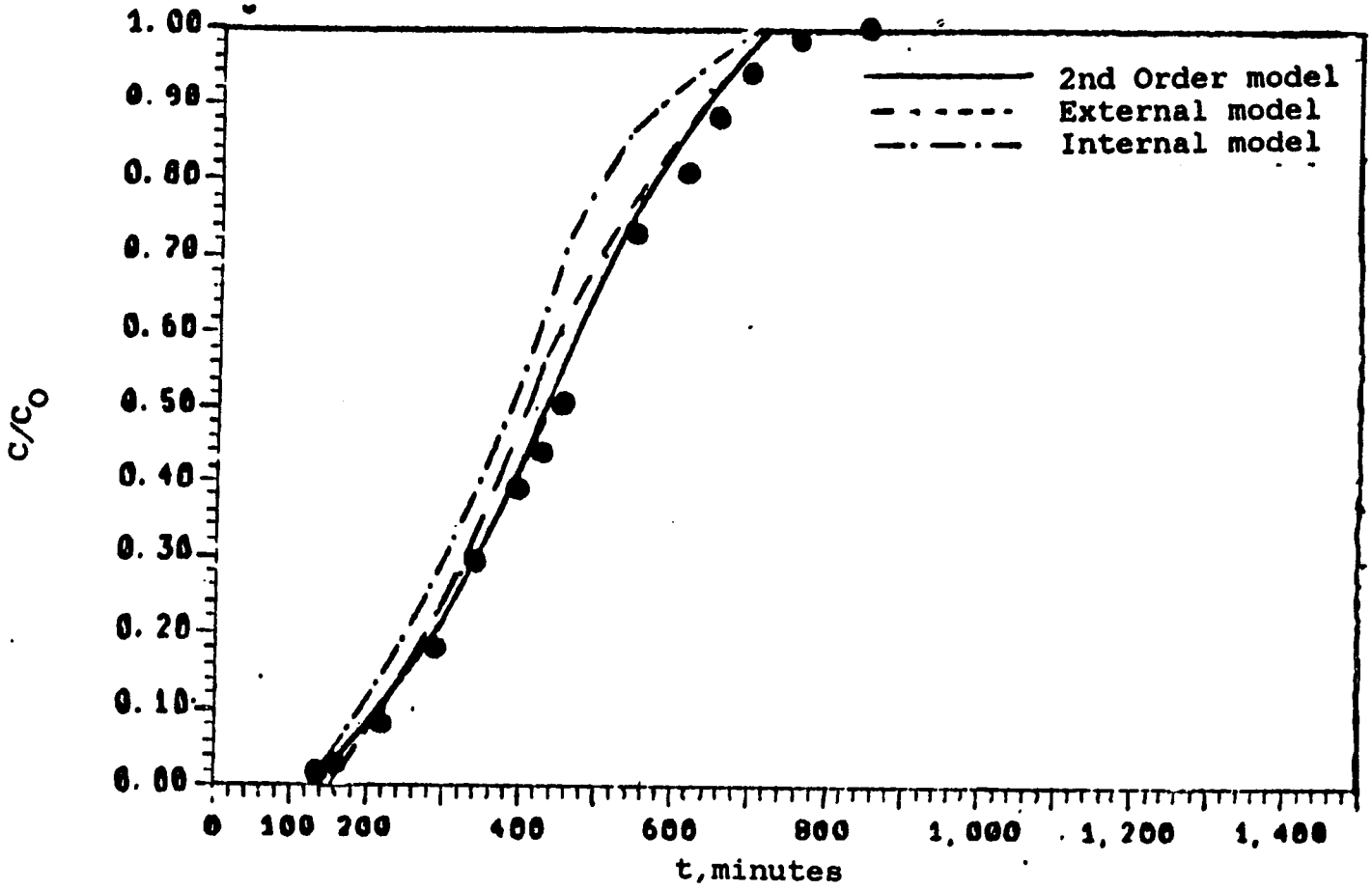

Fig 27 : Predicted Curves Compared to the Experimental data-RUN 4,L2.

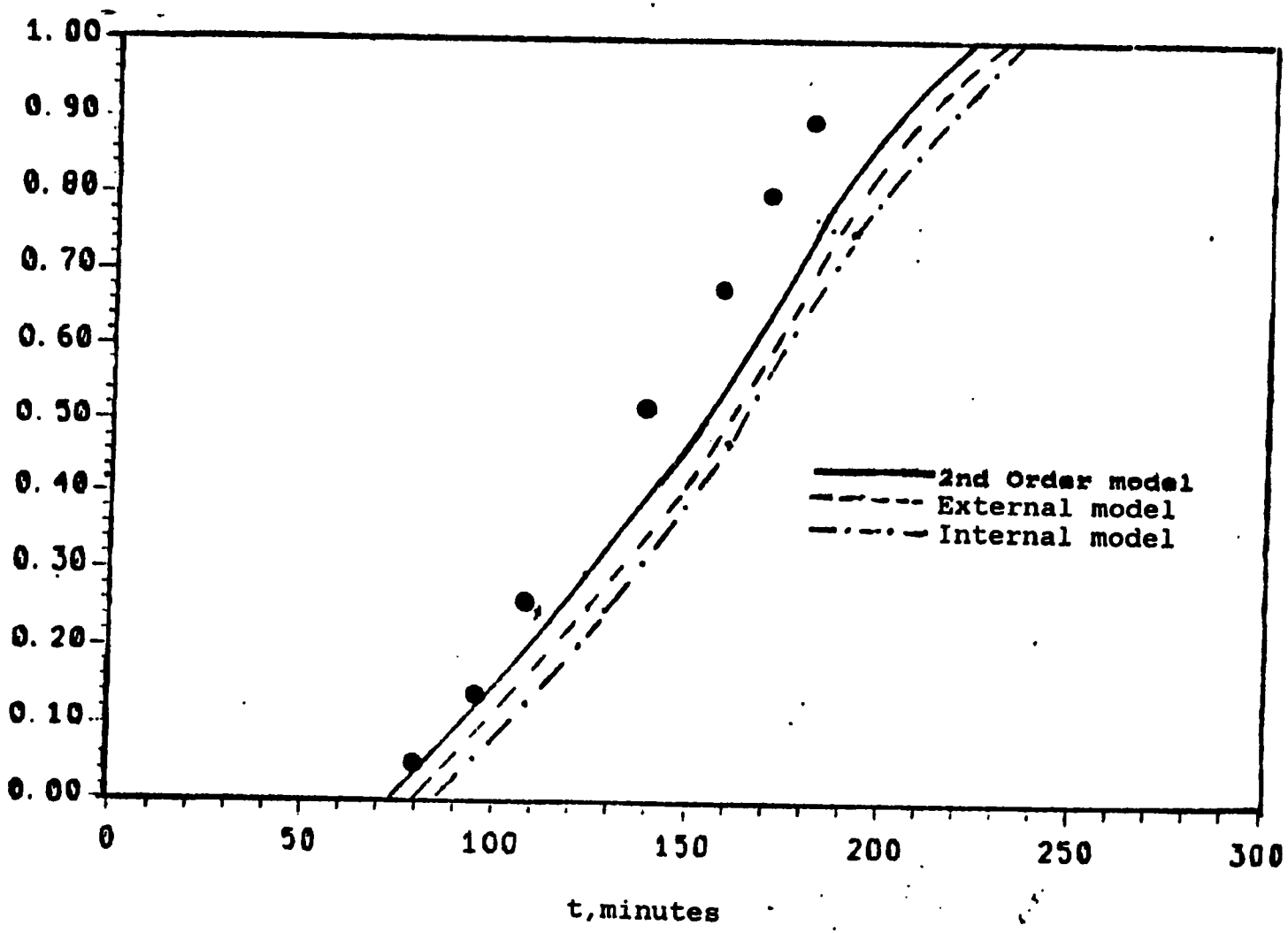

Fig 28 : Predicted Curves Compared to the Experimental data-RUN 5,L2.

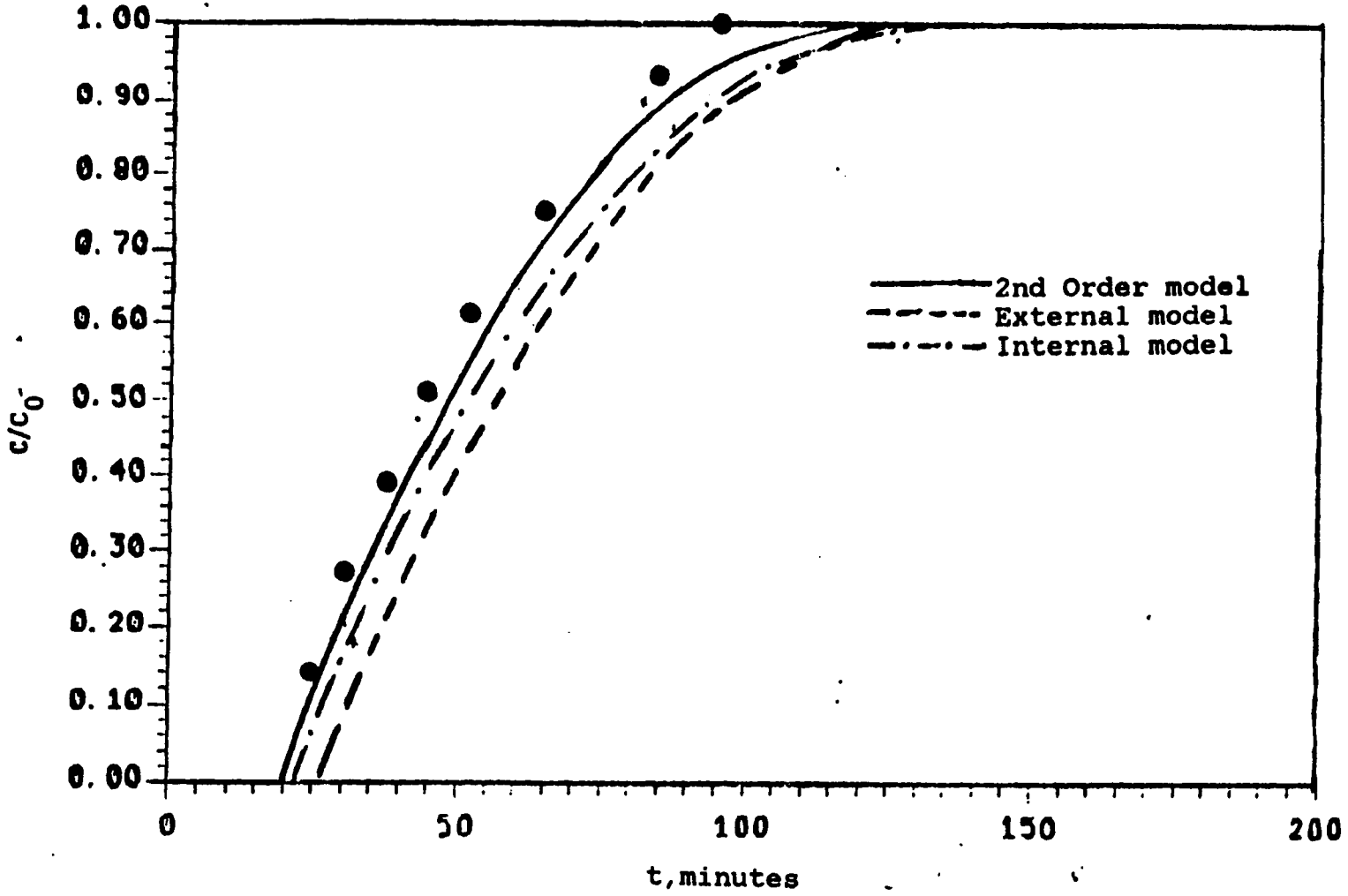

Fig 29 : Predicted Curves Compared to the Experimental data-RUN 5,L4.

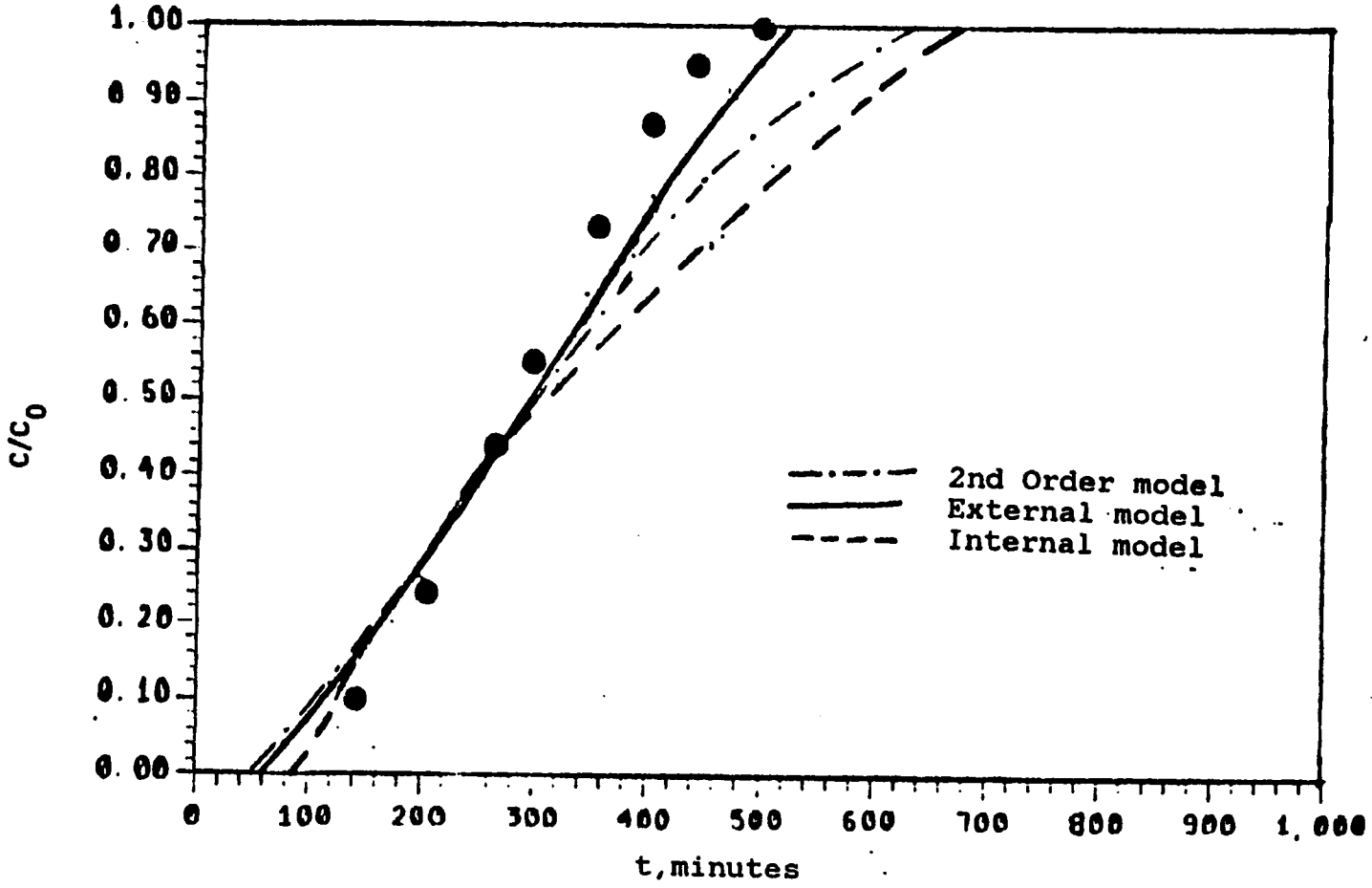

Fig 30 : Predicted Curves Compared to the Experimental data-RUN 6,L2.

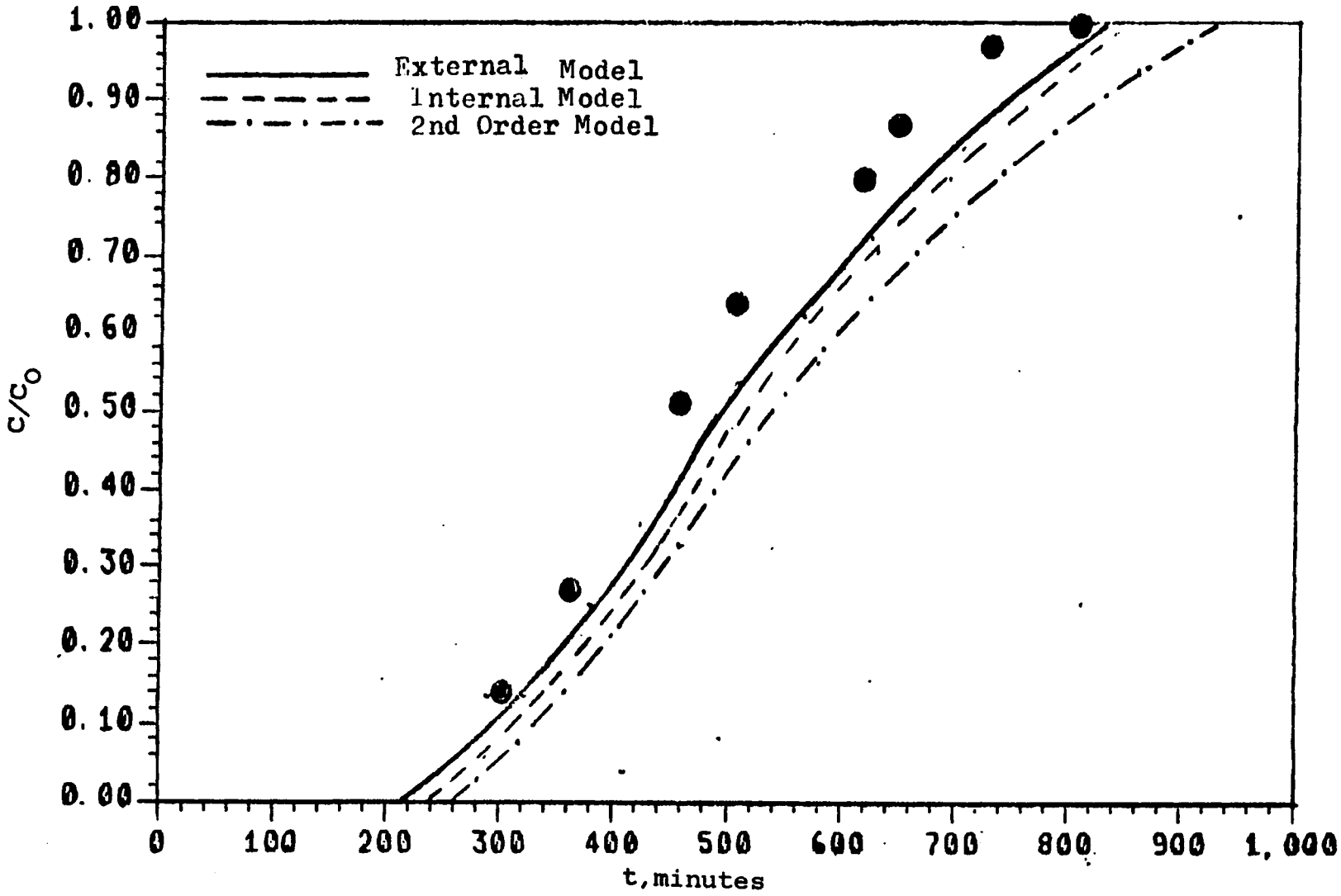

Fig 31 : Predicted Curves Compared to the Experimental data-RUN 6,L3.

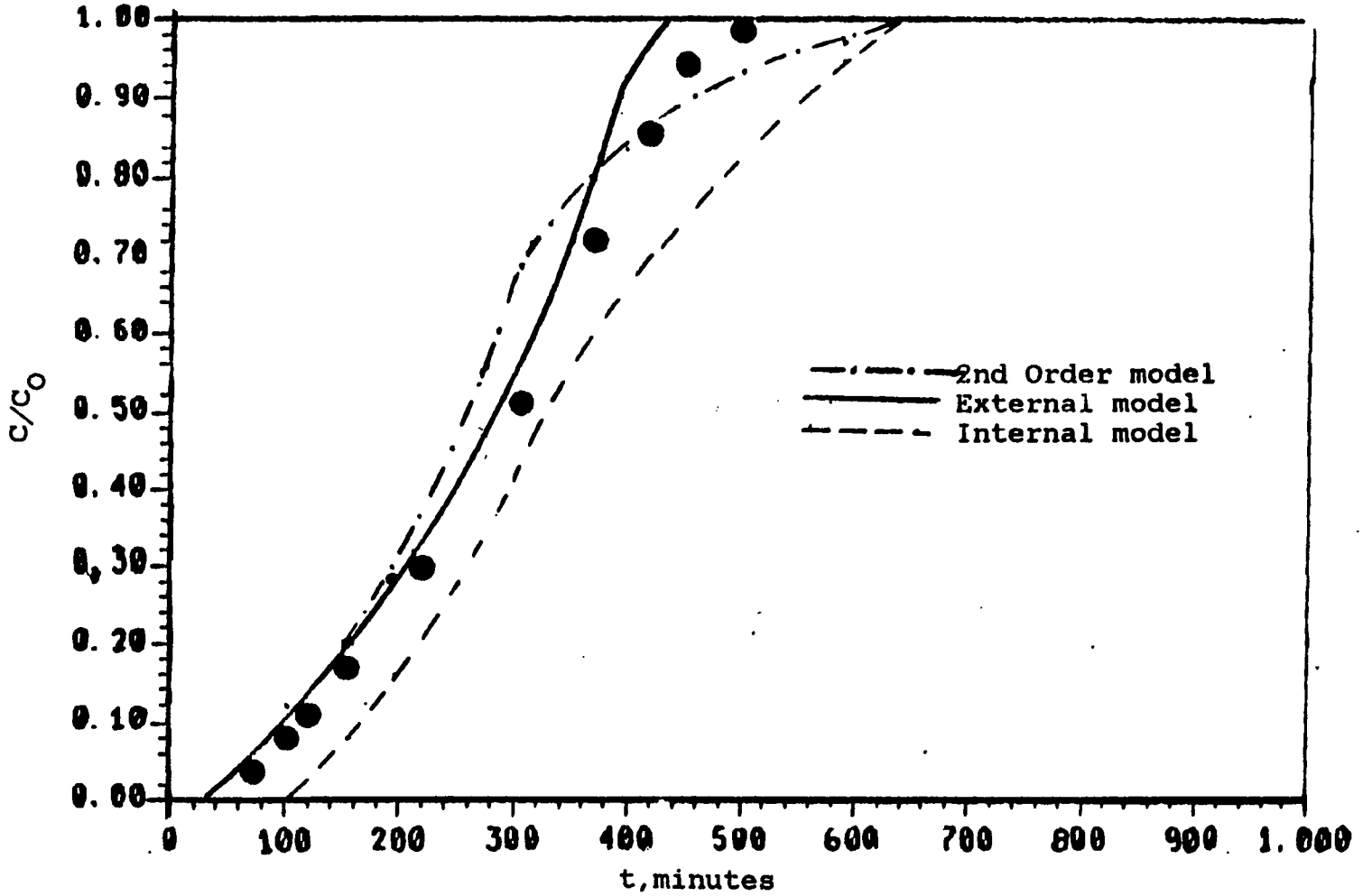

Fig 32 : Predicted Curves Compared to the Experimental data-RUN 3,L1.

the other two curves representing the internal diffusion and second order kinetic limitations. In some cases the theoretical curves are fairly close to one another. From this study it may be concluded that the external diffusion is the controlling mechanism in the case of the phenol. The reaction at the surface is the slowest step in the adsorption of the DPCA acid on the XAD-7 resin.

It is possible to suggest an explanation as to the difference of the rates observed in this study. The DPCA acid is much more acidic than phenol. Though weakly acidic itself, the phenol will behave as a base in presence of an acidic adsorbent such as the XAD-7 resin . Since the DPCA acid is more acidic than the phenol its adsorption on an acidic adsorbent may be expected to be slow. This is actually the case. It seems that the adsorption on the surface is the slowest step.

The adsorption of the phenol on the adsorbent should not present any difficulty because of its relatively basic nature in the presence of the acidic resin. Since the resin is macroreticular, i.e. its

pores have been treated for enlargement, it may be expected that the internal diffusion should not be problematic. The remaining alternative is then the external diffusion. Therefore the results found in this study are plausible.

6.4.2 Regeneration Studies

The last part of the research is to verify the claim that the XAD-7 resin is easily regenerated. This is done by conducting a column experiment starting with a certain initial concentration and flowrate. The solution is passed until saturation of the bed is achieved. Then, distilled water is passed through the bed at the same flowrate.

Tables 51 and 52 show the data obtained for the two runs, one for the acid and the other for the phenol. The corresponding plots are shown in Figs 33 and 34.

For the acid the regeneration curve is a mirror image of the forward curve. This shows that regeneration should present no problem. And since the

equilibrium relationship is linear, it suggests that the controlling mechanism for both the adsorption and regeneration of DPCA acid on the XAD-7 resin is the same.

For the phenol it is seen that the desorption proceeds at a relatively slower rate at the beginning and then increases as the concentration of the solute in the bed decreases. This is expected because the equilibrium isotherm follows the Langmuir model.

Table 51 Experimental data for Phenol regeneration curves

ADSORPTION				DESORPTION			
L1		L2		L1		L2	
t	C/C_0	t	C/C_0	t	C/C_0	t	C/C_0
100	0.12	200	0.03	65	0.96	285	0.91
170	0.27	275	0.16	145	0.79	380	0.79
230	0.52	340	0.28	230	0.60	445	0.61
280	0.65	390	0.38	290	0.44	545	0.38
335	0.78	470	0.58	335	0.29	595	0.23
365	0.83	552	0.73	380	0.20	650	0.11
410	0.89	601	0.80	425	0.12	712	0.07
500	0.99	700	0.91	495	0.09		
		776	0.99				

t in minutes

Table 52 : Experimental data for DPCA acid regeneration curves

ADSORPTION				DESORPTION			
L1		L2		L1		L2	
t	C/C_0	t	C/C_0	t	C/C_0	t	C/C_0
22	0.27	28	0.13	20	0.75	45	0.75
42	0.46	43	0.24	38	0.59	60	0.60
68	0.72	72	0.53	60	0.35	81	0.43
105	0.89	108	0.70	90	0.15	132	0.17
149	0.99	148	0.88	124	0.05	180	0.06
		177	0.93	150	0.01	202	0.01
		204	0.99				

t in minutes

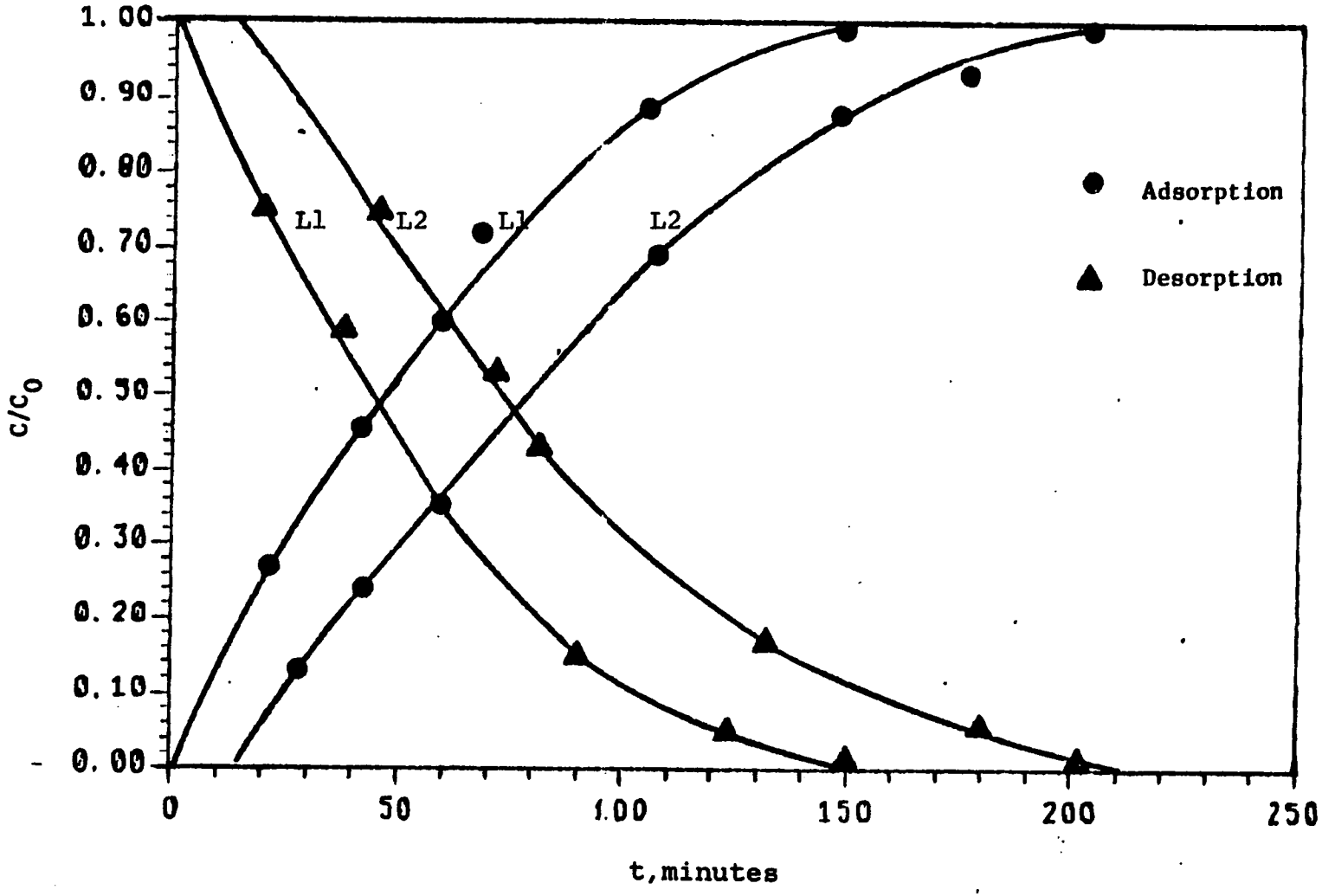

Fig 33 : Regeneration Curve for DPCA Acid.

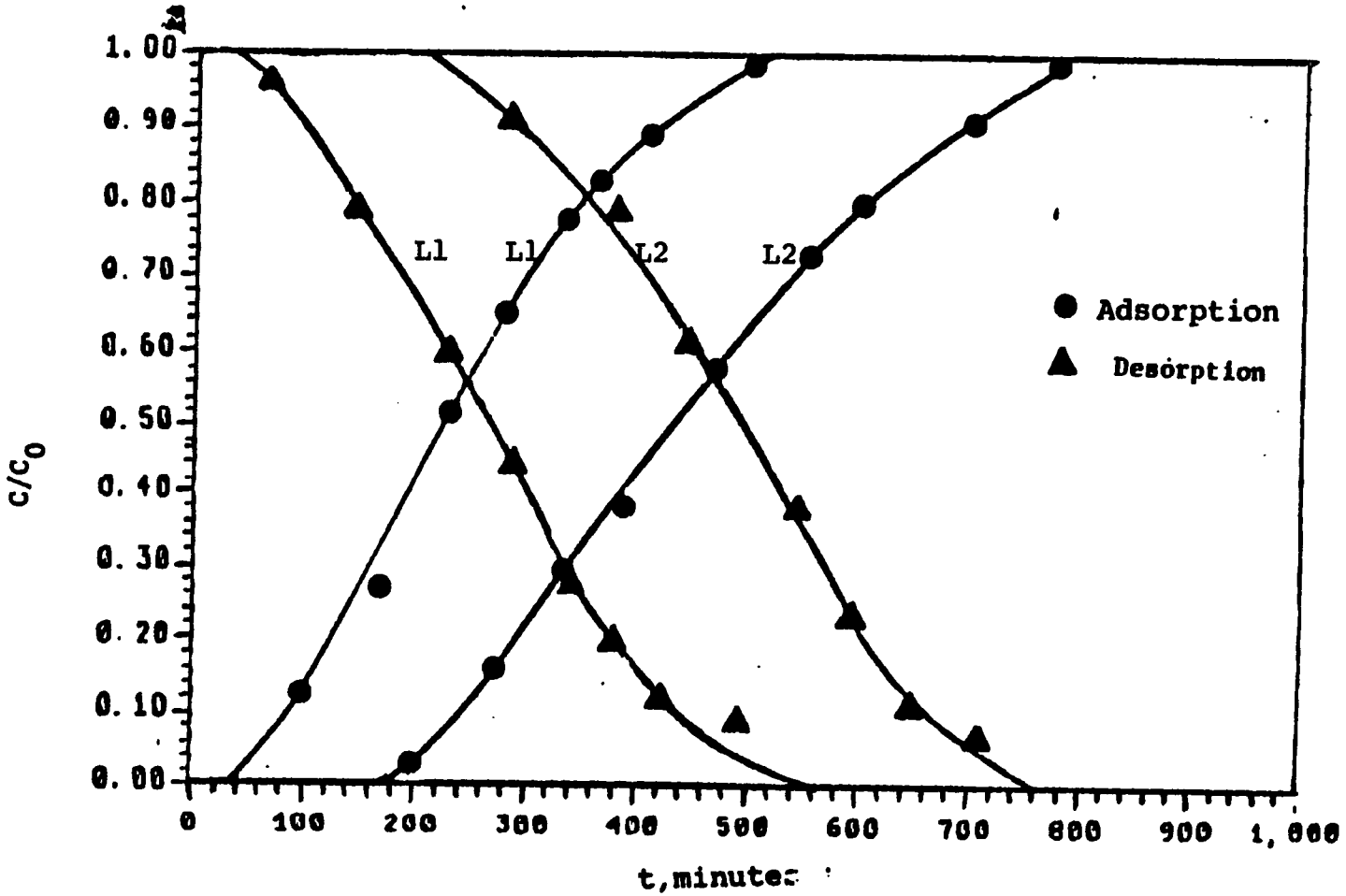

Fig 34 : Regeneration Curve for Phenol.

CHAPTER SEVEN

CONCLUSIONS AND RECOMMENDATIONS

The results obtained in the previous chapter indicate that the macroreticular resin XAD-7 is effective in adsorbing organic matter from waste waters. The XAD-7 resin costs about 19 US dollars per kilogram and the average price of activated carbon is about 15 to 17 dollars per kilogram. For the same concentration, activated carbon adsorbs more organic matter per gram of adsorbent than the phenol. But this is more than compensated for by the ease of regeneration of the resin. In this study it was found that equilibrium is established very quickly, in fact in less than three hours. This suggests that the rate of adsorption on the surface may be faster on the XAD-7 resin than on the activated carbon. Hence, the resin offers an attractive alternative to activated carbon for the removal of organic impurities from waste waters.

The experimental isotherms were found to fit the Langmuir model for the phenol and a linear relationship for the acid. The experimental data were also fitted with the Freundlich equation. The results of mixture adsorption indicate that the phenol and the DPCA acid do not compete with each other for adsorption sites. The heat of

adsorption was calculated for both compounds, and their magnitude indicates that the adsorbate molecules are held by Van der Waals forces or weak chemical bonds. This was further confirmed by the ease of regeneration which took almost the same time as for adsorption.

The experimental adsorption breakthrough curves which were obtained at different conditions showed that the flowrate had an effect on the slope of the breakthrough curves and hence the adsorption rate. The overall rate of adsorption increased with flowrate. Mass transfer coefficients for adsorption of the DPCA acid and phenol were calculated by the differential method. Theoretical breakthrough curves were generated by using the Thomas model and the Langmuir and linear isotherms for phenol and DPCA respectively. These theoretical curves were matched to the experimental data to determine the limiting rate mechanism. The rate mechanisms investigated were internal diffusion, external diffusion and second order adsorption kinetics. The results showed that the layer surrounding the solid was the main resistance to the adsorption of phenol, and that adsorption on the surface was the slowest step for the DPCA acid.

One difficulty encountered in this study was the pressure drop in the bed. For this reason the adsorption

has not been studied with smaller particles, though it was possible to crush the available ones. If the resin is to be used on a large scale in an industrial adsorption bed, it would be advantageous to use a bigger size particle. This can be done by pelletising the resin. An attempt has been made to do this in the laboratory, but the resin was too resilient and the experiment failed. But if a good binder which would not affect the adsorbing properties of the resin could be found, it might be possible to pelletise the resin. It is recommended, therefore, to search for such a binder. Column experiments with mixtures of phenol and DPCA acid should be carried out to study the packed bed adsorption of multicomponent solutions of these two compounds. It is further recommended that studies of adsorption of other organic compounds be carried out to further assess the effectiveness of adsorption of the resin on a greater range of compounds.

LIST OF REFERENCES

1. Gustafson,R.L.,Albright,R.L.,and Reid,O.T,Ind. Eng. Chem. Prod. Res. Dev., 7,107,(1968).

2. Paleos,J.,J. Colloid Interface Sci.,31,7,(1969).

3. Brunauer,S.,Emmett,P.H,and Teller,E.,J. Amer. Soc.,60,309, (1938).

4. Langmuir,I.,J. Amer. Chem. Soc.,40,1368,(1918).

5. Engel,H.C.,and Coull,J., Trans. AICHE,33,947,(1942).

6. Barry,H.M.,Chem. Eng. Prog.,67,105,(1960).

7. Hougen,O.A.,and Marshall,W.R.,Chem. Eng. Prog.,43,197,(1947).

8. Klotz,I.M.,Chem. Rev.,38,241,(1946).

9. Antonson,C.R.,Ph.D Dissertation,Northwestern Univ.,(1968).

10. Hasanain,M.A.,Ph.D Dissertation,Colorado School of Mines,(1980).

11. Radke,C.J.,and Prausnitz,J.M.,Ind. Eng. Chem. Fund.,

11,(4),(1972).

12. Eagleton,L.C.,and Bliss,H.,Chem. Eng. Prog.,49(10),543, (1953).

13. Rosen,J.B.,J. Chem. Phys.,20(3),387,(1952).

14. Masamune,S.,and Smith,J.M.,AICHE J.,10(2),246,(1964).

15. Masamune,S.,and Smith,J.M.,AICHE J.,11(1),34,(1965).

16. Lambaret,F.L.,Ph.D Dissertation,Clemson Univ.,(1970).

17. Thomas,H.C.,J. Amer. Chem. Soc.,66,1664,(1944).

18. Barrer,R.M.,and Lee,J.A.,Surface Sci.,12,354,(1968).

19. Gluekauf,E.,Trans. Faraday Society,51,1540,(1955).

20. Vermeulen,T.,J. Chem. Soc.,London,172,598,(1950).

21. Geser,R,and Kostecki,J.A.,Chem. Eng. Prog. Symp. Ser.,V.63,90,(1967).

22. Vermeulen,T.,and Hiester,N.K.,Chem. Eng. Prog.,48,505, (1952).

23. Sherwood,T.K.,Pigford,A.L.,and Wilke,C.R., 'Mass Transfer',Mc Graw Hill, N.Y.,567,(1975).

24. Hasanain,M.A.,and Hines,A.L.,I&EC Proc. Des. Dev.,20,621, (1981).

25. Pedram,E.,Ph.D Dissertation, Colorado School of Mines,(1978).

26. Satterfield,C.,'Heterogeneous Catalysis in Practice', Mc Graw Hill,(1980).

27. Hsieh,J., Ph.D Dissertation,Syracuse Univ.,(1970).

28. Wilke,C.,and Chang,P., AICHE J.,1,264,(1955).

29. Gaffney,B.,and Drew,T., Ind. Eng. Chem.,41,1124,(1950).

APPENDIX A

A.1 Sample calculations of equilibrium data

Compound : 2,4 dichlorophenoxyacetic acid

Initial absorbance = 0.78

Initial concentration = 560 * Absorbance (eqn. 6.1)

= 560 * 0.78 = 436.8 umoles/liter

Volume of sample = 50 c.c = 0.05 liter

Amount of DPCA acid present = 436.8 * 0.05 = 21.84 umoles

Weight of resin = 1.107 grams

Final absorbance = 0.44

Final concentration = 0.44 * 560 = 246.4 umoles/liter

Amount of DPCA acid in solution = 246.4 * 0.05 = 12.32 umoles

Amount adsorbed = 21.84 - 12.32 = 9.52 umoles

Uptake = amount adsorbed/gram of resin =9.52/1.107 = 8.6 umoles/gm

A.2 Sample calculations of equilibrium data for muticomponent solutions

Compound : 2,4 dichlorophenoxyacetic acid and phenol

slope of phenol at 282 μm, $(S_{phenol})_{282}$ = 0.000501

slope of phenol at 271 μm, $(S_{phenol})_{271}$ = 0.001524

slope of acid at 282 μm, $(S_{acid})_{282}$ = 0.001786

slope of acid at 271 μm, $(S_{acid})_{271}$ = 0.000588

Inital absorbance of solution at 282 μm = 1.1

Inital absorbance of solution at 271 μm = 1.6

Therefore by plugging these values into equations 6.3 and 6.4, and solving simultaneously, it is found that

Initial concentration of phenol = 910 μmoles/lit

Initial concentration of acid = 356 μmoles/lit

Volume of sample = 60 cc

Amount of phenol initially = 54.6 μmoles

Amount of acid initially = 21.36 μmoles

Final absorbance at 282 μm = 0.35

Final absorbance at 271 μm = 0.45

$C_{acid}*(0.001786) + C_{phenol}*(0.000501) = 0.45$

$C_{acid}*(0.000588) + C_{phenol}*(0.001524) = 0.35$

Solving these equations, it is found that

C_{acid} = final concentration of acid in solution
= 210 μmoles/lit

C_{phenol} = final concentration of phenol in solution
= 150 μmoles/lit

Amount of acid in solution = 12.6 μmoles

Amount of phenol in solution = 9.0 μmoles

Total amount of phenol absorbed = 45.6 μmoles

Total amount of acid absorbed = 8.76 μmoles

Uptake of phenol = 45.6/1.2= 38 μmoles/gm

Uptake of acid = 8.72/1.2 = 7.27 μmoles/gm

A.3 Sample calculations of the mass transfer coefficients

RUN # 2

Length 3, z =50 cm

Compound = DPCA Acid

Cross-sectional area = 0.95 cm^2

Volume of bed = 50 * 0.95 = 47.5 cc

Flowrate = 6 cc/minute =.360 lit/hr

Density of resin = 0.9 gm/cc

Density of bed = 0.550 gm/cc

Void fraction, ε = (0.9 - 0.55)/ 0.9 = 0.389

Initial concentration = 274.4 umoles/lit

Measuring the coefficients at C/C_0 = 0.6

C = 164.6 umoles /liter

t = 135 minutes

From Fig 17

$$\frac{dC/C_0}{dt} = .2/36 = 5.555*10^{-3}\ min^{-1} = 0.333333\ hr^{-1}$$

$$\frac{dC}{dt} = 91.46\ umoles/(lit\text{-}hr)$$

From Fig A.1

$$\frac{dC/C_0}{dZ} = -0.36/19.6 = -0.01837 cm^{-1}$$

$$\frac{dC}{dZ} = -5.04 \text{ umoles/cm}$$

Plugging these values into equation 4.8

$$\frac{dq}{dt} = -\frac{(0.36)(-5.04)}{(0.95)(0.55)} - \frac{(0.39)(91.46)}{550} = 3.4 \text{ umoles/(gm-hr)}$$

From Fig A.2, integrating till t = 135 minutes

q = 5.1 μmoles/gm

q^* = 5.761 " (at equilibrium with C = 164.6 μmoles/lit)

q_∞ = 9.6 " (at equilibrium with C = 274.4 μmoles/lit)

C^* = 145.71 umole/lit (at equilibrium with q = 5.1 μmoles)

(1) The Second Order Surface Reversible Kinetics

From the above,

r = 3.4 μmoles/(gm-hr)

Q_m, the maximum capacity of the resin, is 1000 μmoles/gm.

From the linear equation $q = K'Q_mC$

K' = 0.000035 lit/μmoles

q = 5.1 μmoles/gm

Substituting into equation 4.14

k_a = 0.00019 lit/(μmoles-hr)

(2) The Irreversible Surface Kinetics

$r = K_I[C(Q_m - q)]$ (eqn 4.15)

$K_I = 2.08*10^{-5}$ lit/μmol-hr

(3) The External Mass Transfer Coefficient

$r = K_F a_F \varepsilon (C - C^*)/\rho_b$ (eqns 4.10 and 4.34)

$\varepsilon = 0.389$

$K_F a_F = 254.4\ hr^{-1}$

(4) The Internal Mass Transfer Coefficient

$r = K_p a_p (q^* - q)$ (eqns 4.11 and 4.44)

$K_p a_p = 3.4/(5.761 - 5.1) = 5.1437\ hr^{-1}$

(5) The Vermeulen non-linear Mass Transfer Coefficient

Substituting the values of q* and q into equation 4.12

$K_V = 4.8\ hr^{-1}$

(6) The Geser Mass Transfer coefficient

Substituting the values of Q_m and q obtained above into equation 4.13

$K_{GE} = 3.42 * 10^{-3}\ hr^{-1}$

(7) The Klotz Mass Transfer Coefficient

$r = K_K(C)/\rho_b$ (eqn 4.9)

$K_K = 11.4\ hr^{-1}$

These coefficients are tabulated in Table 20.

A.4 Sample calculations of theoretical breakthrough curves for 2,4 dichlorophenoxyacetic acid

Because $r^* = 1$, the equation 4.32 reduces to the simpler form

$$C/C_0 = X = J(\xi, \tau)$$

The values of J are read from the figure A.3. ξ is the variable α and τ is the variable β in this case.

The selected point Z = 50 cm of run 2. The mass transfer coefficients at this point have been calculated in Appendix Three. The external, second order reaction and internal mass coefficients calculated will be used below to predict the theoretical breakthrough curves.

Second-Order Surface Reaction Model

k_a = 0.00019 lit/umole-hr (calculated above). From eqn 4.6

$$\xi_o = \frac{k_a\ v\ Q_m\ \rho_b}{F} = \frac{0.00019 * 47.5 * 1000 * 0.55}{0.36} = 13.83$$

$$\tau = k_a\left(\frac{1}{K'} + C_0\right)\left(t - \frac{\varepsilon v}{F}\right) \quad \text{(eqn 4.17)}$$

$$\tau = 0.00019 \left(\frac{1}{.000035} + 274.4 \right)\left(t - \frac{0.39 * 47.5}{360}\right)$$

$$\tau = 5.48 \ (\ t - .051 \ ) \ (t \text{ in hrs})$$

$$t = 0.1825\tau + 0.051 \text{ (hr)} = 11\tau + 3 \text{ (min)}$$

Values of $J(\xi,\tau)$ are read from Fig A.3 for different values of τ to give the profile of $X = C/C_0$ vs t. The values are given below.

τ	X	t (min)
5	0.04	58
7	0.09	80
10	0.21	113
15	0.51	168
20	0.81	223
25	0.98	298

External Diffusion Model

$$K_F a_F = 254.4 \ \text{hr}^{-1}$$

From equation 4.38

$$\xi = \frac{K_F a_F * \varepsilon * v}{F} = \frac{254.4 * 0.38 * 47.50}{360} = 13$$

from equation 4.39

$$\tau = \frac{254.4 * 0.3888 * 274.4}{9.6 * 550} \left(t - \frac{0.389 * 47.5}{360}\right)$$

$\tau = 5.13\ (t - 0.052)$

$t = 0.1946\tau + 0.052$ (hr)

$= 11.68\tau + 3$ (min)

From Fig A.3

τ	X	(min) t
7	0.18	85
10	0.32	120
15	0.72	178
20	0.90	237
25	0.99	295

Internal Diffusion Model

$r = K_p a_p\ (\ q^* - q\ )$

$K_p a_p = 3.4/(5.761 - 5.1\ ) = 5.144\ \ hr^{-1}$

Substituting the appropriate values into eqn 4.46 and 4.47

$$\xi = \frac{5.144*0.55*9.6*47.5}{0.36*274.4} = 13.06$$

$$\tau = K_p a_p\ (t - \frac{\varepsilon V}{F})$$

$\tau = 5.144\ (t - 0.05)$

$t = 0.1944\tau + 0.05$ (hr) $= 11.66\tau + 3$ (min)

From Fig A.3

τ	X	t
7	0.18	85
10	0.32	120
15	0.72	178
20	0.90	237
25	0.99	295

These results are plotted in Figure 28.

A.5 Sample calculations of theoretical breakthrough curves for phenol

RUN # 4

Compound : phenol

L2, z =30.5 cm

Cross-sectional area = 0.95 cm^2

Volume of bed = 30.5 * 0.95 = 29.26 cc

Flowrate = 9 cc/minute =.540 lit/hr

Density of resin = 0.9 gm/cc

Density of bed = ρ_b = .570 gm/cc

Void fraction, = (0.9 - 0.57)/ 0.90 = 0.3667

Initial concentration = 154 umoles/lit

Measuring the coefficients at $C/C_0 = 0.54$, t = 480 minutes.

C = 88.6 µmoles/liter

From Fig 1 9

$$d(C/C_0)/dt = 0.2/100 \text{ min} = 0.2/1.67 \text{ hr} = 0.1197 \text{ hr}^{-1}$$

$$dc/dt = 19.6 \text{ µmoles/lit-hr}$$

From Fig A.4

$$d(C/C_0)/dz = 0.22/10.5 = 0.021 \text{ cm}^{-1}$$

$$dc/dZ = -3.44 \text{ µmoles/lit-cm}$$

Substituting into eqn 4.8

$$\frac{dq}{dt} = -\frac{(0.54)(-3.44)}{(0.95)(0.57)} - \frac{(0.37)(19.6)}{570} = 3.42 \text{ µmoles/gm}$$

From Fig A.5, the rate is integrated to give the amount adsorbed till t = 480 minutes.

q = 21.2 µmoles/gm

$C^* = 78.1$ µmoles/lit

$$q^* = \frac{0.317*88.6}{1 + 0.001865*88.6} = 24.1 \text{ µmoles/gm}$$

$q_o = 40.8$ µmoles/gm (from the phenol isotherm at 25 degrees C)

The Langmuir constants to be used are

Q_m = 170 μmoles/gm

K' = 0.001865 lit/μmole

$$r^* = \frac{1}{1 + K'C} = \frac{1}{1 + 0.001865 * (164)} = 0.766$$

Second-Order Surface Reaction Model

The equation is

$$r = k_a[\, C(Q_m - q) - q/K']$$

Plugging the values of C, Q_m, q and K',

k_a = 0.00188 lit/μmole-hr

From equation 4.6

$$\xi = \frac{k_a\, v\, Q_m\, \rho_b}{F} = \frac{0.00182 * 29.26 * 170 * 0.57}{0.54} = 9.87$$

From equation 4.17

$$\tau = k_a\left(\frac{1}{K'} + C_0\right)\left(t - \frac{\varepsilon v}{F}\right)$$

$$\tau = 0.00188\left(\frac{1}{.001865} + 164\right)\left(t - \frac{0.37 * 29.26}{360}\right)$$

$$\tau = 1.32\,(\,t - 0.03\,)$$

$$t = 0.76\tau + 0.03\ (hr) = 45.6\tau + 2\ (min)$$

From Fig A.3, the various J values are read and substituted into equation 4.32 to yield the following results:

τ	$r^*\xi$	$J(r^*\xi, \tau)$	ξ	$r^*\tau$	$J(\xi, r^*\tau)$	$X=C/C_0$	t
5	7.56	0.33	9.87	3.83	0.07	0.10	230
7	7.56	0.60	9.87	5.36	0.21	0.28	321
10	7.56	0.80	9.87	7.67	0.46	0.60	456
12	7.56	0.90	9.87	9.19	0.59	0.78	549
15	7.56	0.96	9.87	11.5	0.73	0.92	686

External Diffusion Model

Plugging values of C, C^*, ξ and r into equation 4.34,

$$K_F a_F = \frac{(3.42) * (570)}{(88.6 - 78.1) * (0.366)} = 506 \text{ hr}^{-1}$$

From equation 4.38,

$$\xi = \frac{K_F a_F * \varepsilon * v}{F} = \frac{506 * 0.37 * 29.26}{540} = 10.14$$

Equation 4.39 becomes

$$\tau = \frac{506*0.366*164}{570*40.8*[1+0.5(.766 - 1)]} \left(t - \frac{0.37*29.26}{550}\right)$$

$$\tau = 1.48 \ (t - 0.03)$$

$$t = 0.676\tau + 0.03 \text{ (hr)}$$

$$= 41\tau + 2 \text{ (min)}$$

From Fig A.3, the various J values are read and substituted into equation 4.32 to yield the following results:

τ	$r^* \xi$	$J(r^*\xi,\tau)$	ξ	$r^* \tau$	$J(\xi, r^*\tau) X = \frac{C}{C_0}$		t
5	7.77	0.27	10.1	3.83	0.05	0.08	207
7	7.77	0.50	10.1	5.36	0.11	0.21	289
10	7.77	0.73	10.1	7.67	0.31	0.50	412
12	7.77	0.85	10.1	9.19	0.42	0.70	494
15	7.77	0.94	10.1	11.5	0.59	0.88	617

Internal Diffusion Model

$$r = K_p a_p (q^* - q)$$

$K_p a_p = 3.42/(24.1 - 21.2) = 1.179 \ hr^{-1}$

Substitution of the values of q , r^*, into equation 4.46 and 4.47 gives:

$$\xi = \frac{1.179*0.57*40.88*29.26}{164*0.54} = 9.06$$

$$\tau = 1.34 (t - 0.03)$$

$$t = 0.748\tau + 0.03 \ (hr) = 44.9\tau + 5 \ (min)$$

From Fig A.3,

τ	r*ξ	J(r*ξ,τ)	ξ	r*τ	J(ξ,r*τ)	X=C/C0	t
5	6.9	0.37	9.06	3.83	0.10	0.14	227
7	6.9	0.69	9.06	5.36	0.27	0.37	316
10	6.9	0.83	9.06	7.67	0.57	0.71	451
12	6.9	0.93	9.06	9.19	0.62	0.83	541
15	6.9	0.98	9.06	11.5	0.83	0.96	675

These results are plotted in Figure 30.

A.6 Sample calculations of external mass transfer coefficients

The diffusivity of phenol is calculated by the empirical correlation of Wilke and Chang(28).

$$D_f = \frac{7.4*10^{-8}(\phi M_B)^{0.5} T}{\mu \; \nu^{0.6}}$$

where

M_B = mol. wt. of solvent

T = temperature,K

μ = solution viscosity,centipoises(1.005 for water).

ν = solute molal volume(= 108.8for phenol)

ϕ = association factor for solvent (2.6 for water)

Therefore,

$$D_f = 9.05 * 10^{-6} \ cm^2/sec$$

From Gaffney and Drew(29)

The external mass transfer coefficient is defined as

$$j_D = 1.26 \beta (Re)^{-2/3}$$

where

Re = Reynolds Number = $\rho V d_p/\mu$

V = superficial velocity of solution = 9.5/60 cm/sec

d_p = 100 microns (an average value)

μ = 1.005 centipoises

Therefore Re = 0.158

$Re^{2/3} = 0.2923$

Plugging in the values for Run 4 with $\epsilon = 0.36$

$$\beta = \left[\frac{1 - (1-\epsilon)^{5/3}}{2 - 3(1-\epsilon)^{1/3} + 3(1-\epsilon)^{5/3} - 2(1-\epsilon)^2} \right]^{1/3}$$

$\beta \simeq (24.55)^{0.333} = 2.91$

$j_D = (k_m \ Sc^{2/3})/V$

$j_D = 1.26*2.91*0.2923 = 12.528$

Sc = Schmidt number = $u/\rho D_f = 1030$

$Sc^{2/3} = 102$

$k_m = 12.528*570/102 = 70$

a_m = area of particle / volume of bed

$= 6(1-\varepsilon)/d_p = 384$

$K_F a_F = k_m a_m * C_0/(q_\infty * \rho)$

$= 70*384/141.8 = 190\ hr^{-1}$

$Sc^{2/3} = 102$

$k_m = 12.528*570/102 = 70$

a_m = area of particle / volume of bed

$= 6(1-\varepsilon)/d_p = 384$

$K_F a_F = k_m a_m * C_0/(q_\infty * \rho)$

$= 70*384/141.8 = 190\ hr^{-1}$

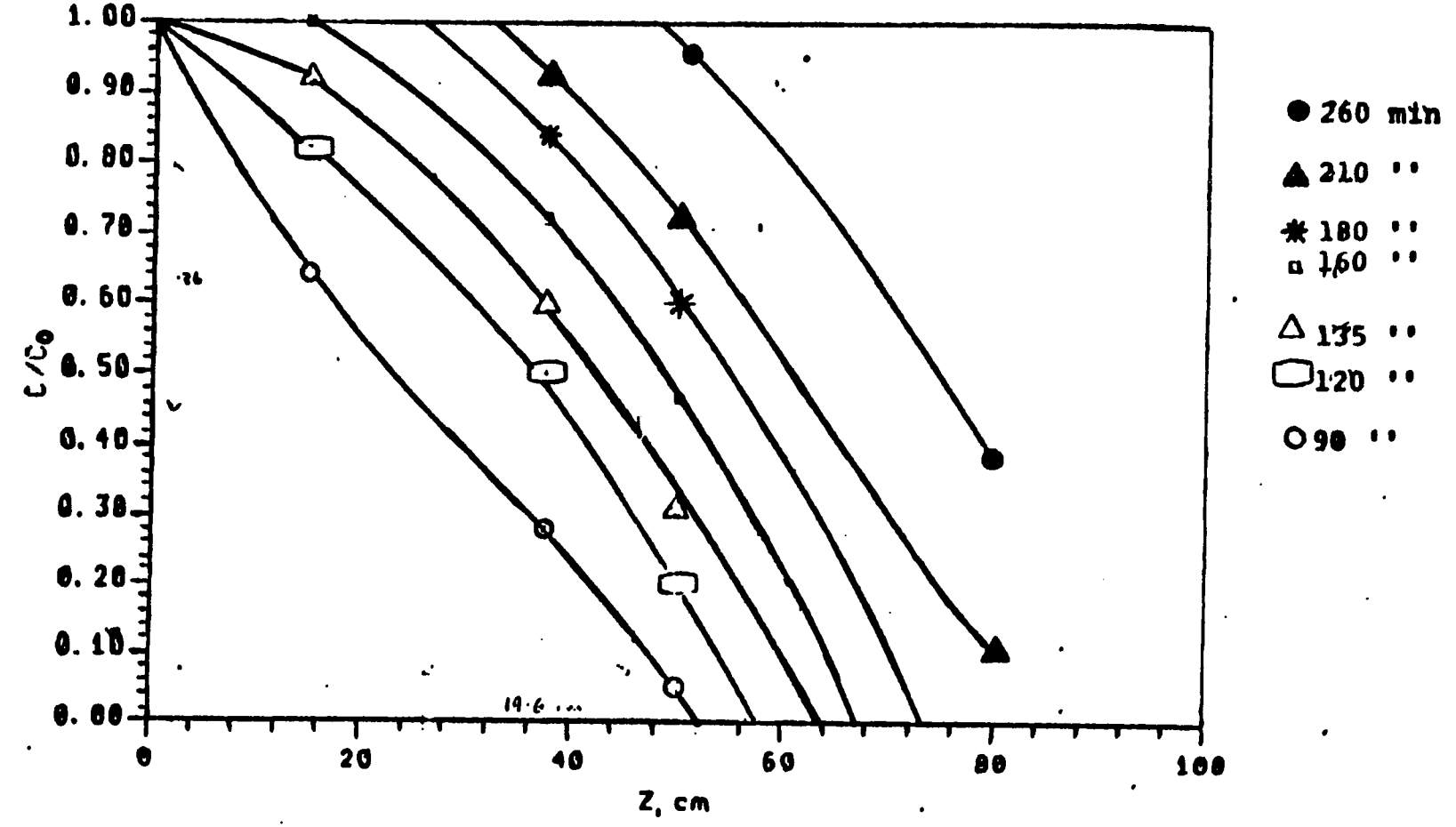

Fig A.1: C/C_0 vs Z for DPCA Acid RUN 2, Z = 50 cm.

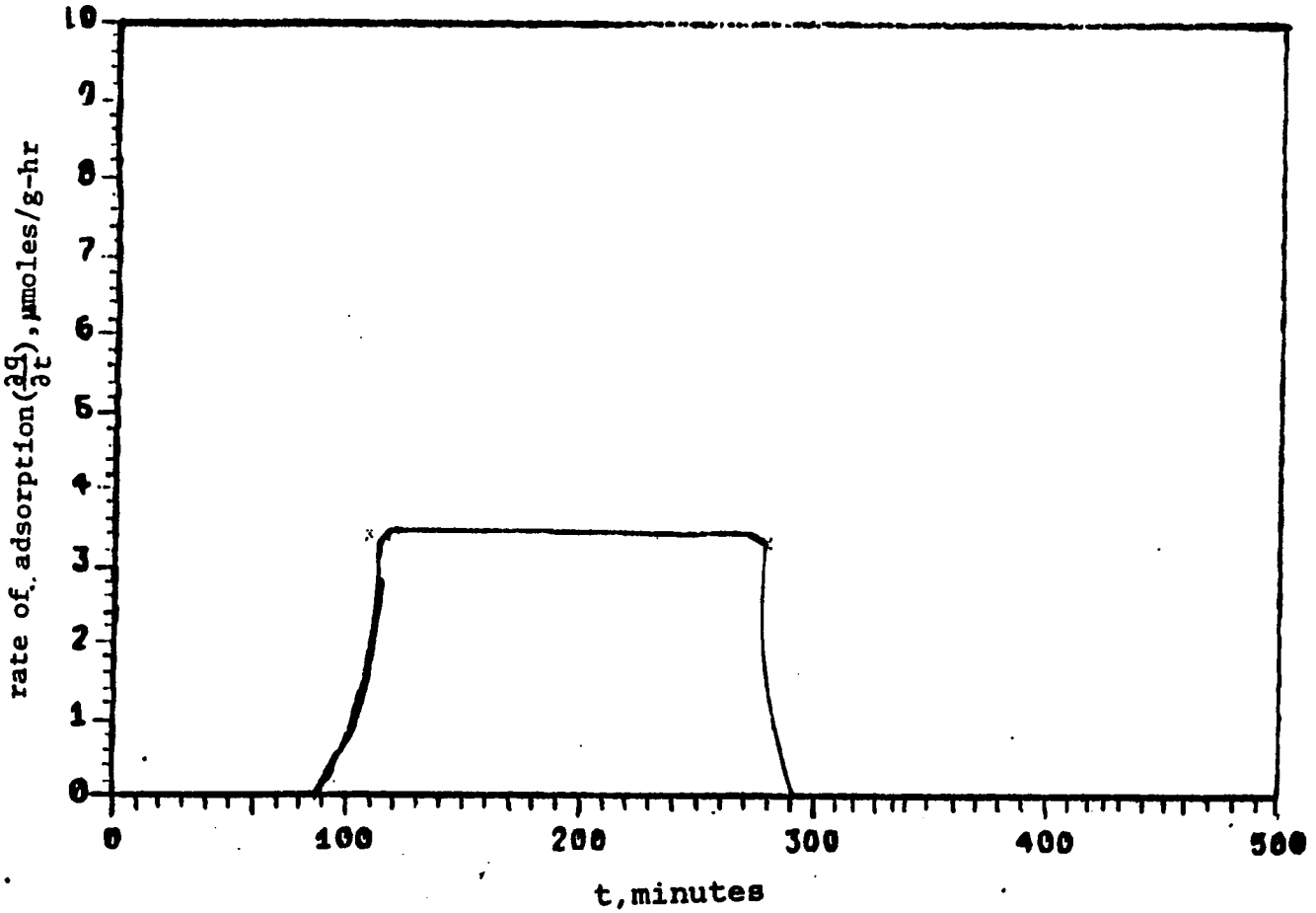

Fig A.2 : Graphical Integration of Rate of Adsorption -RUN 2, Z = 50 cm.

Fig A.3: Function used in calculating the Thomas Function J

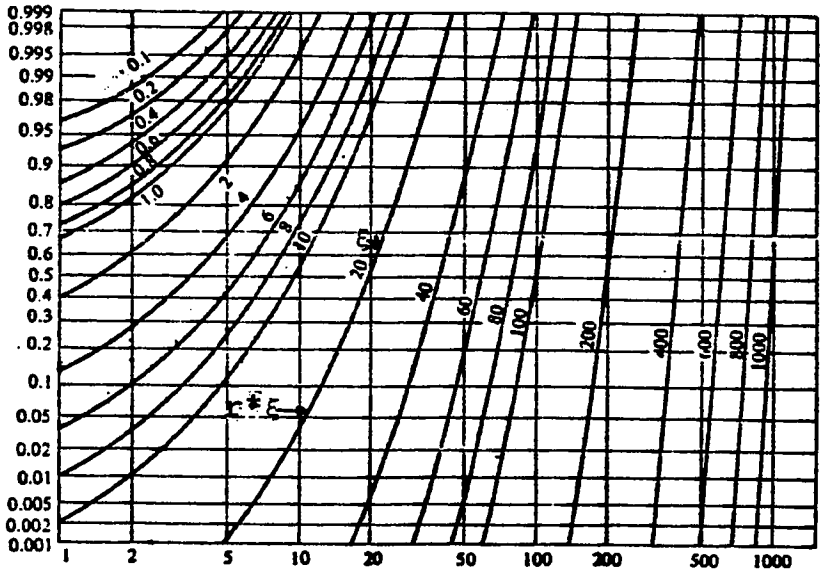

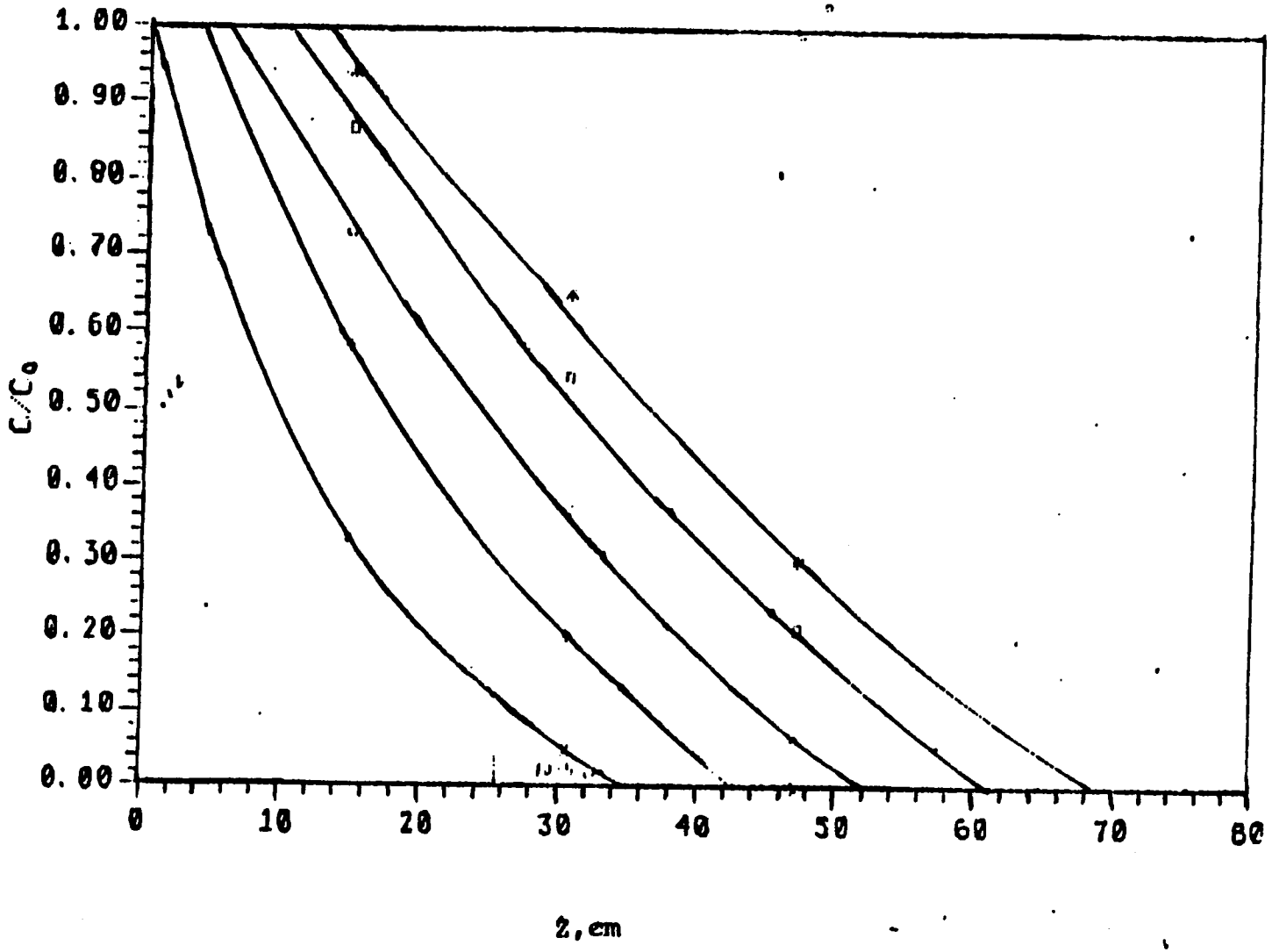

Fig A.4: C/C_0 vs Z for Phenol RUN 4, Z =30.5 cm.

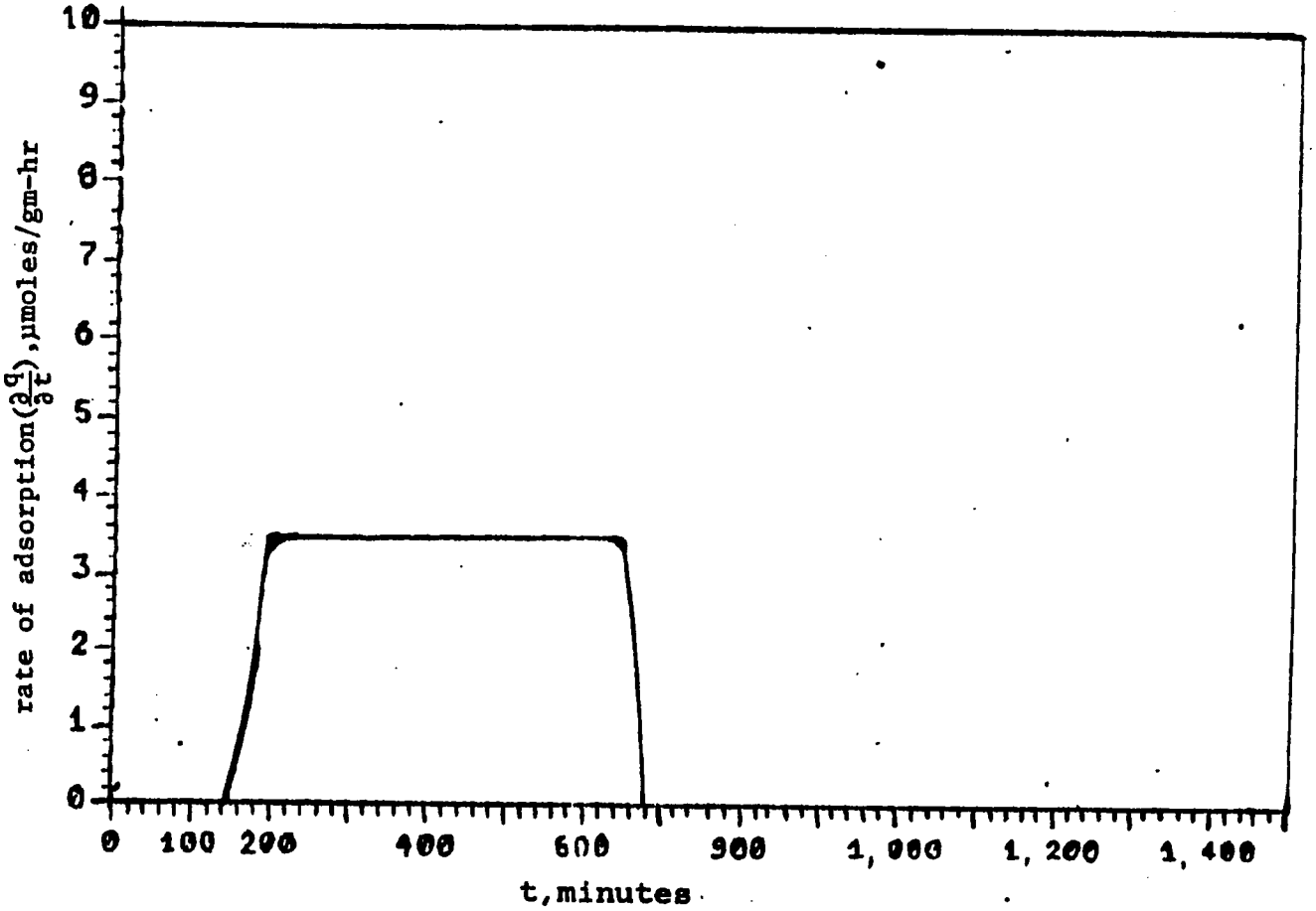

Fig A.5 : Graphical Integration of Rate of Adsorption, RUN 4, Z = 30.5 cm

A.7 Further Confirmation of External Mass Transfer Limitation for Phenol Adsorption on XAD-7

It was found in Sec 6.4.1 that the theoretical external mass transfer coefficients differed significantly from the experimental ones. The explanation advanced was that the particle diameter used in the calculations was assumed to be 100 microns while in reality the particle size ranged from above 200 microms to below 50 microns. A column experiment was made with fresh resin which had been sieved and the size of which was measured under the microscope. Only one length was used. The external mass transfer coefficient was calculated as described in Sec A.6 and used in the Thomas method to generate the theoretical external diffusion limited breakthrough curve. The following gives the operating conditions of the run, and a summary of the calculations.

Compound: phenol

Length of bed = 27.2 cm

Weight of resin = 12.6 gm

$S = 0.95\ cm^2$

density of bed = 12.6/(27.2*0.95) = 0.488 gm/cc

$\varepsilon = 0.458$

F, Flowrate = 9 cc/min

$C_o = 190.24$ umoles/lit

Therefore $q_\infty = 44.5$ umoles/gm

The experimental data for the run are:

C/C_O	.05	.10	.33	.43	.52	.62	.77	.90	1.0
t(min)	46	89	164	215	253	335	455	550	635

d_p, particle diameter = 140 microns

$Re = 0.22$

$Re^{2/3} = 0.364$

$j_D = 1.26 / Re^{2/3}$

$= 2.524$

$j_D = 8.74$

$Sc = 1104$

$Sc^{2/3} = 102$

$K_m = j_D * V / Sc^{2/3} = 48.84$ cm/hr

$a_m = 232.3$ cm^{-1}

$K_m a_m = 11345$ hr^{-1}

$K_F a_F = K_m a_m * C_O / (q_\infty * \rho_b) = 99.4$ hr^{-1}

$\xi = 99.43 * 0.458 * 25.84 / 540 = 2.18$

$r^* = 1/(1+0.001856*190.24) = 0.738$

$\tau = 99.4 * 0.458 * 190.24 / (540 * 44.5 * 0.869)(t - .458 * 25.84/540)$

$\tau = 0.4148(t - 0.0219)$

$t = 2.411\tau + 0.0219$ (min)

$t = 144.7\tau + 1$ (min)

From Fig A.3,

τ	$r^*\xi$	$J(r^*\xi,\tau)$	ξ	$r^*\tau$	$J(\xi,r^*\tau)$	$\bar{X}$	t
0.5	1.61	0.28	0.369	2.2	0.15	0.18	73
1.0	1.61	0.46	0.738	2.2	0.29	0.33	146
1.5	1.61	0.60	1.11	2.2	0.37	0.45	218
2.0	1.61	0.69	1.48	2.2	0.45	0.53	290
3.0	1.61	0.83	2.21	2.2	0.59	0.71	435
4.0	1.61	0.93	2.95	2.2	0.68	0.83	580

These calculated points are compared to the experimental data in Fig A.6, and it is found that the fit is reasonable.Thus the conclusion that external diffusion is limiting the adsorption of phenol on XAD-7 is confirmed.

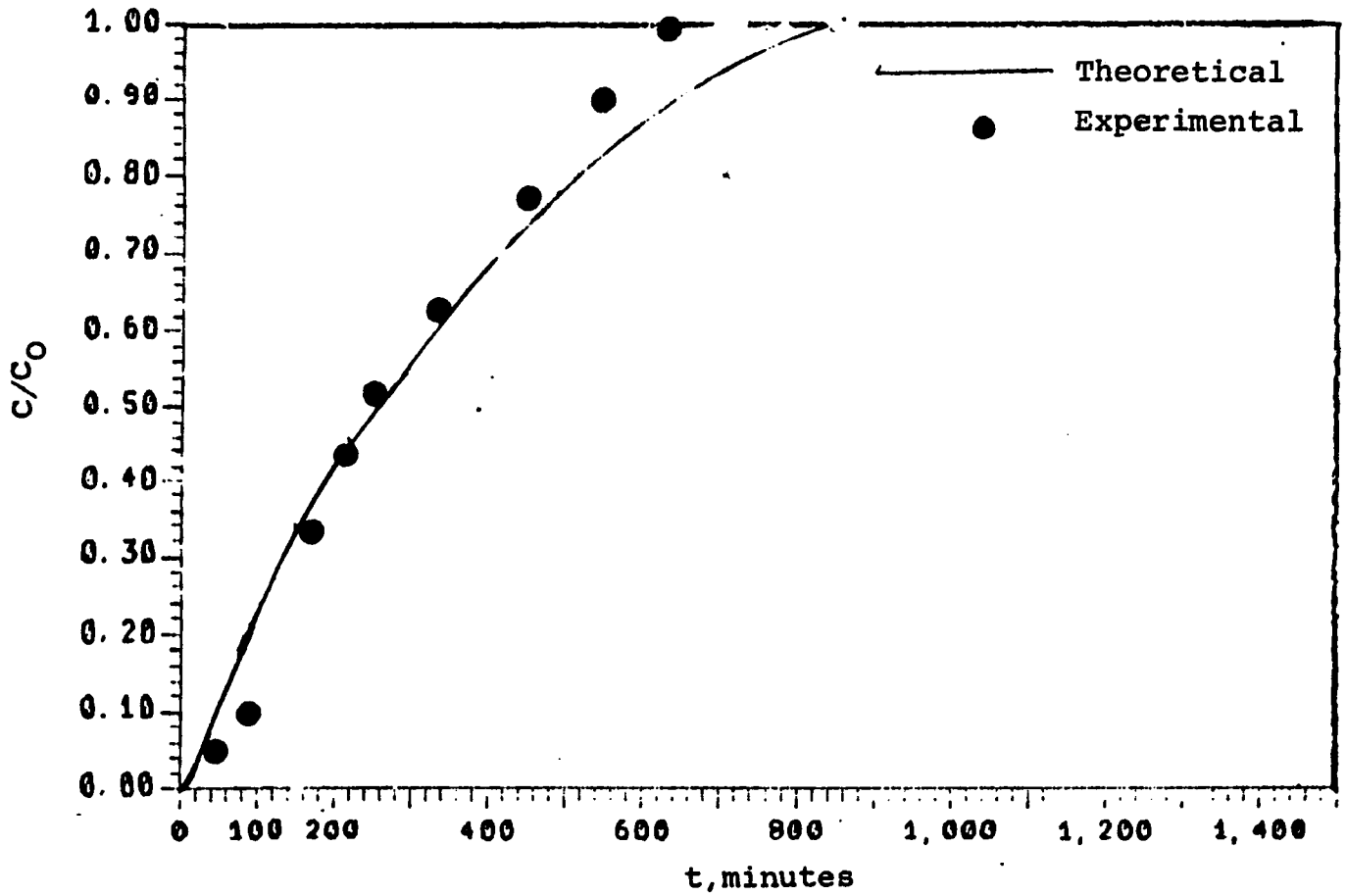

Fig A.6: Predicted Curve Compared to the Experimental data-RUN 10.